EXPERIMENTAL MODELING OF EVA TASKS AND WORKLOAD USING FORCE-TORQUE SENSING APPARATUS

by

Sayan Chakraborty

Bachelor of Science in Aeronautics and Astronautics
Massachusetts Institute of Technology
1989

Submitted in Partial Fulfillment of
the Requirements for the Degree of

MASTER OF SCIENCE IN
AERONAUTICS AND ASTRONAUTICS

at the

MASSACHUSETTS INSTITUTE OF TECHNOLOGY
SEPTEMBER 1990

© Massachusetts Institute of Technology, 1990

Signature of Author ______________________________
Department of Aeronautics and Astronautics
July 16, 1990

Certified by ______________________________
Professor David L. Akin
Thesis Supervisor
Department of Aeronautics and Astronautics

Accepted by ______________________________
Professor Harold Y. Wachman
Chairman, Departmental Graduate Committee
Department of Aeronautics and Astronautics

MASSACHUSETTS INSTITUTE
OF TECHNOLOGY

SEP 19 1990

LIBRARIES

Aero

Experimental Modeling of EVA Tasks and Workload Using Force-Torque Sensing Apparatus

Abstract

To facilitate research into modeling EVA and IVA tasks through the use of neutral buoyancy simulation, a force-torque sensing data acquisition system was designed and constructed. This system centered around three identical six degree-of-freedom, strain gage based, underwater force-torque sensors. These were attached to a left handrail, right hand task board/handrail, and foot restraints; and displayed an accuracy of better than ± 3.75 N in force, and ± 1 N-m in torque.

This test set-up was then used to determine the force-torque versus time profiles for simple tasks performed by six scuba-trained test subjects. These profiles were compared against profiles predicted by Kinematic Chain Link (KCL) models for two cases: subject restrained only at left handrail while performing tasks on the right handrail (Case 1), and subject restrained in foot restraints while performing tasks on the right handrail (Case 2). The KCL model for Case 1 did not provide an accurate predictor of test subjects' force-torque applications, primarily because the subjects' lower bodies were free to rotate, creating dynamic and fluid effects unaccounted for by the model. In the Case 2 restraint system, however, such rotations were inhibited by the foot restraints. As a result, The KCL model for this case provided high fidelity when predicting force-torque profiles.

It had been hoped to use both KCL models developed above to create a general empirical model for predicting force-torque profiles caused when a subject was fully restrained (foot restraints and both handrails, Case 3). This model assumed a distribution of reactions between the restraints which was proportional to values predicted by the previous KCL models for the same input. Due to interactions between the three restraints not predicted by the two-point models, this model could not be validated. However, the data proved useful in confirming hydrodynamic effects as the major cause of error in Case 1.

In addition to this modeling, a methodology for the use of this data acquisition system to estimate a subject's physiological workload is presented.

Finally, peak forces and torques applied by the subjects during the various tasks were investigated. This research found with statistical corroboration that subjects in restraint Case 3 were able to output higher peak forces and torques then the other two cases. It was also found that subjects in the Case 2 restraint system were able to output higher forces than the Case 1 system, and the same seemed true for torque application, although this was not statistically confirmed. The test subject parameters of height and mass were found to have no statistically confirmed general effect on the peak force-torque output, restraint case was indicated as the driving influence. Peak force-torque data taken under normal gravity conditions was also taken as a benchmark to the neutral buoyancy data.

This Research Conducted Under
NASA Grant Number NAGW - 21

Thesis Advisor:
David L. Akin
Assistant Professor of Aeronautics and Astronautics

Dedication

This thesis is dedicated to *my* authors. My parents have always been there for me, and it is through their unceasing hard work and love that I have had the freedom to pursue my dreams.

Acknowledgements

Over one year ago a naive graduate student turned to his thesis advisor and said, "I want to build *something cool that moves.*" And so began the saga of Fafnir, a project which, however cool, cannot move. Such is life. Now that the tale nears its end, I would like to thank those who have had a part in it, however small.

First and foremost, I must thank Dave Akin, who would have let me do this entire page in iambic pentameter. Dave has been my teacher, advisor, and especially friend, throughout my five years at MIT. Dave has a unique ability to turn students into engineers when they aren't really looking, plus he provides lots of snacks. Thanks for everything, Dave, and good luck.

Thanks must also go to Professors Mar and Alexander, who with advice, Peking Raviolis, and soldering iron, have had a very positive impact on this work; and of course to Ping, without whom nothing would have ever been accomplished. Don't forget to pack her, Dave.

Thanks to my test subjects who spent many chilly (and overchlorinated) winter hours in the pool: Anna, Dave, Karl, Kurt, and Matt. And to the contributing members of Fafnir: Les, Sam, and Kurt, box guy extraordinaire, thanks, and good luck at MIT.

To the denizens of Space Systems Lab, a great place to have fun and do cool engineering research on the side: good luck wherever you end up. Those deserving special note, include : Jud and Russ, Terry "too Cruel" Fong, Rich, Killer, Rob, Ender, Beth, Matt, Anna, Kurt, Ella and Ali. And to whoever gets Fafnir, I hope you answer some of the many questions I raised.

To my friends (MIT and non-MIT, Baker and non-Baker), if it is through the quality of your friends that you judge yourself, I must be amazing. Right? Thanks Paul, Ken, Andy, Megan, Joe, CJ, Tracy, and Renee; my amazing roommates Andy, Tim, Sam, Mike, and (in a strange sort of way) Giovanna (thanks for the edit!); my future roommate Cathy, the Unified Dudes; all of the Brockmen; and bunches of others including everyone I inevitably forgot.

And thanks to two of my best friends of all: my big sister Sulagna (the definitively amazing person), and my little brother Simanta, who grew up when I wasn't looking. Also to my little puppy, and obnoxious pet, Raja.

And finally, to Julie-Anne, we've been through a great deal together, good and bad, but mostly very very good. I love you.

Table of Contents

List of Figures

List of Tables

Chapter 1: Introduction

1.1 Background

During the past three decades the astronauts and cosmonauts of Mir, Salyut, Apollo, Gemini, Soyuz, Skylab, and the Space Shuttle have shown that humans can work effectively both inside and outside their spacecraft. It is hoped that this decade will see the advent of a new generation of space station, and the opportunities it will provide those countries with and without access to Mir. To construct, operate, and maintain such a space station will, however, require several thousand hours of EVA (Extra-Vehicular Activity) and IVA (Intra-Vehicular Activity). Space operations on this scale represent a cost, and demand a commitment to safety, far beyond the realm of present experience. This requires that new efforts be made towards fully understanding what is involved when working in zero gravity.

Unlike working on Earth, working in space requires a tremendous amount of effort to be expended towards just maintaining a desired position and orientation when applying forces and torques. Newton's third law pushes back on a pushing astronaut with the same force magnitude and in an opposite direction - action and reaction. Unrestrained tools and astronauts would soon find themselves drifting away from their worksite as a result of reaction forces and torques. To counteract these forces and torques, hereafter referred to simply as reactions, mission planners have provided astronauts with all manner of handholds, as well as foot and leg restraints. Unfortunately, there seems to have been little attempt to model how reactions are produced when designing the actual tasks performed or the restraints used. Such modeling would prevent overdesign of restraint systems and work area structures; in a workplace where every excess pound represents a cost both in mission capabilities and in thousands of dollars, any saving could prove invaluable. In addition, poor restraint designs, which may cause injury, could be redesigned before undergoing testing with actual subjects.

Reaction modeling could also be used to assess the demands a given task places on an astronaut. As mentioned before, a major physical cost of zero gravity operations is in applying the required reactions. And while fatigue has rarely been the limiting factor when performing tasks on orbit in the past, with the advent of advanced suit technology allowing longer EVA durations, and the need for much greater amounts of EVA and IVA, it could soon become an important consideration. Physiological workload can be assessed in a variety of ways, with the predominant methods being heart rate and oxygen consumption measurement at present. These methods do have disadvantages, however. Both methods require that the subject's environment (such as a flight suit) be instrumented. This could not only compromise the environment, but would also require extensive and expensive modifications. An assessment of all forces and torques expended (both those required by the task itself, as well as those required by the reactions), provides a non-invasive method of physiological workload assessment.

Reaction modeling and physiological workload assessment are hardly new topics. Both have been researched extensively throughout this century, but virtually exclusively in the realm of normal gravity operations. This is to be expected, however, as this area of the field of biomechanics is primarily concerned with the physiological demands placed on a worker or athlete when performing their functions. A wide variety of biomechanical models have been developed to mimic human activity (several of which are presented in the following chapter), and these vary both in complexity and the useful regime of operation - usually whether the motions involved are static or dynamic.

It appears obvious that these methods and models might be adaptable to zero gravity conditions, and this generally holds true. Exceptions to this do occur, however, especially in one case of importance. In this case an astronaut is restrained at the feet, grasping a handrail with one hand, and performing some task with the other. This is an essentially static situation if the hand and arm displacements required by the task are small, but the static models (which are developed using structural analysis methods) break down for this case. This is because the case represents a statically indeterminate problem which defies mathematical modeling, but which cannot be ignored as it is often seen in actual space operations. Any model which covers this case must therefore be an empirical model, derived from experimentation. Any such experimentation would best be carried out in simulated zero gravity, as performing these experiments on orbit would be prohibitively expensive.

The simulation of the zero-g environment is difficult on Earth. One such method is employing aircraft to fly trajectories which nullify gravity effects, much as a rapidly descending elevator does. Unfortunately, parabolic-trajectory KC-135 flights are expensive and provide extremely short periods of zero-g test time, less than 30 seconds in duration. A less expensive method is to employ an "air table", a table where jets of forced air offset the downward gravity acceleration, similar to an air hockey table. But being a tabletop environment, air table testing is normally impractical for large scale objects, such as astronauts, and by its nature confines testing to two dimensions. Simulated weightlessness in three dimensions can best be found, then, in the realm of the Scuba diver. Divers use the buoyant force of water (which is proportional to the diver's volume) to support themselves against the pull of gravity, usually requiring air-filled vests and lead weights to trim exactly. This apparently weightless state, called neutral buoyancy, allows the diver a great deal of freedom in the underwater environment. In the realm of research, testing underwater, utilizing neutral buoyancy, provides an environment in which long-duration, large-scale experimentation can be accomplished. Size is limited only by the tank size (some of which can contain mockups of the space shuttle), and maximum testing duration by air supply, available power, or other consumables. Even this simulation method is far from perfect, however, for as motions become larger and occur at higher velocities, water drag and associated effects greatly reduce the fidelity of the simulation. For essentially static operations, however, neutral buoyancy is an attractive medium for performing zero-g experimentation.

It was experience with this type of simulation environment that led the author and MIT's Space Systems Lab towards this investigation of mathematical and empirical zero gravity task modeling. The Space Systems Lab's Lab of Orbital Productivity (SSL/LOOP) has been using neutral buoyancy for over a decade to simulate space operations. Although work has been done in the lab utilizing KC-135 flights, air tables, and even a flight experiment on board the space shuttle *Atlantis*, the emphasis has been on neutral buoyancy. Testing of human SCUBA subjects as well as telerobots at the MIT Alumni Pool and at the Marshall Space Flight Center's facility has produced a wealth of information on how humans and machines can work in space, both together and independently.

The recent discussion of the space station's EVA and IVA requirements, as well as a NASA push for more orbital servicing of satellites by the shuttle, focused SSL's gaze on human task performance in zero gravity. It was determined that the construction of force-torque sensors capable of providing measurements of all applied forces and torques, with a high degree of sensitivity, would allow complete modeling of primarily static tasks under a variety of restraint cases. Sensors placed on a task board, a handrail, and foot restraints could be used to confirm the validity of biomechanical models adapted for zero-gravity, as well as provide the data necessary to attempt to develop an empirical model for the case where the mathematical model breaks down.

Such sensors would also provide the type of data to be used when assessing physiological workload. The integration of all forces and torques expended over time, as measured at the task board and restraints, could be correlated to energy expenditure. If the tasks performed were basic, then more complex tasks could be modeled as a combination of these simple tasks, allowing the analysis to be broadly useful.

It was soon discovered that these sensors could be used for a number of investigations outside of those raised above. Two were selected as being relevant to the research already proposed. The first involved a comparison of the peak forces and torques a subject was capable of exerting in zero gravity for a variety of restraint configurations, and against peaks under normal gravity. This type of investigation had been done previously, but not in conjunction with a defined set of relevant tasks, or used for comparing different restraint cases. The second investigation was a broad comparison of test subject parameters, such as body mass or height, to the peak forces the subject was capable of exerting, in an effort to determine if a trend existed. Thus, the data from these sensors could provide a variety of important conclusions about human operations in zero gravity.

1.2 Related Research

While the following chapter will provide an overview of the field of biomechanics and how it relates to this research, it will prove useful to examine specific work that has already been done in this area, both to provide a sense of what is understood, and to show what remains to be studied. Interestingly enough, the investigation of force-torque reactions in the worksite has been studied for over three decades, and has been heavily motivated by the space program. In July of 1970, R. H. Huston and C. E. Passerello opened their paper on modeling human body dynamics with a comment that, "the manned space program is primarily responsible," for increased interest in human body dynamics; two decades later that statement still rings true [Huston, 1970]. Huston and Passerello go on to model the equations of motion of humans engaged in such activities as lifting objects under reduced gravity, swimming, or kicking while in free fall. The paper is interesting because it approaches the problem with mathematical rigor, at a time when analytical biomechanics was still a fairly "rule-of-thumb" oriented field. However, these models were never verified experimentally, which underlines the gulf that existed between the theoreticians and experimenters at that time.

The first extensive experimental force-torque analysis of human actions was performed using a "Lauru platform" by Brouha in 1960 [Brouha, 1960]. The force platform was outfitted with piezoelectric crystals which changed polarization under compression. Given a triangular arrangement of these crystals, the platform was capable of measuring a broad range of forces in the downward, frontal, and transverse directions. By the very nature of the device, however, it was incapable of measuring any torques produced by a subject. A series of experiments were performed, and were designed to mimic actions in a normal gravity workplace, the area of the Brouha's interest. Many of the ideas developed here are broadly applicable to the entire field, however. Brouha presents the force-time profiles of several actions, such as typing or lifting heavy bags, and then correlates the peak expended forces to both heart rate and oxygen consumption as estimates of workload. Correlation coefficients of 0.83 to 0.96 were found when comparing force profiles to oxygen consumption, confirming the possibility of using force analysis to estimate energy expenditure.

Confirming mathematical models with real world experimentation had actually been done for the case of simulated weightlessness, a notable exception in a clearly divided field. As early as 1964, C. E. Whitsett began modeling astronauts floating unrestrained, where, "any force or torque applied by or to man will result in translational and/or angular accelerations or decelerations" [Whitsett, 1964], the same reactions which this work focuses on for the restrained cases. Whitsett models the moments of inertia for body segments as well as those for a complete individual, in order to simulate changes in body orientation as a result of applying torques of under two second durations. To confirm the models, a subject applied torques while in weightlessness simulated via KC-135 parabolic trajectories. Both the torque applied, and the subject's resulting angular velocity were estimated, and the resulting inertial values were within 10% of the analytical predictions. Among other conclusions, Whitsett discovered that subjects peak torques were reduced by 1/3 for 0-G versus their 1-G peaks. This research also provided useful information on the dynamic motion of unrestrained astronauts, information which would not be used for actual space operations until the advent of the Skylab Astronaut Maneuvering Unit (AMU), and later the shuttle Manned Maneuvering Unit (MMU).

Underwater experiments have also been performed for some time. The University of Wisconsin Mechanical Engineering department performed experiments in the late Sixties on human reaction forces underwater [Seireg, 1970]. To perform the experiments, a set of foot restraints were instrumented with nine springs, in order to detect all six directions of force and torque (Fx, Fy, Fz, Tx, Ty, Tz in a three-dimensional orthogonal coordinate system, X, Y, and Z). Accuracy of this measurement system was not discussed; however the force-torque estimates did depend on summation and amplification of analog signals without any apparent attempts to reduce or estimate noise. The testing involved subjects being placed in the restraints and performing simple arm motions on the surface and then in a water tank. Using the equations of motion for the arm movements, the authors were able to experimentally estimate the drag effects and, more specifically, the drag coefficient, Cd, for the underwater motions. Although not concerned with simulating weightlessness, the research does provide a methodology for estimating drag effects during dynamic neutral buoyancy simulation. In addition, it estimated peak forces in zero-g at 12% of one-g maximums for tasks with low drag effects, such as pushing an object directly forward.

Actual application of this type of analysis to simulated space operations did not occur until the late Seventies and early Eighties. A good deal of work was done in MIT's Space Systems Laboratory towards attempting to model dynamic motions of humans in neutral buoyancy [Tomusiak, 1978]. This work dealt mainly with examining the validity of the neutral buoyancy environment for modeling unrestrained motions, such as arm motions with held masses [Bowden, 1981]. Work was also done, however, on modeling human dynamic motions, both in restraints and out, with the use of experimental force-torque values [Cousins, 1987]. To this end a circular cross-section beam was instrumented with waterproofed strain gages to provide measurements of five directions of forces and torques (Fx, Fy, Tx, Ty, and Tz, as axial beam forces (Fz) were not instrumented for). This Instrumented Beam System (IBS) provided a basis for experimentally verifying a model of subjects performing simple, very dynamic, tasks, called the Task Mechanics Model. The subjects performed four tasks: large mass translation, large mass rotation (both while in foot restraints attached to IBS), subject body translation, and subject body rotation (on handrails attached to IBS). Accuracy of the IBS was estimated at ± 2 %, and as only one

IBS was available, tests were limited to the one-point restraint case. It was this work, however, which chiefly motivated the present research's look into static operations modeling with multiple-point restraints.

Finally, work has been done towards bringing force-torque sensing into actual space operations. The Jet Propulsion Laboratory (JPL) has developed a full six direction force-torque sensor for use on the shuttle's remote manipulator system (RMS) [Hanson, 1988]. This sensor is designed to provide force-torque reaction profiles of a working astronaut attached to foot restraints on the end of the shuttle arm. It could also provide a major component in a force-feedback loop for use in arm operations. At present that loop is envisioned as continuing through a human operator by simply providing force-torque values on a screen. Later improvements might include a complete closed loop through the hardware. JPL originally specified a device accuracy (for forces) of better than ± 10 N, as they predicted that most astronaut and RMS force expenditures would be in the 10-100 N range. However, the device had to be constructed to withstand shuttle launch loads of nearly 45000 N through one axis. To prevent yield failure the device was made more robust, driving sensitivity down. The device accuracy is now estimated at ± 125 N, well beyond the range of many astronaut and RMS task force magnitudes. This underlines the suitability of neutral buoyancy simulation for this type of sensor use, as with present technology very high accuracies can be achieved.

Chapter 2: Biomechanics

The term "biomechanics" can be defined in many ways, but in essence it provides an engineering approach to the analysis of the human body and its various subsystems. Here a line can be drawn separating the two major fields of biomechanics. The first field examines motions of the entire human body, or at least of the muscoskeletal system (kinesiology) through modeling, and it is in this area that this research lies. The second field attempts to model the actions of various organs and structures of the body, such as the heart or lungs, and these models are used when designing artificial replacements for such parts.

The models used when studying the entire human body have tremendous variation in terms of complexity as well as regions of validity. They can be loosely classified into biodynamic, mathematical, and kinematic/kinetic models, although a good deal of overlap does exist [Roozbazar, 1973].

2.1 Biodynamic Models

Biodynamic models are primarily concerned with how the human body reacts to a specific type of force environment, such as acceleration, impact, blast, acoustics, pressure, or vibration. The model generally used in this type of experimentation views the human body as a collection of masses, springs, and dampers. Each body subsystem, such as the upper arm, uses lumped parameterization - i.e. the mass of the entire subsystem is lumped at its center of mass. An example of such a model can be seen in Figure 2-1 [Coermann, 1970].

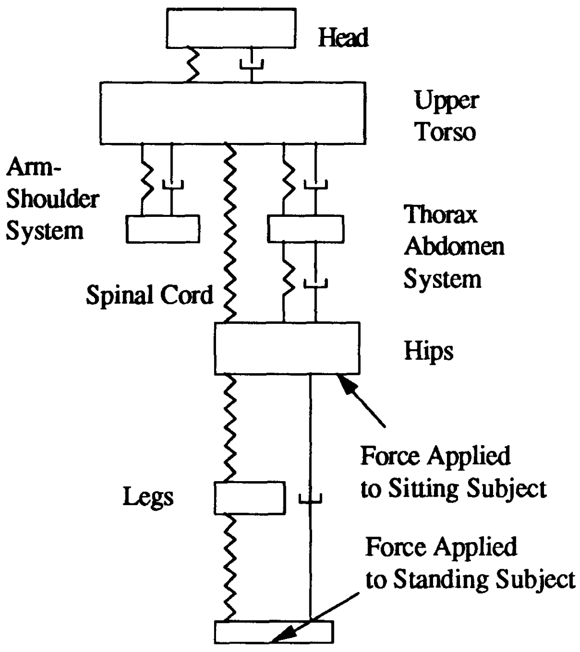

Figure 2-1: Biodynamic Model

As a rule, such a model is only used to determine response to forces along the vertical axis. The segment masses are determined by examination of human cadavers, but to determine the values of the various spring and damping constants, animals and live humans are subjected to the environments to be studied in a safe regime, and their responses noted. In several cases the models were then actually built, and compared to human subject responses in actual experiments, to fine tune the physical constants. An example of one such experiment placed a human, the mass-spring-damper model, and a simple mass into tractor seat simulators. All three were then subjected to vibrations well within human safety limits. While the mass had little correlation to human response, the biodynamic model was iteratively adjusted until it mimicked the human subject well. The model could then be used to estimate human response for hazardous environmental regimes [Suggs, 1973]. The major use of these models has proven to be in examining the resonance effects of blasts, impacts, accelerations, and vibrations, in terms of the body systems' frequencies and peak amplitudes.

2.2 Mathematical Modeling

Mathematical models have their name not because they are the only class of biomechanical models which require mathematical development, but because mathematical calculations and assumptions are made to determine the inertial properties of various human subsystems. These inertial properties are important because mathematical models attempt to simulate human dynamic motion. Biodynamic models tend to concentrate on resonance of an essentially static human, while kinematic/kinetic models concentrate on static force and torque applications by and on a human. As a result of this, biodynamic models can be seen as mass-spring-damper systems and easily built, while kinematic models can be viewed as sets of structural links. It is the dynamic mathematical models which have no simple experimental analog, and thus depend on more extensive mathematical analyses.

To begin the process of mathematical modeling, the human form is divided into various segments, each of which is to be modeled separately. The number of segments depends on the needs of the experiment, but a typical model might have 15 such parts, specifically, the head, neck, torso, upper arms, lower arms, upper legs, lower legs, feet, and hands. Each part is then modeled by a geometric shape with the same general center of mass characteristics. From various studies of live humans and cadavers [Chaffin, 1984], average values for the various segment dimensions, centers of mass, densities, and overall masses are taken. In fact, equations for segment masses and dimensions as functions of overall subject height and weight have been developed, simplifying the modeling process when personalizing these values for a test subject. During this process, three basic assumptions have been made:

1) The human body can be modeled as simple geometric shapes of constant density.

2) The average values for segment parameters not taken from the test subjects themselves can be validly interpolated from existing surveys.

3) The segments move about fixed pivot points, i.e. all the joints have been modeled as groups of single degree-of-freedom (DOF) rotational joints.

Typical geometric shapes which are used to model the various segments can be seen in Figure 2-2.

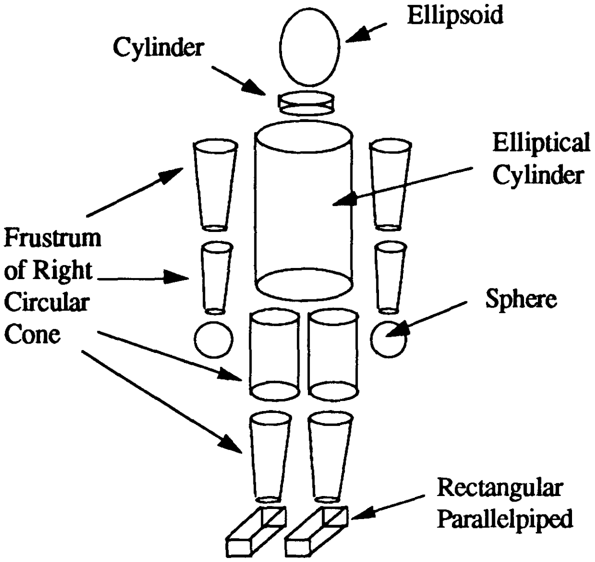

Figure 2-2: Mathematical Modeling of a Human Form

Once each segment is modeled, human motion can then be described as the correct rotations of the various segments about the joints. Equations of motion must account for inertial and torque effects of each segment in relation to itself and to the overall center of mass. These equations are taken from classical mechanics, and lend themselves to matrix notation and solutions employing computers. In fact, in his survey of biomechanical models , Aziz Roozbazar places the mathematical models which require extensive computer processing power to properly use in their own category [Roozbazar, 1973]. These models divide the human form into more segments and with more degrees of freedom, in full three-dimensional analysis, but with the vastly increased availability and power of computers, separate classification is no longer necessary.

In fact, the author implemented part of a 15 segment model in software, and this may be illuminating for the reader. Appendix A: Software, contains a Microsoft Excel™ 2.2 worksheet entitled *Moments of Inertia*, which covers some steps basic to any dynamic modeling process. This process usually proceeds along the following lines:

1) The body is divided into simple geometric shapes, as described above. Using references [Chaffin, 1984] body segment densities and masses are calculated.

2) Also using references some sample segment dimensions can be gleaned, the rest are derived from the knowledge of segment mass and density. At this point, segment and total body centers of mass can be calculated.

3) The various moments of inertia for each segment can now be developed as formulae are known for the geometric shapes being considered. These moments of inertia will play an important role in the next step.

4) The equations of motion for the pertinent body segments are developed using the major dynamic forces involved; such as virtual mass, water drag, and inertial effects for underwater experiments.

The program developed performs the first three functions of this modeling process. As sophisticated dynamic models were not directly used in this research, the mathematics are not developed more fully here. Far more thorough development of this topic can be found in Space Systems Lab Report #13-87 *Biomechanics of EVA and its Neutral Buoyancy Simulation* [Cousins, 1987].

2.3 Kinematic/Kinetic Modeling

Kinematic/kinetic modeling techniques are used to simulate a restrained human operating under essentially static conditions. The tools used in this area are those of the structural mechanist, and the basic assumptions vary from those made for dynamic modeling. For example, in this modeling environment elasticity and damping of the human body are regarded as having little pertinent effect.

The kinematic model is composed of a collection of rotational joints, which model the degrees of freedom available to a human, connected by rigid links. These links are not equivalent to the corresponding bones, rather they are a kinematic abstraction of the straight line distance between two joints. Figure 2-3 shows an example of such a link system, hereafter called a Kinematic Chain Link, or KCL. Each node represents a single degree-of-freedom rotational joint. The shoulder, for example, is composed of two such joints. It should also be noted that the head, hands, and feet are considered links beyond the terminal joints, and are ignored in most KCL models.

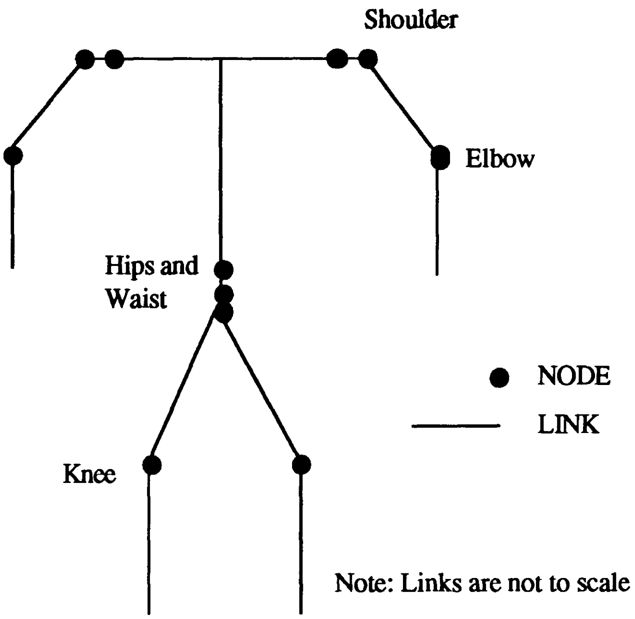

Figure 2-3: Kinematic Chain Link (KCL) Model

The model presented above has 11 degrees of freedom, represented by the nodes. To fully describe this system one would need to specify the lengths of the 10 links and the angular position of the 11 joints. If working in normal gravity, the mass and center of mass of each link would also be required inputs into the model.

For the zero gravity case, a force on an end of a link causes a resultant force and moment at the other end that are functions of the magnitude and direction of the input force as well as the angle(s) of the joint(s), and the lengths of the links. These resultant forces and moments are developed by the subject to prevent the link from changing its position translationally or rotationally. The equal-and-opposite effects of these resultants are then inputs for the next link and so on, until reaching a restraint upon which the total reactions are expended.

Chaffin succinctly describes this process of solving the distributions of forces and torques through a human body represented as a kinematic chain link by stating that, "the analysis starts at the point of application (often the hands) and proceeds in sequence, solving the equilibrium equations for each body segment, until reaching the segment that supports the body (usually the feet)." [Chaffin,1984]

A critical assumption in this type of analysis is that the reactions follow a one-way path from the input point to the restraints. This would not be the case if a subject produced more reactions to aid in performing a task, just as pushing off with one's feet might aid in moving a mass with the hands.

Figure 2-4 shows two links in zero gravity, and the resultants caused by an input force. In this case the two links are the forearm and upper arm. It is important to note that this is for the weightless case; under normal gravity additional reactions would be produced by the weight of each body segment operating through each link's center of mass (joints are modeled as massless units).

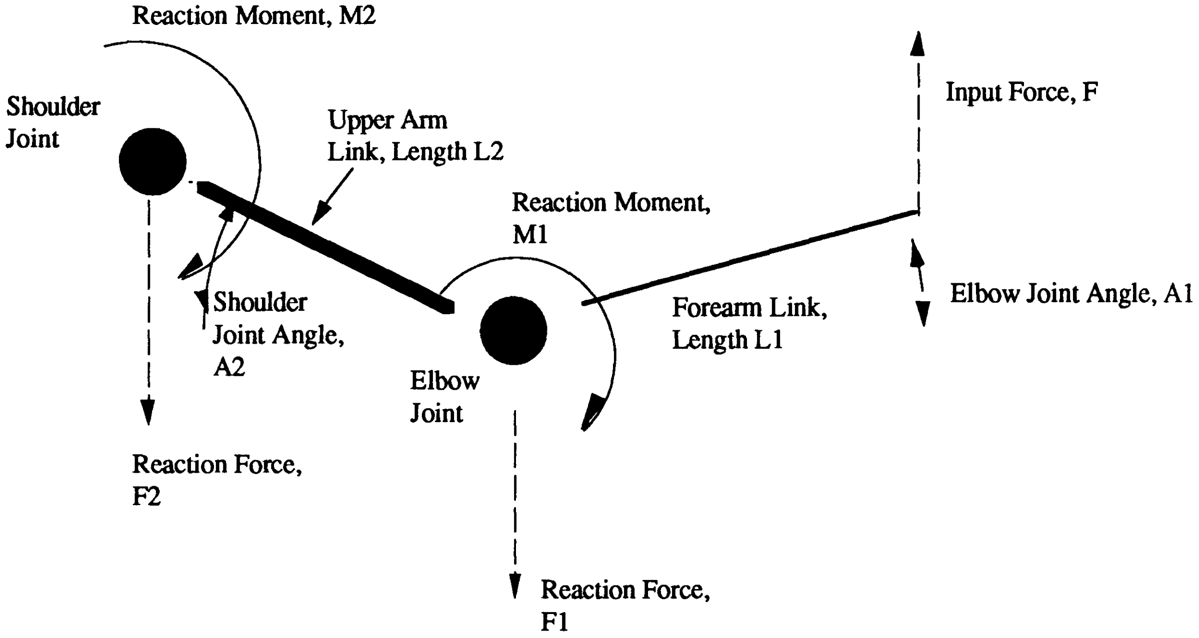

Figure 2-4: KCL Link Analysis

The equations of equilibrium of each joint can be calculated in a relatively straightforward fashion. Equations (2.3-1) and (2.3-2) are the equations for the elbow, while (2.3-3) and

(2.3-4) are for the shoulder. Developing these types of equations on each subsequent link is the process that Chaffin speaks of.

Elbow, Force Equilibrium:

$$\sum F=0: F + F1 = 0; \quad F1 = - F \tag{2.3-1}$$

Elbow, Moment Equilibrium:

$$\sum M=0: F(L1)\cos(A1) + M1 = 0; \quad M1 = - F(L1)\cos(A1) \tag{2.3-2}$$

Shoulder, Force Equilibrium:

$$\sum F=0: F + F2 = 0; \quad F2 = - F \tag{2.3-3}$$

Shoulder, Moment Equilibrium:

$$\sum M=0: M2-M1 - F(L2)\cos(A2) = 0; \quad M2 = M1 + F(L2)\cos(A2) \tag{2.3-4}$$

An examination of the force equations reveals that the joints must maintain force equilibrium by applying an equal but opposite force at each joint. This prevents any joint from translating. Moment equilibrium is more complex, as each joint must not only develop enough moment to counteract the input force over the length of the lever arm (a function of link length and joint angle) but must also counteract the moment developed at the previous joint. These opposing moments prevent joint motion, allowing the subject to maintain position and rotational orientation. Please note that throughout the paper the nouns torque and moment are used interchangeably, unless otherwise specified.

Unfortunately, these reaction equations cannot always be completely determined. In many human activities, KCL models appear as "open" chains. This refers to the fact that equations of motion for an unconstrained or overconstrained human are indeterminate, i.e. the number of describing independent equations is less than the number of unknown joint positions. The total number of unconstrained degrees of freedom for the body is represented by m-n, where m is the number of unknowns, and n is the number of describing equations.

In an attempt to provide more constraints on human motion, the "minimum principle" from structural analysis has been employed [Nubar, 1961]. This principle, when applied to the statically indeterminant system representing the human form, can be defined as the following: "A mentally normal individual will, in all likelihood, move (or adjust his posture) in such a way as to reduce his total muscular efforts to minimum consistent with the constraints." The muscular efforts can be described by the following effort equation:

$$E = (c_1M_1^2+c_2M_2^2+...+c_mM_m^2)\Delta t+A_0 \qquad (2.3\text{-}5)$$

where E is the total effort, M is the moment at a particular joint, c is a joint constant, delta-t is the duration of effort, and A_0 represents the initial conditions. The constraints on the effort function are normally of the form of Equation 2.3-6.

$$\begin{array}{c} f_1(M_1,M_2,...,M_m,t)=0 \\ \cdots\cdots\cdots\cdots\cdots\cdots\cdots\cdots \\ f_n(M_1,M_2,...,M_m,t)=0 \end{array} \qquad (2.3\text{-}6)$$

The above equation indicates that at all times the net moment on the model must equal zero, or the subject would be in motion and no longer subject to static analysis.

This effort-driven constraint is a quite useful unless, as will be true for this research, the subject tends to maintain a given orientation. In this case constraints are provided by the joint angles and moments required to maintain this orientation, which will not necessarily be an orientation of least effort. Since the orientations are still essentially static, however, Equation (2.3-6) is still satisfied.

In the following chapter, KCL models will be developed with force inputs at the right hands, and then terminating at either the feet or the left hand. For the case where the link terminates at the left hand, a mathematical model will also be developed in order to estimate the effects of water drag. Finally, KCL principles will be applied to attempt to model the indeterminate three-point case, where force inputs at the right hand can terminate either at the feet or the left hand.

Chapter 3: Modeling

As stated previously, this chapter is about applying the tools discussed in Chapter 2 to the problems of interest. These problems are modeling weightless humans, performing simple, essentially static tasks with one hand while restrained by the other hand, the feet, or both. For all three problems some of the same basic assumptions were made, including neglecting the masses of links and joints, and very importantly, assuming that changes in the joint angles of the chain link in question would be small. This was the single most important constraint in modeling and experimentation, and while it failed at points, it did allow for a much simpler modeling and experimental process. Finally, it was also assumed that any task performed by the subject could be decomposed to a set of three forces and three torques along and about a set of orthogonal coordinate axes, such as Fx, Fy, Fz, Tx, Ty, Tz. The actual tasks and coordinate system used are discussed in Sections 6.1 and 6.2 respectively.

3.1 Case 1: Two-Point Restraint - Both Hands

3.1.1 The KCL Model

Under these circumstances the subject being modeled is performing a static task with one hand (for the purposes of this work, all tasks were performed with the right hand), and is maintaining position with the left hand. The kinematic chain link in question runs from the right hand, up the right arm, across the shoulders, and down the left arm to the left hand. The lower body and the head do not appear at all in this reaction path and so are not included in the KCL model (except the waist angle about the z axis, which rotates the upper body). The hands themselves are not included since any moments developed across a link representing the hand would be very small. So, too, are the three degrees of freedom available at the wrists ignored. Since the tasks will be static, as is subject orientation (joint angles are constant), the chain link can begin just after the wrists.

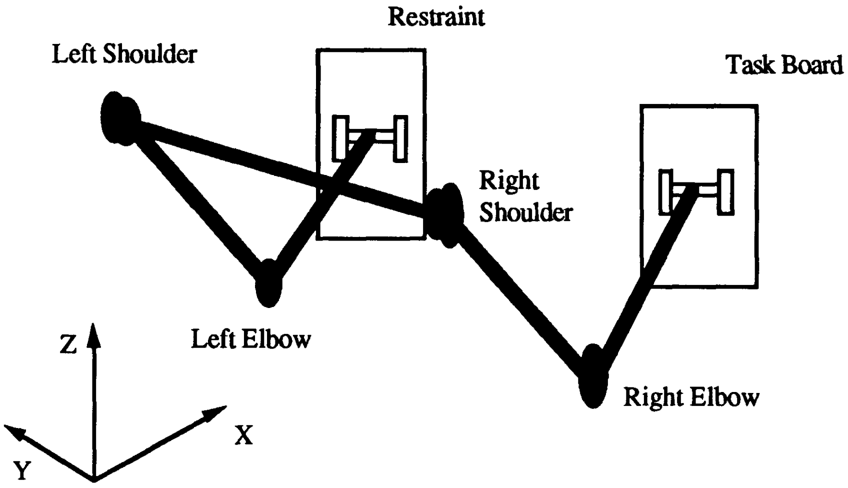

Figure 3-1: Chain Link for Case 1

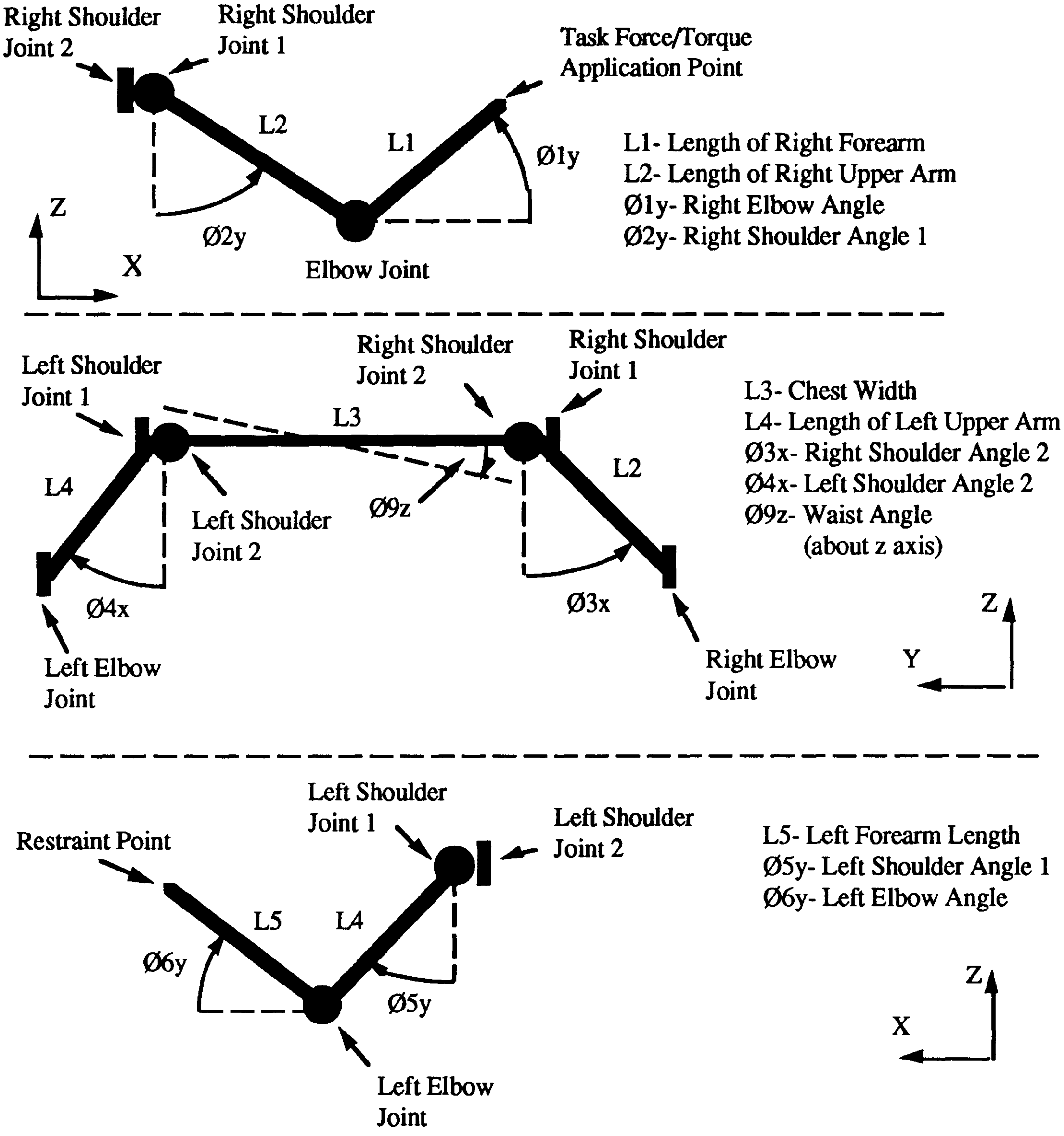

Figure 3-2: Breakdown of Chain Link for Case 1

Figure 3-1 shows the KCL chain model used for this case while Figure 3-2 breaks it down to show all the relevant angles and link lengths. The angles are numbered in order along the chain, with the letter subscript denoting the coordinate axis the joint rotates about. For comparison to experimental data, the link lengths were provided via measurement of the test subjects, and angle data was provided by examination of videotapes of the tasks being performed and the arrangement of the test rig. It is hoped that ongoing work in the SSL towards the development of a fiber optic body suit will soon allow a more direct measurement of subject joint angle data. For the purposes of modeling, however, retaining these inputs as variables does not present a difficulty.

Calculating force and moment equilibriums for each joint, while following the chain from input point to restraint, allowed the development of the model. Again, since the assumption was made that any task could be decomposed into a combination of six components, the model was developed using each component as a possible input, and then the six were superposed to produce the total model.

What follows are the force and moment equilibrium equations at each joint along the link; these were implemented on a Microsoft Excel 2.2™ spreadsheet, available in Appendix A: Software, under the title *Kinematic Chain Link*. Along with the basic spreadsheet, are six personalized versions, one for each test subject.

Beginning at the elbow (position 1) (task inputs are subscripted with zeros),

Force Equilibrium:

$$\sum Fx=0;\ F_{x1}=-F_{x0} \qquad (3.1\text{-}1a)$$

$$\sum Fy=0;\ F_{y1}=-F_{y0} \qquad (3.1\text{-}1b)$$

$$\sum Fz=0;\ F_{z1}=-F_{z0} \qquad (3.1\text{-}1c)$$

Since no single joint can translate, it becomes obvious that all the joints in the link will have force equilibrium equations of the same form, and this is also true of the restraint point. Thus, the overall force equilibrium equation is presented below, with n being any of the three coordinates x, y, or z, and k being any point on the chain link.

$$\sum Fn=0;\ F_{nk}=-F_{n0} \qquad (3.1\text{-}2)$$

This is not true of the moment equilibrium equations, however. The notation used in the equations for the angles and link lengths is from Figure 3-2 and is consistent in the software. The numerical subscripts denoting the point being considered are available in Table 3-1.

ANALYSIS POINT	NUMBER	ANGLE
Right Elbow Joint	1	Ø1y
Right Shoulder Joint 1	2	Ø2y
Right Shoulder Joint 2	3	Ø3x
Left Shoulder Joint 2	4	Ø9z
Left Shoulder Joint 1	5	Ø4x
Left Elbow Joint	6	Ø5y
Restraint Point	7	Ø6y

Table 3-1: Analysis Points- Case 1

What follows are the moment equilibrium equations along the chain link, up to and including the restraint point.

$$M_{x1} = - M_{x0} + F_y \sin(Ø_{1y})L1 \tag{3.1-3a}$$
$$M_{y1} = - M_{y0} - F_x \sin(Ø_{1y})L1 + F_z \cos(Ø_{1y})L1 \tag{3.1-3b}$$
$$M_{z1} = - M_{z0} - F_y \cos(Ø_{1y})L1 \tag{3.1-3c}$$

$$M_{x2} = M_{x1} + F_y \cos(Ø_{2y})L2 \tag{3.1-4a}$$
$$M_{y2} = M_{y1} - F_x \cos(Ø_{2y})L2 - F_z \sin(Ø_{2y})L2 \tag{3.1-4b}$$
$$M_{z2} = M_{z1} + F_y \sin(Ø_{2y})L2 \tag{3.1-4c}$$

$$M_{x3} = M_{x2} + F_y \cos(Ø_{3x})L2 - F_z \sin(Ø_{3x})L2 \tag{3.1-5a}$$
$$M_{y3} = M_{y2} - F_x \cos(Ø_{3x})L2 \tag{3.1-5b}$$
$$M_{z3} = M_{z2} + F_x \sin(Ø_{3x})L2 \tag{3.1-5c}$$

$$M_{x4} = M_{x3} - F_z \cos(Ø_{9z})L3 \tag{3.1-6a}$$
$$M_{y4} = M_{y3} - F_z \sin(Ø_{9z})L3 \tag{3.1-6b}$$
$$M_{z4} = M_{z3} + F_x \cos(Ø_{9z})L3 + F_y \sin(Ø_{9z})L3 \tag{3.1-6c}$$

$$M_{x5} = M_{x4} - F_y \cos(Ø_{4x})L4 - F_z \sin(Ø_{4x})L4 \tag{3.1-7a}$$
$$M_{y5} = M_{y4} + F_x \cos(Ø_{4x})L4 \tag{3.1-7b}$$
$$M_{z5} = M_{z4} + F_x \sin(Ø_{4x})L4 \tag{3.1-7c}$$

$$M_{x6} = M_{x5} - F_y \cos(Ø_{5y})L4 \tag{3.1-8a}$$
$$M_{y6} = M_{y5} + F_x \cos(Ø_{5y})L4 + F_z \sin(Ø_{5y})L4 \tag{3.1-8b}$$
$$M_{z6} = M_{z5} + F_y \sin(Ø_{5y})L4 \tag{3.1-8c}$$

$$M_{x7} = M_{x6} + F_y\sin(\emptyset_{6y})L5 \qquad (3.1\text{-}9a)$$

$$M_{y7} = M_{y6} - F_x\sin(\emptyset_{6y})L5 + F_z\cos(\emptyset_{6y})L5 \qquad (3.1\text{-}9b)$$

$$M_{z7} = M_{z6} - F_y\cos(\emptyset_{6y})L5 \qquad (3.1\text{-}9c)$$

This last set of three equations (3.1-9a through 3.1-9c) represent the torque reactions at the restraint, which along with equation (3.1-2) comprise the reaction equations for this case. As mentioned above, these were implemented in software to allow easy comparison to experimental data. Obviously, it is hoped that the decomposed task inputs measured experimentally should produce reactions, via these equations, which are very close to the measured reactions.

3.1.2 The Dynamic Model

It became apparent when the experiments for this restraint case were being designed that subjects would inevitably rotate. This is because the lower body, representing the bulk of the mass and inertia, is not restrained. As subjects became acclimated to the tests it was expected that the problems maintaining orientation would lessen. It was still expected, however, that this dynamic motion would have some effect on the results.

Rotation of the body about the pivot point represented by the restrained left hand would result in some lessening of the braking reactions needed because of the retardant effects of water drag, inertia, and virtual mass, which is the force needed to displace the still water in the direction of motion. As a result, measurable conservation of reactions is not maintained. The KCL model is unable to account for these effects as they are in the dynamic regime. It was therefore decided that a dynamic mathematical model analysis must be performed to estimate these effects in order to assess their error-creating potential.

The basic principles of Section 2.2 allow development of a simple analysis of these effects to gage how negligible they are. In fact, for the first cut the 15 element model is probably not required, and the entire human can be modeled as a right circular cylinder (especially since it is assumed that the legs act as a single unit). In fact, a cylinder with the same outer dimensions as a "more human" model has a greater surface area, which means the forces calculated will be higher than those actually present. This provides a comfortable margin in the analysis.

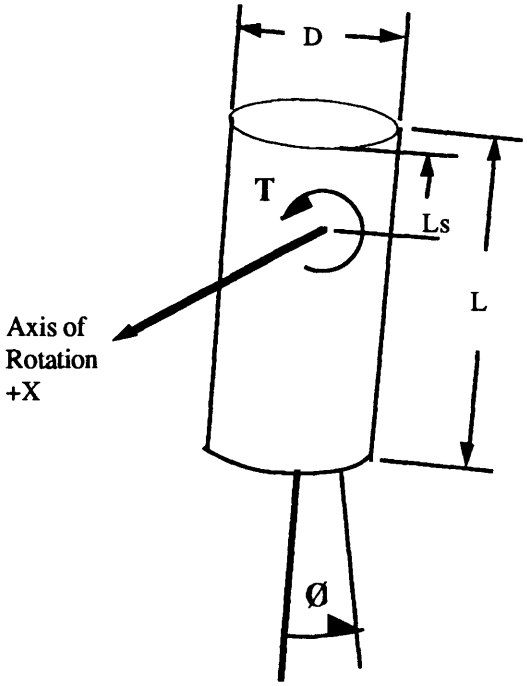

Figure 3-3: First Cut Dynamic Model

Figure 3-3 shows the model being considered. It is apparent that rotation about the long axis of the cylinder will cause negligible effects, especially when compared to rotation about the transverse axes, due to the greatly lessened surface area and moment of inertia in that direction. The following equations have therefore been developed for rotations about the transverse axes [Cousins, 1987].

The torque developed counter to the direction of rotation can be expressed as:

$$T_{total} = T_{inertial} + T_{drag} + T_{virtual\ mass} \tag{3.1-10}$$

where,

$$T_{inertial} = M\left(\frac{L^2}{3} + LL_s + L_s^2\right)\ddot{Ø} \tag{3.1-11}$$

$$T_{drag} = \frac{1}{8}C_D\rho D\left(L_s^4 + (L - L_s)^4\right)\dot{Ø}^2 \tag{3.1-12}$$

$$T_{virtual\ mass} = C_V\rho\left(\frac{\pi}{12}\right)D^2\left(L^3 + (L - L_s)^3\right)\ddot{Ø} \tag{3.1-13}$$

Equation (3.1-10) does not account for other fluid effects such as lift forces, multi-body effects, and end effects. A complete discussion of the role of these forces can be found in [Paines, 1986], but are ignored in this analysis. Note that the term in parentheses in Equation (3.1-11) represents the cylinder's moment of inertia about the axis of rotation. The variables used in 3.1-11 through 13 are defined in Table 3-2, which also provides their values or methods of determination.

VARIABLE	DEFINITION	VALUE	SOURCE
M	Cylinder Mass	per subject mass	subject data
L	Cylinder Height	per subject height	subject data
Ls	Distance to Rotation Axis	calculated	subject data
Ø	Angular Displacement	calculated	experiments
Cd	Coefficient of Drag	~1.2	Cousins, 1987
ρ	Water Density	1000 kg/m3	Cousins, 1987
D	Cylinder Diameter	calculated	*Moments of Inertia,* Appendix A
Cv	Coefficient of Virtual Mass	~1.3	Cousins, 1987

Table 3-2: Dynamic Model Variables

This model is actually implemented to determine its impact on the experimental results in Chapter 7; as an example, selecting a 95th percentile male subject with a height of 1.725 m and a mass of 70 kg reduces the torque equations to:

$$T_{\text{inertia}} = 100\,\ddot{\emptyset} \quad \text{N-m} \tag{3.1-14}$$

$$T_{\text{drag}} = 251\,\dot{\emptyset}^2 \quad \text{N-m} \tag{3.1-15}$$

$$T_{\text{virtual mass}} = 315\,\ddot{\emptyset} \quad \text{N-m} \tag{3.1-16}$$

It can easily be seen that for relatively constant angular velocities the drag moment dominates. Using some SCUBA subject sample data [Cousins, 1987] on a subject rotating 1.4 radians ($\dot{\emptyset} = 0.4$ rad/sec, $\ddot{\emptyset} = 0.05$ rad/sec^2), the resisting torque total is estimated at 61 N-m (45 ft-lbs) two-thirds of which is caused by fluid drag.

This value is certainly large enough to indicate that it should be considered during experimental data analysis, although the model should be customized for the subject in question. Analysis performed on test data estimated from videotape of tasks conducted during this experimentation ($\O = 0.52$ rad, $\dot{\O} = 0.17$ rad/sec, $\ddot{\O} = 0.02$ rad/sec^2, typically) estimated torque effects about the transverse axes at about 15.6 N-m (47% from fluid drag).

3.2 Case 2: Two-Point Restraint - Hand and Feet

The process involved in developing the KCL model for this restraint case is very similar to the previous one. The reaction path has changed from hand-to-hand to hand-to-feet, of course, but the methodology remains identical. Figure 3-4 shows the chain link system required, while 3-5 provides a breakdown of the linkages. It should be noted that reaction transference from the shoulder to the back is performed by a link one-half the length of L3 (chest width) used in Section 3.1.

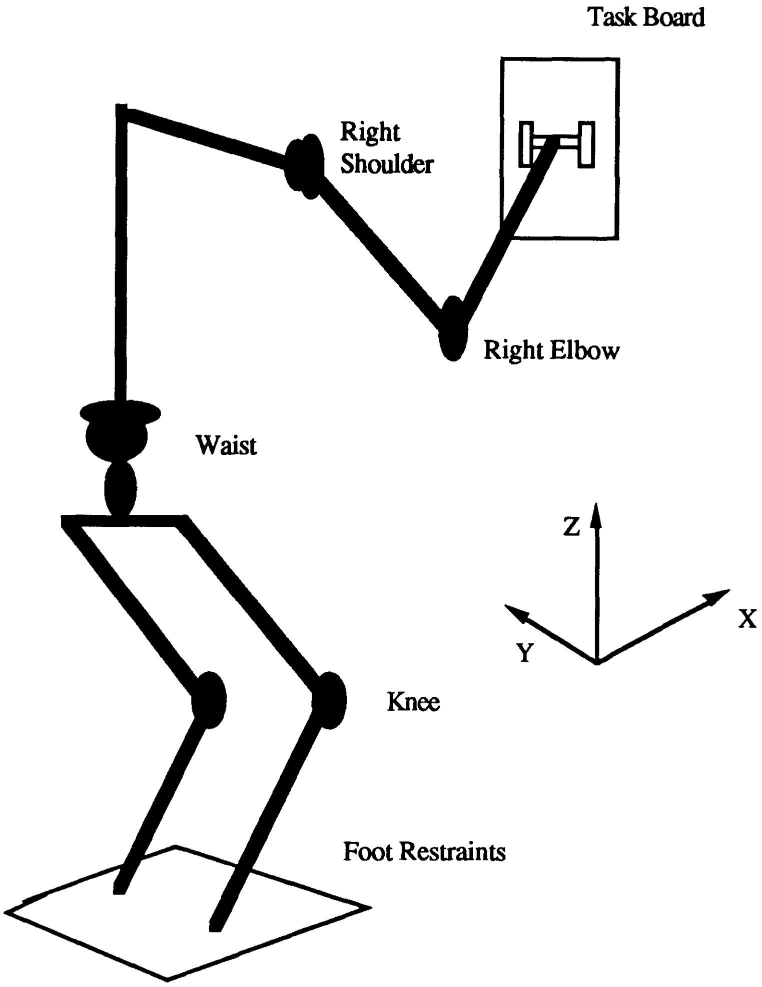

Figure 3-4: Chain Link for Case 2

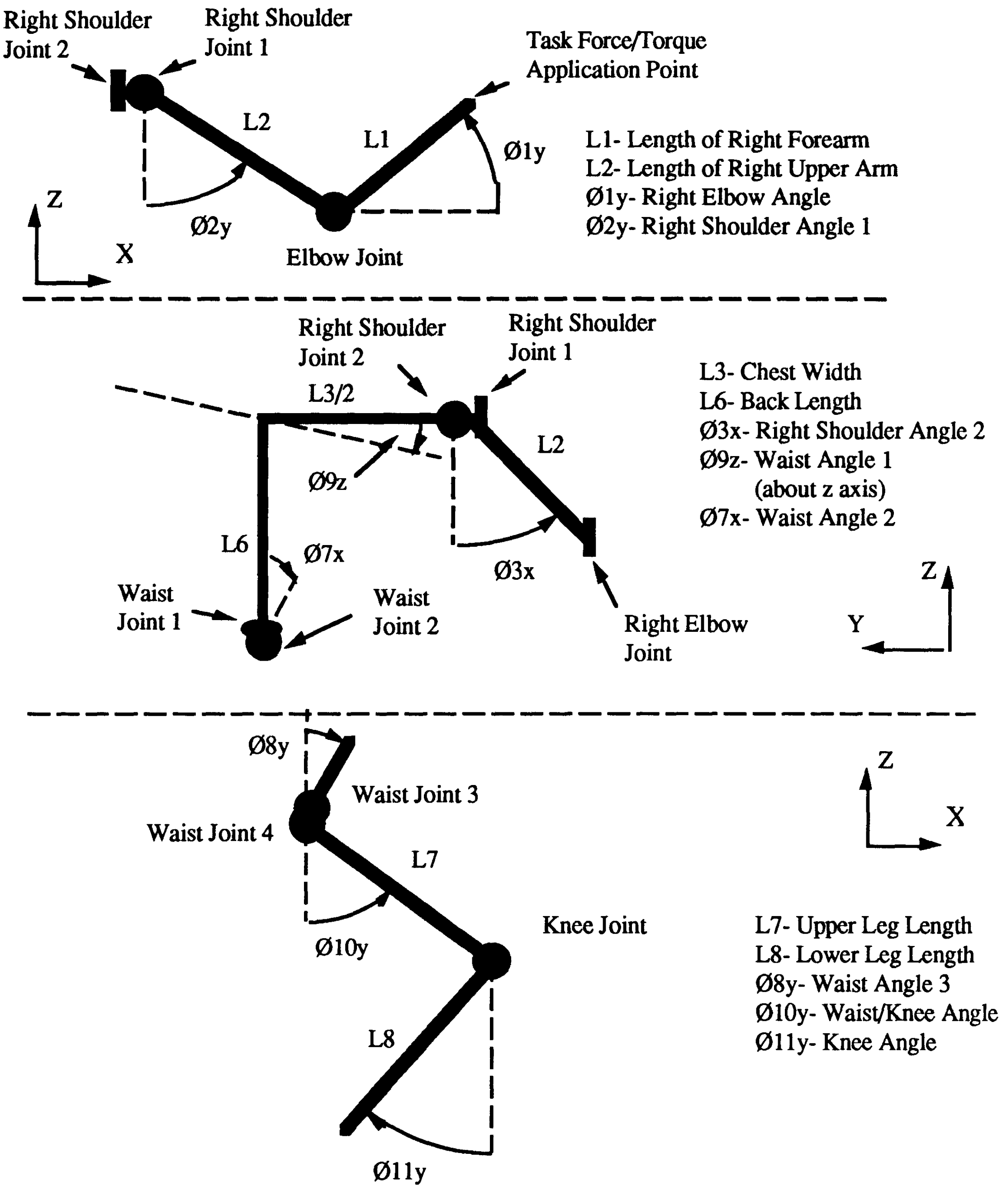

Figure 3-5: Breakdown of Chain Link for Case 2

Once again, the wrist and hand are ignored, and for this case, the ankles and feet are similarly omitted. The degree of freedom about the y-axis for the ankles was subsumed into the knee angle measurement; all other degrees of freedom are completely constrained by the foot restraints. A very important assumption made for this analysis was that since the feet are to be restrained beside each other, the legs could be modeled as a single unit. Thus, all leg movements apply to both legs working in tandem. Once again the equations of equilibrium are developed, Table 3-3 providing information on the analysis points, as the reactions are followed from the right hand, across to mid-chest, down the back, through the legs and finally, to the foot restraints.

ANALYSIS POINT	NUMBER	ANGLE
Right Elbow Joint	1	Ø1y
Right Shoulder Joint 1	2	Ø2y
Right Shoulder Joint 2	3	Ø3x
Mid-Chest	4	Ø9z
Waist Joint 1	5	Ø7x
Waist Joint 2	6	Ø8y
Knees	7	Ø10y
Restraint Point	8	Ø11y

Table 3-3: Analysis Points- Case 2

It can be readily seen that the analysis for Case 2 will be similar to Case 1. Force equilibrium determination once again results in the solution constraining translation at any analysis point, Equation (3.1-2).

$$\sum \mathrm{Fn}=0;\ F_{nk}= -F_{n0} \qquad (3.1\text{-}2)$$

Moment or torque equilibrium determination is identical for analysis points 1 through 3 (along the right arm), but the relevant equations are reproduced below.

$$M_{x1} = - M_{x0} + F_y\sin(\text{Ø}_{1y})L1 \qquad (3.2\text{-}1a)$$

$$M_{y1} = - M_{y0} - F_x\sin(\text{Ø}_{1y})L1 + F_z\cos(\text{Ø}_{1y})L1 \qquad (3.2\text{-}1b)$$

$$M_{z1} = - M_{z0} - F_y\cos(\text{Ø}_{1y})L1 \qquad (3.2\text{-}1c)$$

$$M_{x2} = M_{x1} + F_y\cos(\text{Ø}_{2y})L2 \qquad (3.2\text{-}2a)$$

$$M_{y2} = M_{y1} - F_x\cos(\text{Ø}_{2y})L2 - F_z\sin(\text{Ø}_{2y})L2 \qquad (3.2\text{-}2b)$$

$$M_{z2} = M_{z1} + F_y\sin(\text{Ø}_{2y})L2 \qquad (3.2\text{-}2c)$$

$$M_{x3} = M_{x2} + F_y\cos(\text{Ø}_{3x})L2 - F_z\sin(\text{Ø}_{3x})L2 \qquad (3.2\text{-}3a)$$

$$M_{y3} = M_{y2} - F_x\cos(\text{Ø}_{3x})L2 \tag{3.2-3b}$$
$$M_{z3} = M_{z2} + F_x\sin(\text{Ø}_{3x})L2 \tag{3.2-3c}$$

The following equations then progress from mid-chest to the foot restraints, once again the numerical subscript on the moments indicates the analysis point (see Table 3-3), while the letter denotes the axis about which the moment occurs.

$$M_{x4} = M_{x3} - F_z\cos(\text{Ø}_{9z})\frac{L3}{2} \tag{3.2-4a}$$
$$M_{y4} = M_{y3} - F_z\sin(\text{Ø}_{9z})\frac{L3}{2} \tag{3.2-4b}$$
$$M_{z4} = M_{z3} + F_x\cos(\text{Ø}_{9z})\frac{L3}{2} + F_y\sin(\text{Ø}_{9z})\frac{L3}{2} \tag{3.2-4c}$$

$$M_{x5} = M_{x4} - F_y\cos(\text{Ø}_{7x})L6 - F_z\sin(\text{Ø}_{7x})L6 \tag{3.2-5a}$$
$$M_{y5} = M_{y4} + F_x\cos(\text{Ø}_{7x})L6 \tag{3.2-5b}$$
$$M_{z5} = M_{z4} + F_x\sin(\text{Ø}_{7x})L6 \tag{3.2-5c}$$

$$M_{x6} = M_{x5} - F_y\cos(\text{Ø}_{8y})L6 \tag{3.2-6a}$$
$$M_{y6} = M_{y5} + F_x\cos(\text{Ø}_{8y})L6 - F_z\sin(\text{Ø}_{8y})L6 \tag{3.2-6b}$$
$$M_{z6} = M_{z5} + F_y\cos(\text{Ø}_{8y})L6 \tag{3.2-6c}$$

$$M_{x7} = M_{x6} - F_y\cos(\text{Ø}_{10y})L7 \tag{3.2-7a}$$
$$M_{y7} = M_{y6} + F_x\cos(\text{Ø}_{10y})L7 + F_z\sin(\text{Ø}_{10y})L7 \tag{3.2-7b}$$
$$M_{z7} = M_{z6} - F_y\sin(\text{Ø}_{10y})L7 \tag{3.2-7c}$$

$$M_{x8} = M_{x7} - F_y\cos(\text{Ø}_{11y})L8 \tag{3.2-8a}$$
$$M_{y8} = M_{y7} + F_x\cos(\text{Ø}_{11y})L8 - F_z\sin(\text{Ø}_{11y})L8 \tag{3.2-8b}$$
$$M_{z8} = M_{z7} + F_y\sin(\text{Ø}_{11y})L8 \tag{3.2-8c}$$

As before, the most significant equations are the final three, which denote the reaction moments produced at the foot restraints for this case. These equations are also implemented in *Kinematic Chain Link*, found in Appendix A. In fact, when using the spreadsheet, selecting values for the component input forces and torques produces the reaction values for both cases simultaneously. This feature will become important in the following section.

3.3 Case 3: Three-Point Restraint - Hands and Feet

The third restraint case involves the complete link system, all eight links and eleven joints. Here there is a subject restrained at the left hand and at foot restraints, and herein lies the ambiguity. What is not covered by the kinematic chain link model is the reaction path followed in Figure 3-6. Inputs at the right hand progress normally to the mid-chest and are then distributed somehow between the hand and foot restraint chains. It is the question of how these reactions are distributed that motivates much of this experimentation.

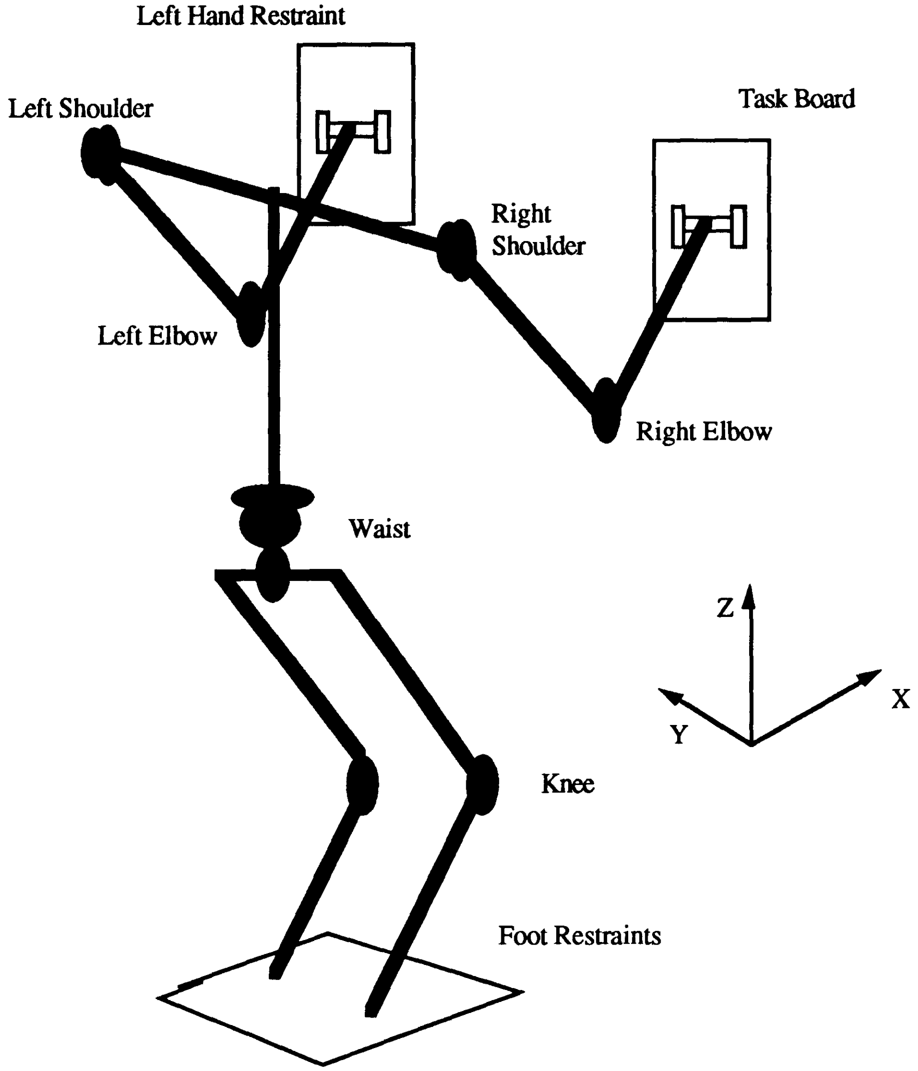

Figure 3-6: Chain Link for Case 3

The model that will be used for this case is a simple superposition of the previous two models, and all of the assumptions made in those models again hold true. If superposition is a valid modeling technique, then the reaction equations will be in essentially the same form as before, save for the multiplication of unknown factors. For example, the force and moment equilibrium equations at the left hand restraint for this case could be described as:

$$F_x = A(F_x)_{\text{case 1}} \tag{3.3-1a}$$
$$F_y = B(F_y)_{\text{case 1}} \tag{3.3-1b}$$
$$F_z = C(F_z)_{\text{case 1}} \tag{3.3-1c}$$

$$M_x = D(M_{x7})_{\text{case 1}} \tag{3.3-2a}$$
$$M_y = E(M_{y7})_{\text{case 1}} \tag{3.3-2b}$$
$$M_z = F(M_{z7})_{\text{case 1}} \tag{3.3-2c}$$

where A-F are the unknown factors. If those were removed Equations (3.2-1 through 6) would reduce to the reactions found for Case 1, represented by Equations (3.1-2) and (3.1-9a through c).

Similarly, the expected reactions at the foot restraints for the three-point restraint case are:

$$F_x = G(F_x)_{\text{case 2}} \tag{3.3-3a}$$
$$F_y = H(F_y)_{\text{case 2}} \tag{3.3-3b}$$
$$F_z = I(F_z)_{\text{case 2}} \tag{3.3-3c}$$

$$M_x = J(M_{x8})_{\text{case 2}} \tag{3.3-4a}$$
$$M_y = K(M_{y8})_{\text{case 2}} \tag{3.3-4b}$$
$$M_z = L(M_{z8})_{\text{case 2}} \tag{3.3-4c}$$

where G-L are the unknowns (the noted Case 2 reactions are found in Equations (3.1-2) and (3.2-8a through c)). These unknowns cannot be found mathematically. Therefore, experiments which can measure the reactions produced for the three point case and decompose them into their directional elements are the remaining method available. Using data from these experiments, the values of A-L can be found empirically, creating a KCL model for a situation not valid for normal KCL analysis, but often found in actual space operations. The remaining chapters describe these experiments and other experiments performed for different purposes, such as estimating energy expenditure.

Chapter 4: Experimental Objectives

The purpose of this experimentation was to apply the techniques discussed in the previous chapters to develop models, and to employ the force-torque sensing apparatus (described in the following chapter) in examining a number of related issues. Primarily, the KCL concepts could be used to empirically model a three-point restraint case. In addition, however, examination of force profiles achieved underwater could be used to assess energy expenditure for a given task. Finally, peak force data from the force-torque measurement system could be examined for correlations to any of several test parameters, as well as compared against peak performance in a 1-G environment.

4.1 KCL Related Models

The process of static modeling discussed in Chapters 2 and 3 provides a basis for much of this experimentation. However, as noted, the model fails in a major region of interest, the three-point restraint case. How reaction forces are distributed between two equally viable chain links cannot be determined within the model itself. But it is possible that the three-point case can be modeled as a simple superposition of the two two-point cases modeled in Chapter 3. Then the search is for what combination of reactions (the coefficients A-L) from the two-handrail and handrail-and-foot-restraint cases produces the reaction profile seen for the three-point case.

The justification behind this formulation is that reactions are produced instinctively by people for most tasks. The subject, once familiar with their environment, does not have to think about the forces and torques which must applied to maintain position and orientation, any more than an experienced commuter does while standing in a subway car . Therefore, different subjects performing the same task could apply reactions similarly if they have the same general training and familiarity with the task and environment.

To confirm the validity of this approach is a two step process. The KCL model in Chapter 3 calculates reactions for a given input force or torque (the input required to complete a task). If a task were to be performed in neutral buoyancy and its measured force-torque profile fed into the model, the resultant reaction profile should match the reaction profile actually measured at the restraint, for the two-point cases.

Once the validity of KCL is confirmed for the two-point cases, a model can be constructed by superposition for the three-point case. Underwater testing for this case provides empirical values for the model: values which describe what aspects of the two two-point case reactions are present, and to what magnitude (the coefficients A-L described in Section 3.3).

As an example, a task involving direct application of force away from the subject is performed. If the subject has their legs free, but is restrained by holding on to a handrail, KCL predicts an equal but opposite force produced at the restraint as well as positive torques about the axes orthogonal to the direction of force application. Assuming that the subject is in foot restraints but no longer grasping the supporting handrail, KCL again predicts an equal but opposing force at the restraint, but the predicted torques, while about the same axes, vary in direction and magnitude. Testing should confirm these reaction profiles, and, when the subject is using both the handrail and the foot restraints, should reveal that some combination of the two previous reaction profiles is produced between the two restraints. The proportion by which the opposing force is divided between the two restraints, and how the torques are expressed at each restraint, is the essence of this search.

4.2 Energy Expenditure

Workload is a term used to refer to several things, but is commonly viewed as the mental or physical cost of performing some task. Workload in space operations usually indicates mental workload, as subjects are not commonly operating near the edges of their strength and endurance envelopes. However, as large-scale operations become more the norm, as exemplified by the proposed expansion of Mir and the advent of the Space Station, the physical assessment of workload will become more vital. Accurately predicting the physical cost of a task will be a driving force in scheduling, workstation design, task design, and a number of other important areas.

The commonly accepted methods of assessing task workload cost include oxygen consumption and heart rate. An exception is Brouha, who, as mentioned in Section 1.2, used a limited reaction sensing platform to correlate reaction forces to oxygen consumption, and used force-time areas to estimate workload [Brouha, 1960]. The sensors used in the current experimentation provide a much more complete picture of the reaction forces expended, as Brouha only determined the applied forces while ignoring torques. The force-torque cost of a task is the sum of the absolute values of the reactions and the task inputs, if one ignores the compliance of the subject and suit, if any. Integrating this profile over the task duration produces a force-time area, which can be used as an estimate of energy expenditure. Brouha concentrated on correlating the peak forces in the profile to energy expenditure rather than force-time areas, while this experimentation allows for either.

4.3 Peak Forces

4.3.1 1-G versus 0-G

The peak forces measured can provide insight into the differences between operating in normal gravity and zero gravity situations. Previous experiments have revealed that subjects in neutrally buoyant conditions can only achieve peak forces far below their land capabilities. This has been measured as a factor of anywhere between 0.1 - 0.4. The tasks being performed for these experiments provide a somewhat more "real world" simulation of force applications, and the peak forces can be noted and compared against the 1-G case to pin down the reduction factor, at least for these cases.

4.3.2 Parameter Correlation

Finally, the peak force data can be sifted for another reason, in an effort to see if there is some overall correlation to the peak forces achieved by individual test subjects. Among the parameters one might expect to have an effect on this performance include: subject mass, height, arm and leg lengths, experience in neutral buoyancy, and strength. Many of these would seem to have obvious correlation to peak forces achieved, but this data taking process provides an opportunity to statistically confirm some of these correlations.

Specifically subject height and mass were selected as parameters which would be examined for correlations to the peak forces achieved.

Chapter 5: Experimental Apparatus

As discussed in the previous chapters, a test set-up capable of measuring reaction forces and torques was required to correlate neutral buoyancy tasks with existing mathematical models, and to develop new models. To this end, a test station was designed, built, and used for experimentation at the MIT Alumni Pool. Figure 5-1 depicts the underwater elements of the station, with major dimensions included, while Figure 5-2 presents a block diagram of the major components of the test set-up. Each of these elements will be discussed as individual topics in the subsections.

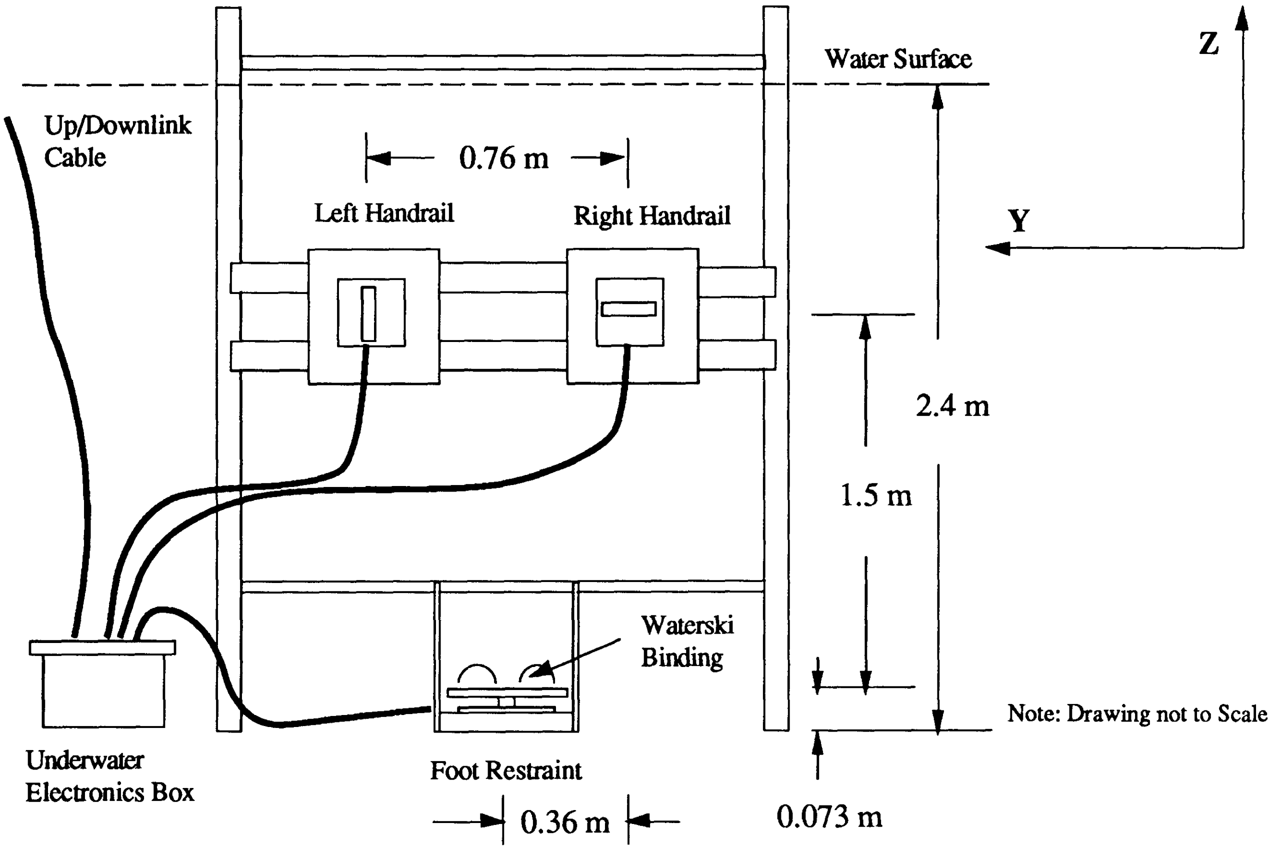

Figure 5-1a: Test Set-Up (Forward View)

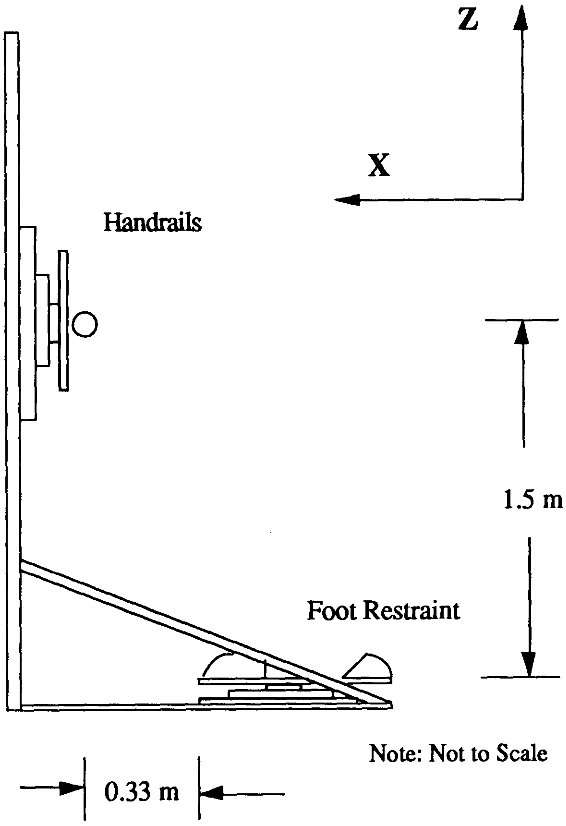

Figure 5-1b: Test Set-Up (Side View)

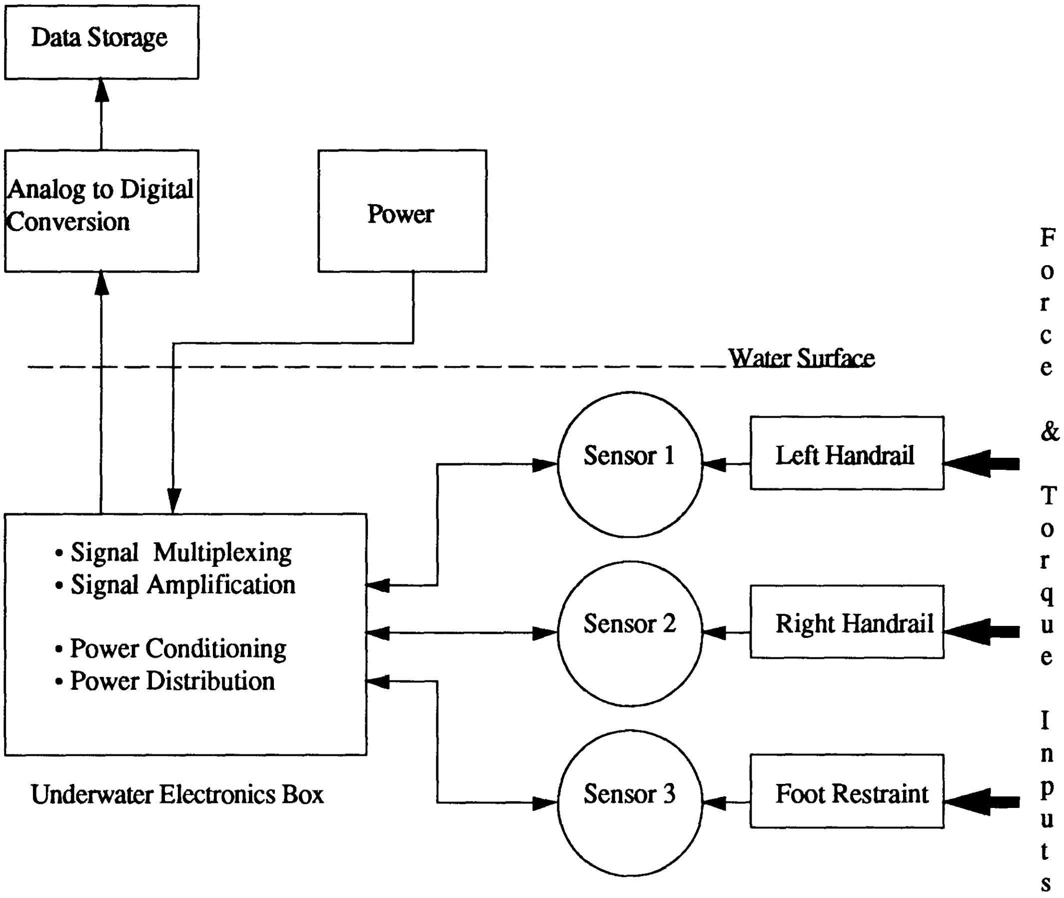

Figure 5-2: Test Set-Up Block Diagram

5.1 Force-Torque Sensors

5.1.1 Sensor Design

The strain gage transducers were designed with the ability to uniquely measure all six directions of forces and torques. The basis for the design is a "Maltese Cross" format with four main flexures which are gaged for measurement in bending, as seen in Figure 5-3, with both side and top views.

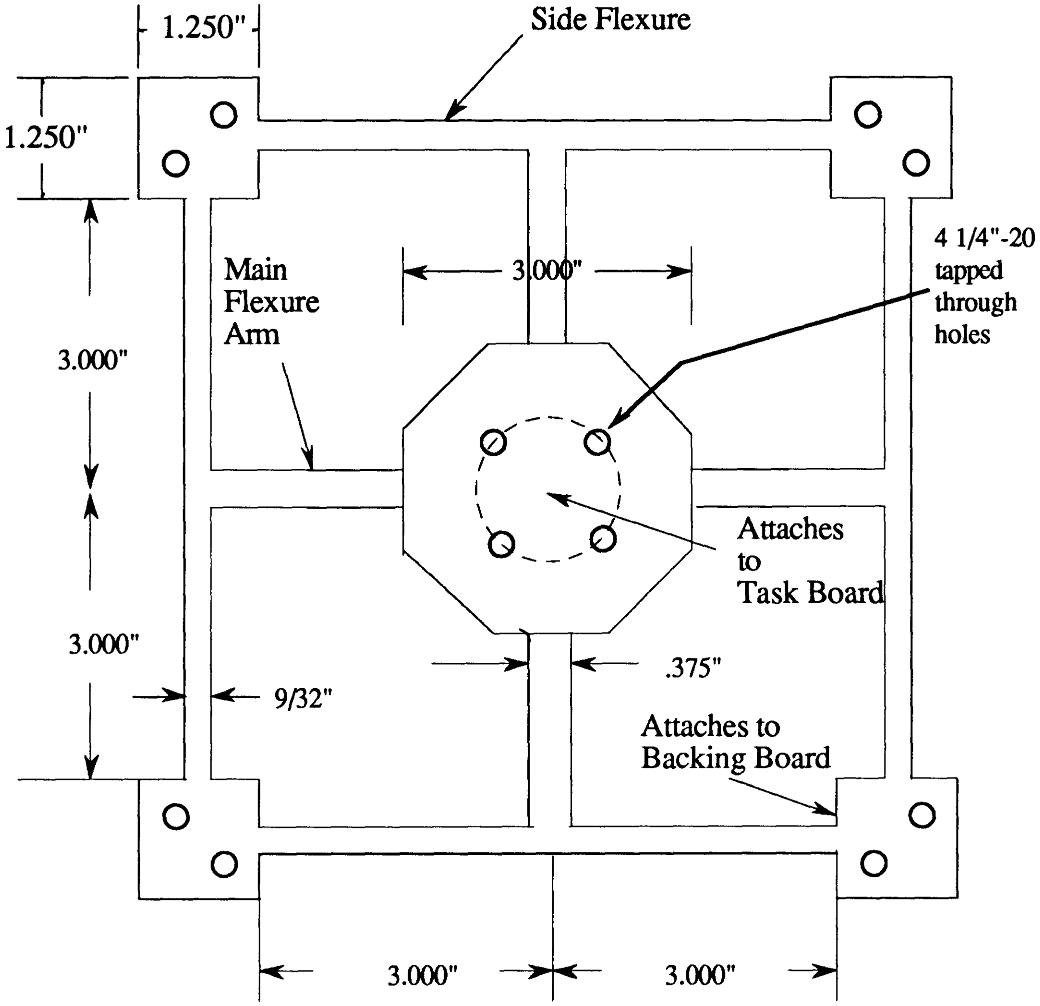

Figure 5-3a: Sensor Element (Top View)

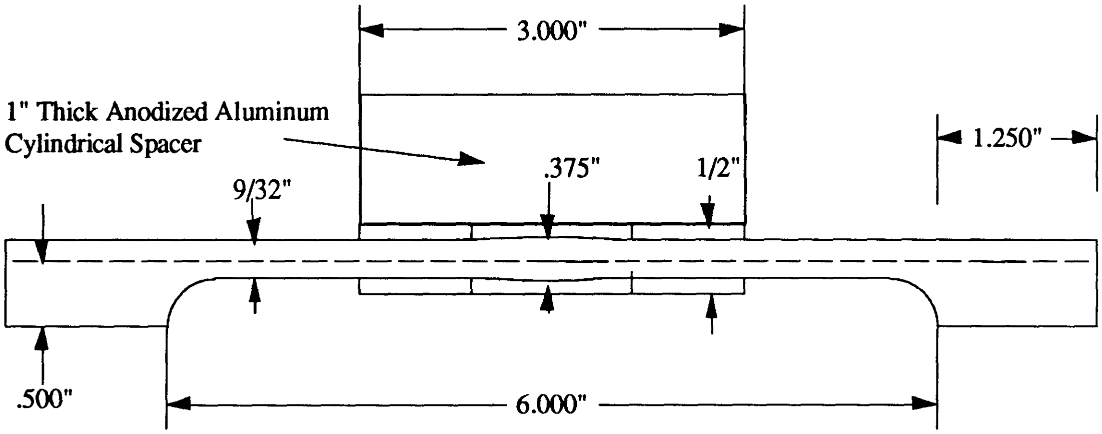

Figure 5-3b: Sensor Element (Side View)

The four square-cross-section main flexures meet at the 3" diameter load application area, which mates with the individual task boards. The side flexures were designed to reduce the loss of forces into axial compression or tension of the main flexures, for reactions producing bending in the plane of the sensor. The side flexures meet at attachment points for the backing boards; these boards in turn provide hardpoints for attachment to the static test rig.

The major tradeoff on sensor design was a choice between the device sensitivity and the yield strength. Secondary considerations were material availability, machinability, and cost. For these reasons, the sensors were fashioned from 7075-T6 Aluminum alloy. Al 7075 has a modulus of elasticity, E, of 7.31×10^{10} Pa (10.6×10^{6} psi), and a yield strength of 4.83×10^{8} Pa (70×10^{3} psi). By varying several parameters, namely flexure length and cross-section as well as side flexure length and cross section, an optimal design was achieved. The actual design process is detailed in Appendix C: Sensor Design, but some important values have been collected in Table 5-1.

Main Flexure Thickness:	0.375	inches	0.953	cm
Main Flexure Length:	2.00	inches	5.08	cm
Side Flexure Thickness:	0.281	inches	0.714	cm
Side Flexure Length:	6.00	inches	15.24	cm
Design Force Accuracy:	± 0.500	pounds	± 2.224	N
Design Torque Accuracy:	± 0.127	foot-pounds	± 0.172	N-m
Minimum Yield Force:	538	pounds	2393	N
Minimum Yield Torque:	86	foot-pounds	116	N-m
Force Measurement Range:	± 152	pounds	± 676	N
Torque Measurement Range:	± 86.5	foot-pounds	± 117	N-m

Table 5-1: Sensor Design Values

The design accuracy was determined assuming that the smallest measurable strain value would be 10 µstrain; the final accuracies are, of course, further degraded through such vehicles as signal loss, signal noise, compliance, and the addition of gages and their coating on the flexures. The actual operational force accuracy is ± 3.72 N and the operational torque accuracy is ± 0.99 N-m for out-of-plane forces and torques. The sensor, due to the design, is twice as sensitive to the in-plane forces and torques. The determination of the sensor measurement error (the accuracy), is discussed in Appendix E: Error Analysis.

As seen in Figure 5-4, each main flexure was instrumented with 8 strain gages, comprising two full Wheatstone bridges, one on the two sides and one on the top and bottom of the flexures. Figure 5-5 delineates the Wheatstone Bridge configuration used. Note that tensile forces produce positive strain, compressive forces negative strain.

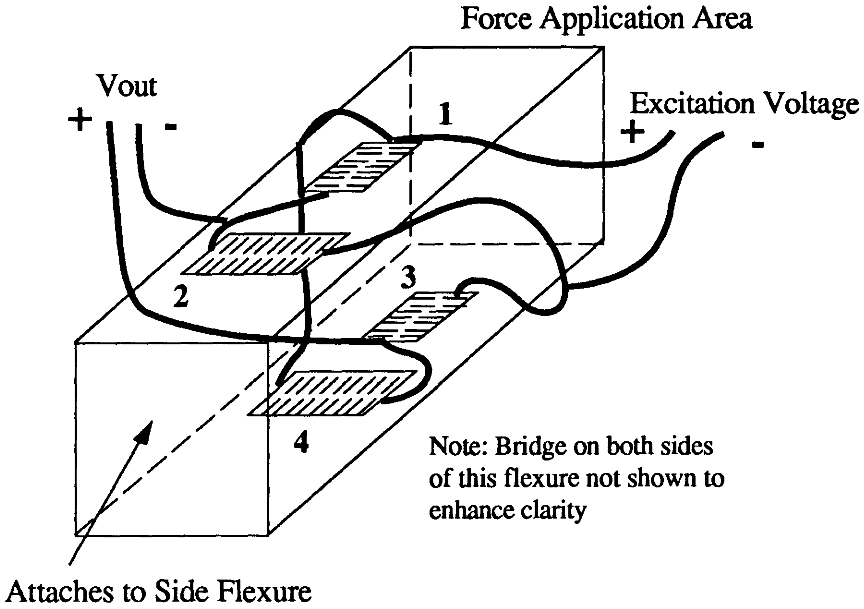

Note: Bridge on both sides of this flexure not shown to enhance clarity

Figure 5-4: Gaged Main Flexure

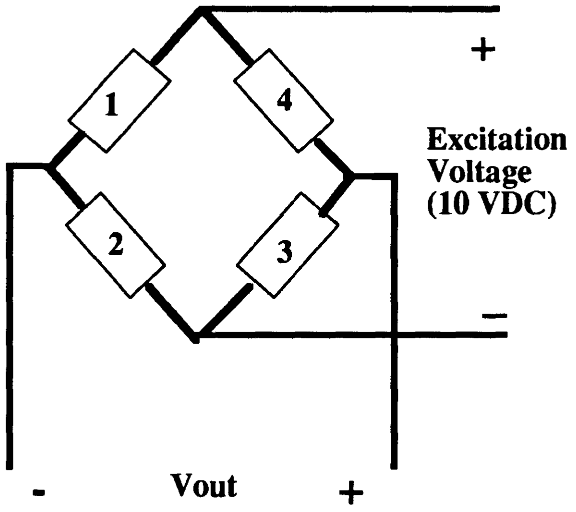

Figure 5-5: Wheatstone Bridge Configuration

Equation (5.1-1) gives the total strain value produced by each bridge.

$$\text{Total Strain, } \varepsilon\ (\mu\text{strain}) = \varepsilon 1 - \varepsilon 2 + \varepsilon 3 - \varepsilon 4 \qquad (5.1\text{-}1)$$

The four-element bridges each have only two gages in the bending direction, the other two gages being placed perpendicularly. These gages are placed to provide temperature compensation between the opposing faces of the main flexures, so their strain values sum to zero. Thus, it can be seen that for any bending force, each bridge will display a strain value of twice the magnitude of the induced strain (the sum of bridges 1 and 3, the bending bridges).

The gages themselves are EA-13-125AC-350 gages with a gage resistance of 350.0 ± 15% ohms, and a gage factor of 2.135 ± 0.5%. Each bridge was balanced to within ± 50 μstrain per inch, and a bridge resistance of 350 ± 2 ohms. The gages were bonded with M-Bond 610 and were coated with 1204 Primer/H-Coat for protection against the water. Before the gages were installed the aluminum sensor was clear-coat anodized to prevent corrosion.

Each sensor thus contains 8 complete bridges, which connect to the Underwater Electronics Box, or UEB (discussed in 5.3), via 8 feet of 28 gage wire in shielded cables, and through 25-pin underwater Amphenol connectors. These wires carry the +10 VDC bridge excitation to the sensors, as well as the resulting strain-caused voltage signals to the UEB. The bridges are numbered sequentially, with odd numbers denoting the top and bottom face bridges; even numbers denote the side face bridges. Numbering starts with the lowest main flexure for the handrails, and the flexure in front of the subject's feet for the foot restraints, and proceeds counter-clockwise. Figure 5-6 displays this numbering scheme; for more details concerning the coordinate system see Section 6.2.

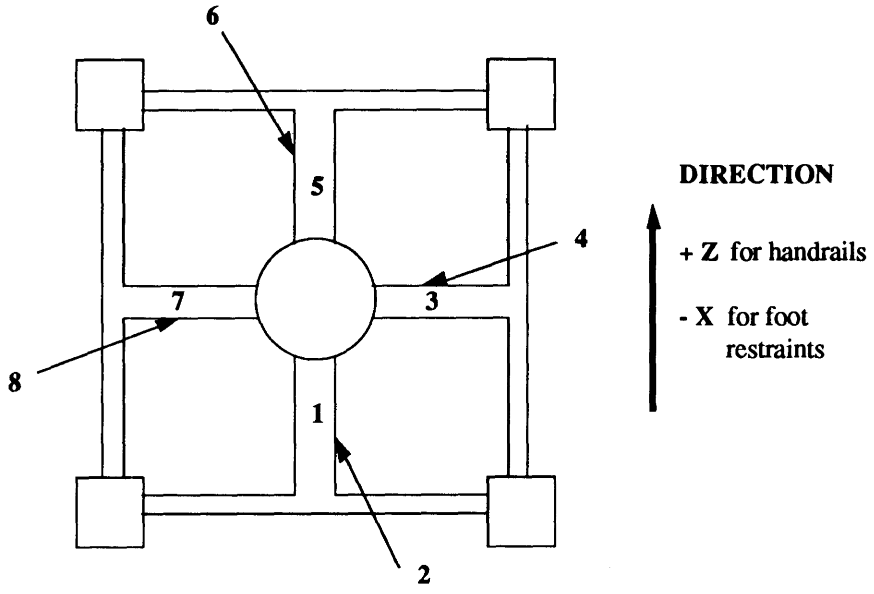

- Odd numbered bridges on top and bottom faces of main flexure
- Even numbered bridges on side faces of main flexure

Figure 5-6: Sensor Bridge Numbering Scheme

5.1.2 Force-Torque Value Determination

The six unique forces and torques (± Fx, ± Fy, ±Fz, ±Tx, ±Ty, ±Tz) are determined by various responses of the bridges. It is important to note that the coordinate system was defined such that for the left and right handrail sensors, X is the out of plane direction, while for the foot restraints Z is the out of plane direction (as mentioned above Section 6.2 discusses the coordinate system in some detail). Figure 5-7 illustrates through exaggeration (obviously, the actual deflections are miniscule) how the flexures bend for each of the forces or torques; the coordinate system used is for the foot restraint sensor.

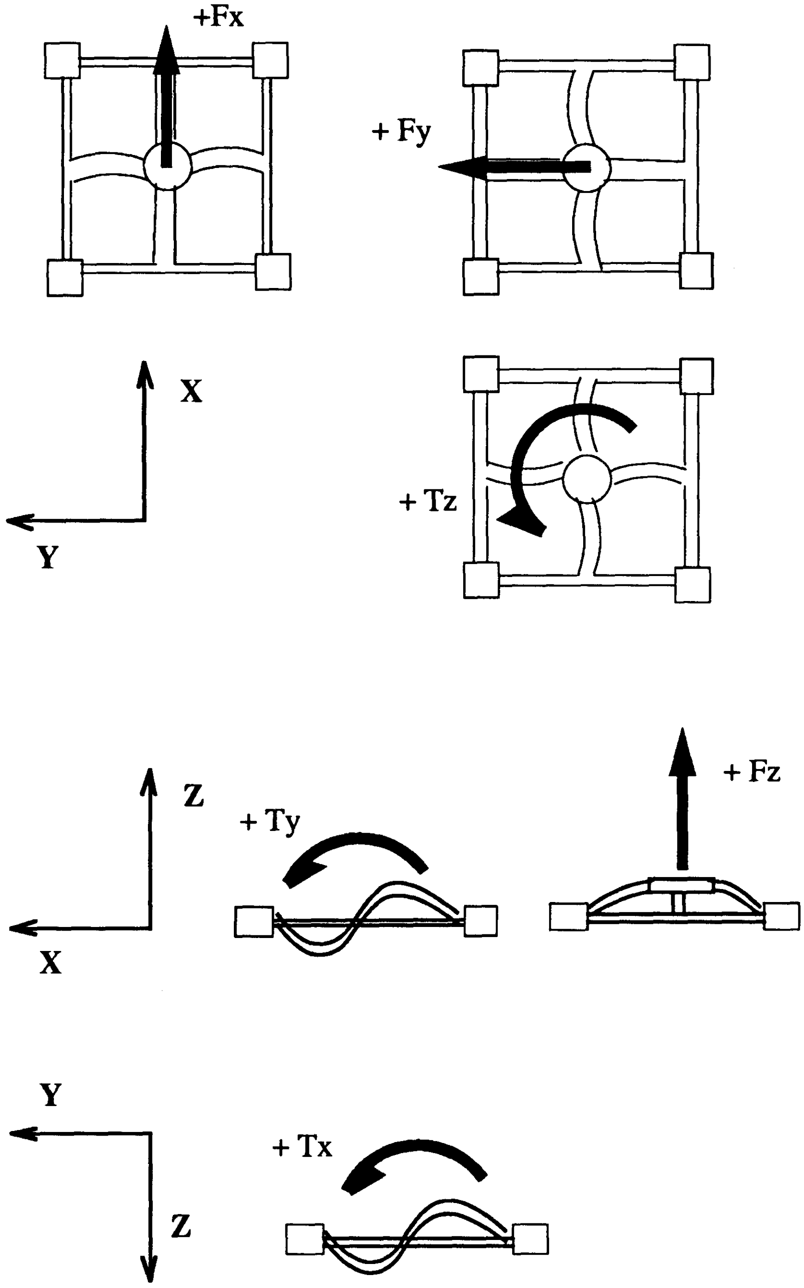

Figure 5-7: Sensor Bending Modes

As shown in the figure, for Fx and Fy, two flexures are in bending, while the other two flexures are not loaded due to the presence of side flexures. Fz and Tz bend all four flexures. Tx and Ty bend two flexures while placing the other two flexures (along the torque axis) in torsion.

The values returned by the complete data acquisition system are the 24 digitized bridge voltage signals within a value range from -4.095 VDC to +4.095 VDC. With 12-bit conversion (see Section 5.4), the smallest distinguishable increment is 1 millivolt. This voltage range effects the measurement range limit on the sensor. This limit is ± 676 N in force, and ± 181 Nm in torque, setting the force range, while the torque range is limited by the yield case to ± 117 N-m. These bridge voltages are then examined to determine the types of reaction forces and torques present.

The method for this conversion requires both the sensor model developed in Appendix C as well as empirical calibration results. For a square cross-section beam in bending the strain produced on a face of the beam is defined by:

$$\text{strain} = \frac{6\,M}{E\,h^3} \qquad (5.1\text{-}2)$$

where h is the beam thickness, E the Modulus of Elasticity, and M the moment at the point of measurement. The moment is a function of the applied reactions as well as the beam length and edge conditions. It is known from Equation (5.1-1) that each bridge measures twice the actual strain present, so Equation (5.1-2) becomes:

$$\text{strain}_{\text{measured}} = \frac{12\,M}{E\,h^3} \qquad (5.1\text{-}3)$$

It has already been mentioned that the actual strain value is not available, rather a voltage value is recorded. The voltage value is proportional to the measured strain, so substituting the measured voltage, V, and a constant of proportionality, c, into Equation (5.1-3) and solving for the moment results in Equation (5.1-4).

$$M = \frac{E\,h^3\,c\,V}{12} \qquad (5.1\text{-}4)$$

There now remains a two step procedure, first to determine the relationship between the moments measured by the eight strain gage bridges and the applied reactions, second, to determine the value of c in the previous equation. The process of modeling the sensor has already been performed for the sensor design in Appendix C. It is from this information that the equations which will convert the eight moments to combinations of the six forces and torques can be determined. Figure 5-7 delineates how the flexures respond to the applied reactions; for a given reaction anywhere from 2 to 4 main flexures are in bending, and in two cases two flexures are also in torsion. Torsion of a square cross-section beam produces the following strain value [Young, 1989]:

$$\text{strain}_{\text{torsional}} = .601 \frac{T}{E\,(.5\ h)^3} \qquad (5.1\text{-}5)$$

where T is the torque applied to a single main flexure. Substituting cV for strain in the above equation provides a direct relationship between the torque (which is 1/4 of the torque applied to the sensor) and the measured voltage, for the torsion case. As will be mentioned again below, the torsional strain is of low enough magnitude as to be considered negligible.

The beams in bending require formulation of the moment equations as was done in Appendix C, with the analysis point being the strain gage application point halfway on any main flexure. Examples of these equations follow:

For an applied in-plane force, F:

$$M = F\left(\frac{x}{2} - \frac{L_1}{8}\right) \qquad (5.1\text{-}6)$$

Out-of-plane force, F:

$$M = \frac{F}{2}\left(\frac{x}{2} - \frac{L_1}{8}\right) \qquad (5.1\text{-}7)$$

In-plane torque, T:

$$M = -\frac{3Tx}{2L_1} + \frac{T}{4} \qquad (5.1\text{-}8)$$

Out-of-plane torque, T:

$$M = \frac{T}{4}\left(-\frac{3x}{L_1} + \frac{1}{2}\right) \qquad (5.1\text{-}9)$$

where x is the measurement point (L/2), and L1 is the length of the force application area and two main flexures (2L + 0.0762 m). Each main flexure is length L, where L equals 0.0508 m.

Once the moment equations are composed for the various applied torques and forces shown in Figure 5-8, they can be substituted into Equation (5.1-4) as the right side. This can then be rearranged to provide the applied forces as a function of the voltage measurements, and the calibration constant, c.

The value of the constant, c, relating measured voltage to strain, was determined by direct calibration. A sensor was loaded with weights of known value, and the voltage responses recorded. This was equivalent to the axial force case as seen in Figure 5-7. It was found that the response was linear over the range of loading (5-55 N), with a value of 0.027 volts per 4.448 N (1 lbf). This can be seen in Figure 5-8, which shows the relationship between applied force and voltage change.

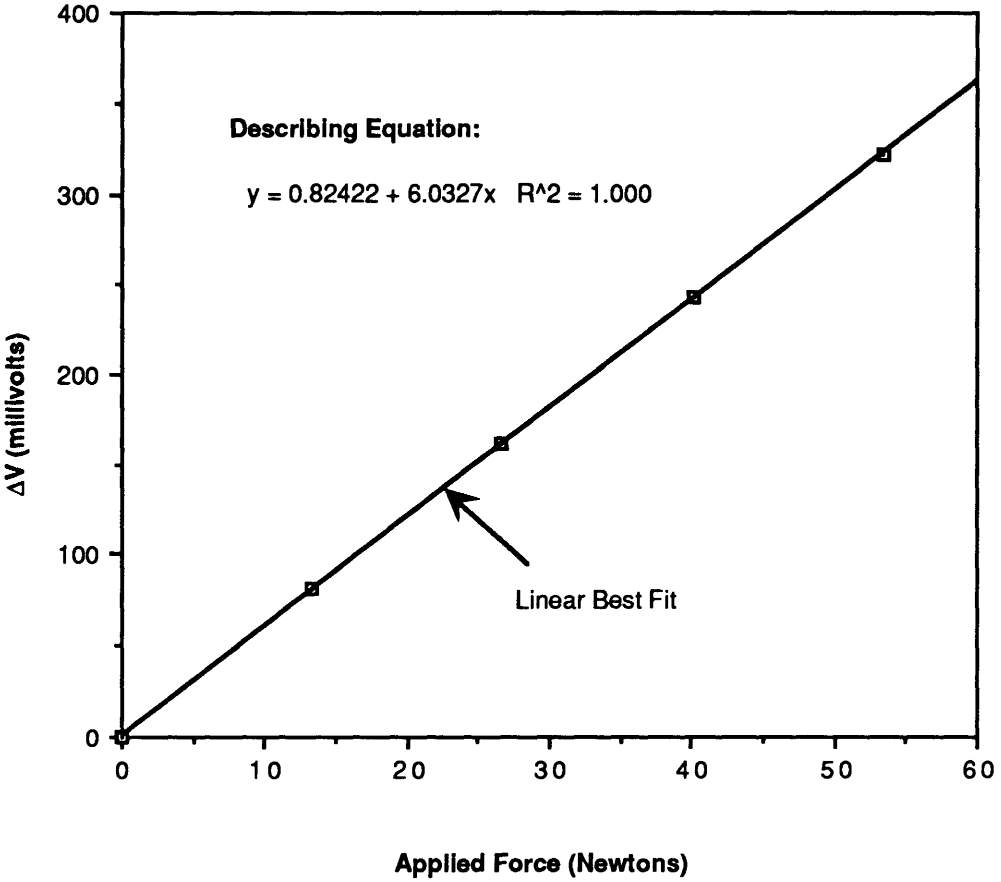

Figure 5-8: Calibration- Applied Force versus Voltage Change

The relationship between applied axial force and strain at the point of measurement, assuming all end conditions are fixed, is:

$$\text{Strain} = \frac{6\,F\,(x/2 - L_1/8)}{E\,h^3} \qquad (5.1\text{-}10)$$

where F is the force applied to the sensor (each perpendicular set of two flexures sees 1/2 the total force), x the position of the strain gages (at the center of each flexure, 0.0254 m), and L1 is the length of a beam composed of two flexures and the force application area (0.1778 m). Equation (5.1-10) was determined by substituting Equation (5.1-7) into (5.1-4). Further substituting cV for the strain, and setting the value of V equal to 0.027 volts and F equal to 4.448 N, c is found to be 0.00015259 strain per volt.

Once both c and the various moment relationships have been found, the equations describing the conversion between voltages and reactions can be composed. Note that these equations assume all end conditions as fixed from the model analysis performed in Appendix C, as this correlated with the calibration data. Employing Equation (5.1-4), (5.1-5), and Equations (5.1-6) through (5.1-9), and substituting in for the known constants c, E, h, L1, and x, the conversion equations are as follows:

Applied in-plane force:

$$F = -\ 82.3707\ V \qquad (5.1\text{-}11)$$

Out-of-plane force:

$$F = -\ 164.7414\ V \qquad (5.1\text{-}12)$$

In-plane torque:

$$T = 21.9683\ V \qquad (5.1\text{-}13)$$

Out-of-plane torque:

$$T = 43.9366\ V \qquad (5.1\text{-}14)$$

where V is the calibrated voltage, in volts, of a single bridge in bending. The data made available from *puff.c* must be calibrated prior to use in Equations (5.1-11 through 14), however. This is done using the following equation:

$$V = Vstrained - Vunstrained \qquad (5.1\text{-}15)$$

where Vunstrained is a bridge reading taken prior to performing a given task (obtained via the calibration reading described in Section 6.3), and Vstrained is the voltage reading during a given task [Omega, 1988]. It should be noted that *puff.c* provides voltage values in millivolts and these must be converted to volts before using them to determine the reactions.

The actual process of data conversion from voltage readings to reactions requires a step prior to implementing the equations and after calibrating the voltages. This step involves confirmation that the bridges which should be reading for a given force are in fact reading (i.e. only the bridges on the bending faces should be registering voltage values). Combining this confirmation with the actual conversion equations (5.1-11 through 14) leads to a conversion matrix, **A**. For sequentially numbered bridges, Equation 5.1-16 reveals this 6x8 matrix, which converts the 8x1 matrix of bridge voltages, **V**, to the 6x1 matrix of reactions, **R** (bridges recording a low-level response due to torsion are denoted by an asterisk). Note that Fx and Tx are the out of plane force and torque for this case, which is true for the two handrails. Fz and Tz are the out of plane reactions for the foot restraint sensor, and the conversion matrix must be adjusted accordingly.

Equation (5.1-16):

$$\mathbf{R} = \begin{bmatrix} Fx \\ Fy \\ Fz \\ Tx \\ Ty \\ Tz \end{bmatrix} = \begin{bmatrix} -41.19 & 0 & -41.19 & 0 & -41.19 & 0 & -41.19 & 0 \\ 0 & -41.19 & 0 & 0 & 0 & -41.19 & 0 & 0 \\ 0 & 0 & 0 & -41.19 & 0 & 0 & 0 & -41.19 \\ 0 & +10.98 & 0 & +10.98 & 0 & +10.98 & 0 & +10.98 \\ +10.98 & 0 & * & * & +10.98 & 0 & * & * \\ * & * & +10.98 & 0 & * & * & +10.98 & 0 \end{bmatrix} \begin{bmatrix} V1 \\ V2 \\ V3 \\ V4 \\ V5 \\ V6 \\ V7 \\ V8 \end{bmatrix} = \mathbf{A}\mathbf{V}$$

A quick study of the elements of the conversion matrix, **A**, shows that the conversion values found in Equations (5.1-11 through 14) have been changed to account for the additions taking place as a result of the matrix multiplication.

This two part conversion process is conducted by the Think C™ v4.0 program *smaug.c*, which takes the output of the program *puff.c* described in Section 5.4 and converts the voltage values to the appropriate forces and torques. *Smaug.c* is available in Appendix A along with *puff.c*.

5.2 Task Boards

The three task boards serve several purposes: they provide restraint for the test subjects, they provide a site to perform the tasks as well as to apply the reaction forces and torques, and they provide an interface to, and protection for, the sensors behind them. In this experimental set-up the task boards are used for the left and right handrails, and the foot restraints. All three are fashioned from anodized 6061 or 2024 aluminum.

The handrails are identical save that the left handle is placed vertically, while the right handrail is placed horizontally. Both handles are 0.0349 m (1.375") in diameter and attach to backing plates, which attach in turn to the force-torque sensors.

The foot restraint attaches similarly to its sensor, although it is placed perpendicularly to the plane of the other two task board sensors . The SCUBA test subjects are restrained with a pair of waterski-type rubber bindings. Unfortunately there was a great deal of compliance in the boots; however the ease of subject access and egress was considered an important safety factor.

5.3 Underwater Electronics Box

The underwater electronics box contains both power and analog signal conditioning electronics, in a watertight, anodized aluminum box. The box is sealed by an O-ring resting in a groove between the box lip and lid. Also sealed by O-rings are the four Amphenol connectors on the lid (1 out to each sensor, 1 uplink/downlink to the surface).

The electronics are contained on three boards: one for each sensor, dedicated to signal conditioning; and one for power conversion and supply (see Section 5.5). These electronics are needed for two reasons: the A-to-D board available can only handle 16 of the 24 signal lines (see Section 5.4), so another level of multiplexing is needed; and it is necessary to amplify the extremely low-voltage strain gage signals before transmitting them up the 40 foot uplink/downlink cable. To accomplish both tasks Analog Devices 2B34J RTD/Strain Gage Conditioners were used. In strain gage mode, each can accept 4 gage inputs and has two digital address select lines to multiplex between them (ADR0 and ADR1). The strain gage signals are also amplified 166.67 times by the 2B34J. As each can handle 4 strain gage bridges, two are required for each sensor and placed on a single board together. Figure 5-9 diagrams the electronics needed by the entire data acquisition system; those in the UEB are within the dashed box. To allow a degree of clarity, the electronics necessary for half of a single sensor's bridges are depicted. The figure does indicate the number of components required by the full three sensor set-up. Appendix B contains electronics specifications for the components used in the set-up.

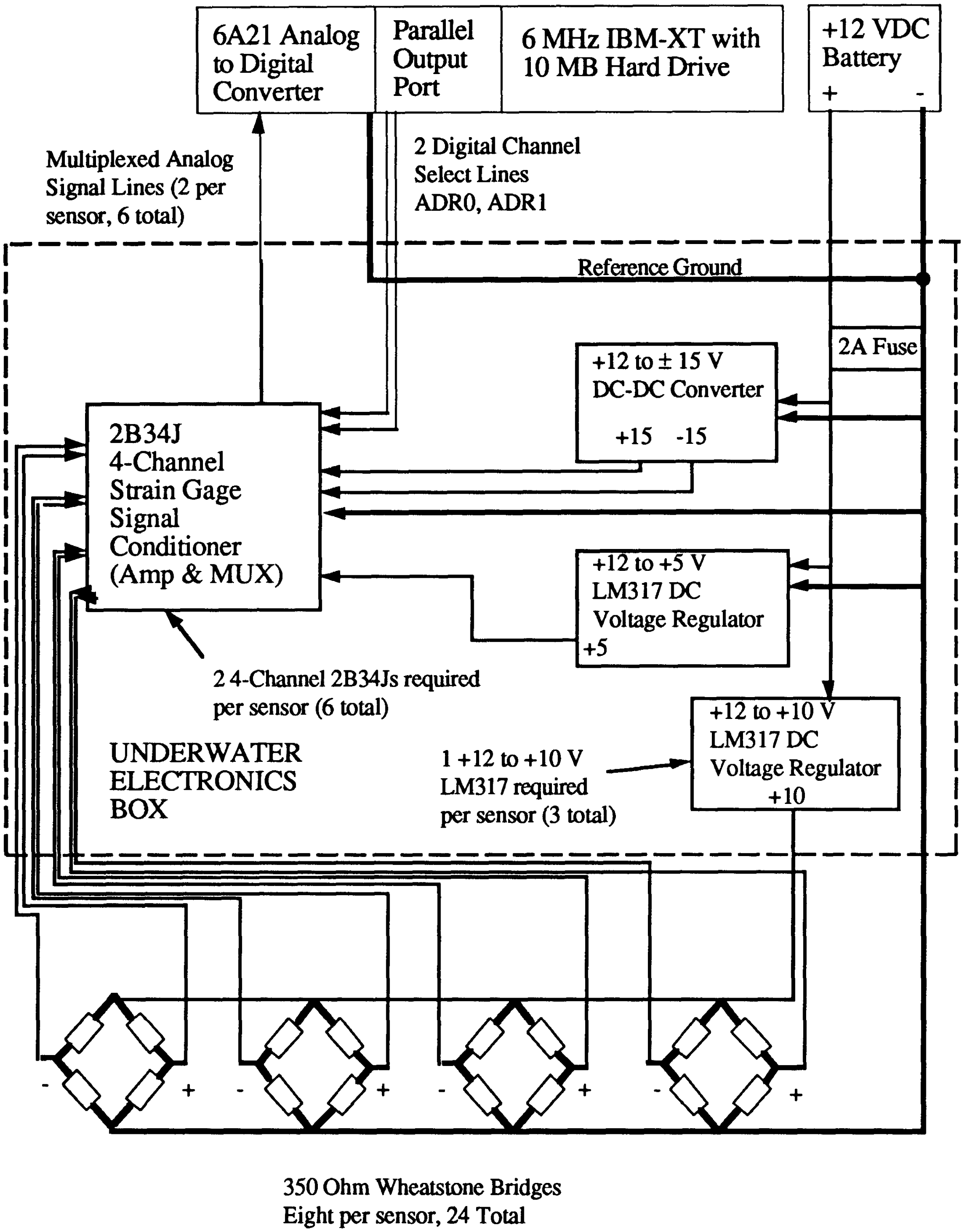

Figure 5-9: Electronics Block Diagram

5.4 Data Conversion

From the Underwater Electronics Box, an uplink cable carries the six multiplexed analog signals to the surface. This 40-foot shielded cable is separate from the power cable, but the 2B34J channel select lines, ADR0 and ADR1 are also contained in it. Each of these lines is 18-gage stranded copper wire. These analog signals are then fed, via a ribbon cable, to a Analog-to-Digital Conversion Board installed in an IBM PC-XT. The PC-XT is a 6 MHz machine with a 10 Megabyte hard drive used for data storage.

The A-to-D Board is a 6A21 Analog Input Card manufactured by the Industrial Computer Source. It is a 12-bit, bipolar, all CMOS card, with an output range of ± 4.095 VDC. It can accept up to 16 single-ended inputs and thus has the onboard multiplexing capability to deal with the six inputs. It also has a 6-bit output port onboard, allowing the 2B34J address select lines to be written to via the card. The maximum conversion rate possible with this card is 15 conversions per second, which is far slower than might have been hoped, as each 24 data point set (8 bridges on 3 sensors) is taken at a rate of 0.625 Hz. Full specifications are available in the 6A21 Reference Manual [ICS,1988].

The following list of tasks is completed by the Microsoft C™ program *puff.c* running on the IBM-XT:

1) Writing address selects to the 2B34J modules (ADR0, ADR1) via the I/O port
2) Channel selecting for the A-to-D board multiplexer (Channels 1-6)
3) Performing the A-to-D conversion
4) Writing the data to the hard drive
5) Detecting file overwrite errors and overrun errors

After receiving a destination data file name the software starts data recording on the striking of the enter key, and converts while looping through the channel and module select loops until halted by the press of the escape key. The various delays set the final data acquisition frequency at virtually 0.5 Hz. The data is stored in text files which are CricketGraph™, Kaliedograph™ and Excel™ readable. The fully commented code used is available in Appendix A: Software.

The A-to-D card also has the ability to amplify inputs by 10 or 100 times, but the gain on board the 2B34J modules was found to be sufficient.

5.5 Power System

Power for the majority of system operation was provided by a rechargeable, unregulated 12 volt battery with a 20 ampere-hour capability. The exceptions are the A-to-D Conversion Board and the computer itself, which operated from a normal 120 VAC wall source with ground fault interrupts. The +12v signal is provided by the battery at approximately +12.6 volts due to the 0.6 volt drop across the 16 gage downlink cable to the electronics box. The operational current draw is 1 ampere, and the system has a 2 ampere fuse for component protection. The +12v signal arrives at the electronics box and is regulated and conditioned on the power board. ±15 volts is required by the signal conditioners, as well as a +5 logic "high"; both are provided through the use of a +12 to ±15 DC-DC voltage converter and a +12 to +5 adjustable voltage regulator respectively. There is a common ground throughout the data acquisition electronics. The sensor excitation value was 10 ± 0.1 volts DC, and each sensor sports 8 350-ohm strain gage bridges, for a total of 686 milliamps current draw, the bulk of the power requirement.

5.6 System Upgrades

As can be seen from Section 5.4, the analog conversion board that was available restricted the data acquisition rate to 15 conversions a second at best, and given the software run time and the 24 element data set, operations were at virtually 0.5 Hz. This limitation prevented investigation of dynamic response in the 10-50 Hz range during task performance, which would be possible otherwise with this test set-up. The original system design had incorporated a much faster 12-bit A-to-D Board, which could not be procured in an acceptable time frame, that operated at a data conversion rate two orders of magnitude better. In addition, it was available memory-mapped to a single board computer. This package was to be placed in the underwater electronics box, leaving the topside computer responsible for only receiving and storing serial data ported up between tests. This system could therefore record data underwater at rates higher than could be uplinked serially, as well as reducing the line noise introduced by the analog uplink cable to the topside computer. When operating, the power system would be required to provide a $^{\pm}12$ volt regulated signal as well as a small additional amperage. It is hoped that future experiments using the hardware will incorporate such a distributed data acquisition scheme.

Chapter 6: Experimental Tasks and Procedure

The experiments which were conducted had to provide a great deal of information, yet be relatively simple, static, and amenable to the data reduction procedures available. Data taken in NBS, using the experimental set-up described in Chapter 5, needed to confirm the validity or invalidity of the Kinematic Chain Link model proposed in Chapter 3. In addition to this, the NBS data would provide information on how reaction forces were distributed by a subject in three-point restraint, allowing an attempt at empirical modeling. All of these tests could be used to assess task workload in terms of energy expenditure, and the same data examined for correlations with the test subject parameters.

The same essential equipment used in NBS testing was used again for 1-G testing in the laboratory, although only one sensor was used. These tests allowed for comparisons of task workload and peak forces possible between 0-G and 1-G workstations.

6.1 Task Selection

The design of the tasks conducted during experimentation was the result of several factors. One consideration was the desire for essentially static testing, i.e. tasks which did not require large body movements or displacements. The models (described in Chapter 3) that were to be confirmed and elaborated on, applied to static regimes only. In addition, as had been seen in past NBS testing in the laboratory, as velocity and displacement increased, the water drag forces made the useful correlation to space operations suffer. These forces are difficult to model in any case, and as work on a dynamic human motion model in NBS was the subject of a previous PhD thesis [Cousins, 1987], it was not repeated in this work. Finally, while the sensors were capable of measuring dynamic response, the Analog-to-Digital conversion board in place at the time was incapable of providing a data rate above 0.625 Hz (as discussed in Chapter 5).

The tasks were also to be kept simple. The KCL model requires body angles as input, and for complex and/or lengthy tasks it would be difficult to maintain high joint measurement accuracy. Also, simple tasks provided easy repeatability and a quick learning curve, considerations important when one considers the limited communication between the surface and the test subject. The slight learning curve effects also meant that all the data sets could be used, allowing more data to be used towards the conclusions made. Simple and short tasks allowed fatigue effects to be largely ignored in the workload and peak forces analysis. Finally, simple tasks could be seen as "building blocks", several of them together comprising more complex or "real" tasks. This would allow reaction force modeling of any task which can be broken down into simpler components.

Almost immediately, an examination of actual IVA and EVA tasks revealed many of them to be simple displacements. Displacement of a mass in zero-g involves a relatively straightforward application of force. Therefore, six possible tasks were forces in the three coordinate directions and in the negative coordinate directions. One-handed object rotation, such as would occur when using a screwdriver, was seen as another common, yet simple, task. Therefore, the remaining six tasks became torques about the three coordinate directions and their corresponding negative torques.

These tasks: $\pm$ Fx, $\pm$Fy, $\pm$Fz, $\pm$Tx, $\pm$Ty, $\pm$Tz, were performed both in zero and one gravity situations. All the tasks were conducted on the right handrail while the left handrail, the foot restraints, or both provided the location for the subject to apply reaction forces. Figure 6-1 shows these tasks being performed:

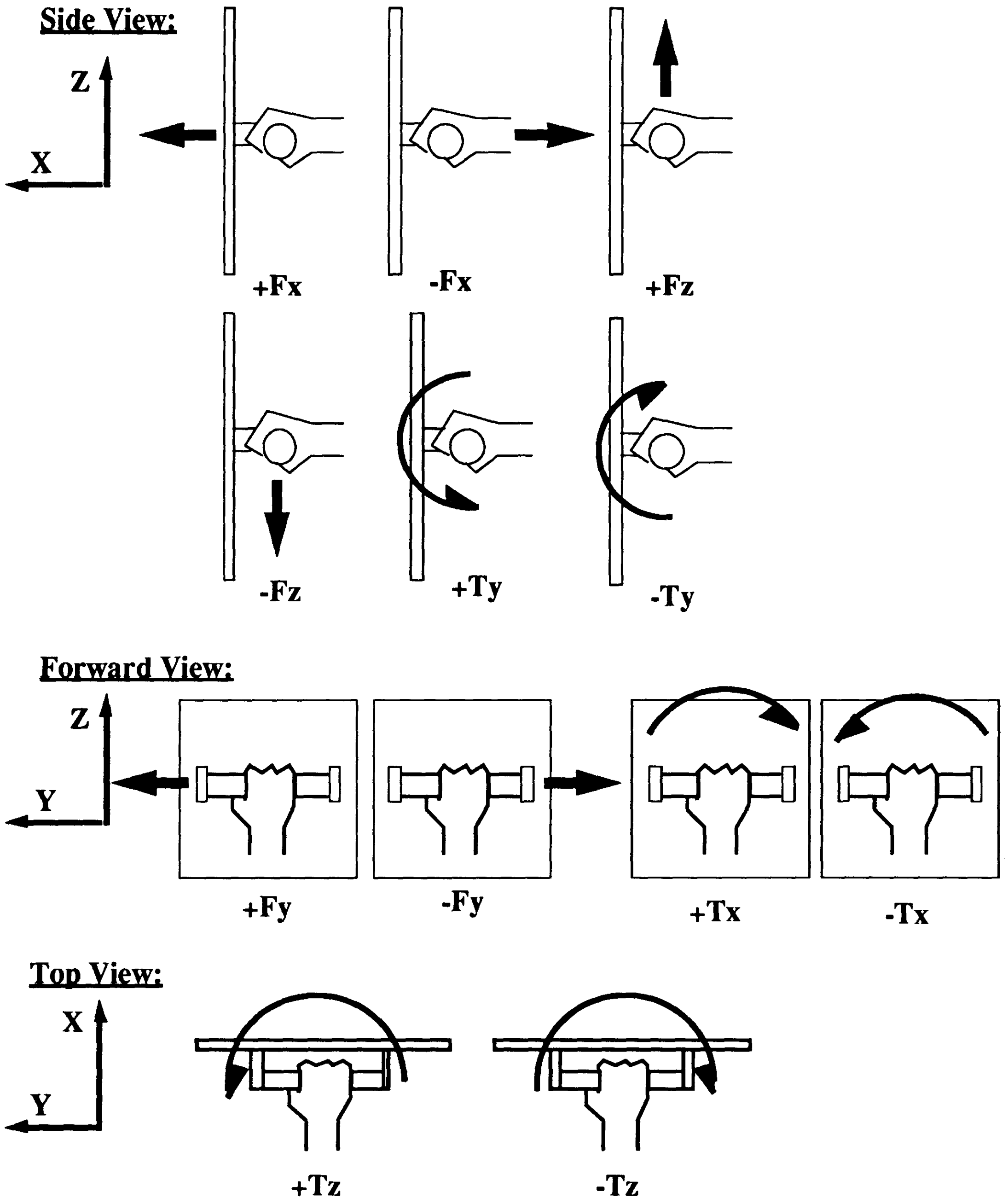

Figure 6-1: Tasks

Fx involved grasping the right handrail's center and pushing forward for the positive direction, and pulling back for negative X. Positive Fy involved grasping the handrail and pulling towards the left handrail in the plane of the handrails, while -Fy was pushing away from the left handrail. Fz had the subject grasping the handrail and pushing up, and pushing down for -Fz.

The torques applied were somewhat more complex. X Torque involved rotation about the defined X-axis in both senses. Positive involved grasping the handrail and rotating the wrist and forearm in a clockwise direction, or pronation, while -Tx was performed through wrist and forearm supination (counterclockwise rotation). +Ty involved wrist extension, -Ty wrist flexion. Finally, +Tz was produced by right wrist adduction, -Tz by right wrist abduction.

These 12 tasks fulfilled the criteria discussed above, and were used in the actual testing. It is important to note that in the vast majority of cases, the 12 tasks do not translate directly into forces and torques of the same type at the sensor itself. This is due to the fact that the site of task application differs from the point at which the sensors measure the tasks. Therefore, before continuing any farther, it is important to specify the exact coordinate system used in the experiments, and the locations of the restraints and their sensors relative to each other.

6.2 Coordinate Axes

Virtually all references in this text use one set of axes, to avoid the confusion developed when several sets are used and transformations become necessary.

The system origin is located at the center of the foot restraints, on its upper surface. The Z-axis extends vertically from that point, and the subject faces in the positive X direction with the positive Y-axis extending to his/her left. Figure 6-2 provides a rendering of the axis position, while Table 6-1 enumerates the coordinate locations of the sensors' force application points, the handrails, and the foot restraints for neutral buoyancy testing. It should be noted that the foot restraint is in the defined X-Y plane, while both handrails are in the Y-Z plane. This indicates that the central axis of the foot restraint sensor is the Z-axis, while for the handrail sensors it is the X-axis.

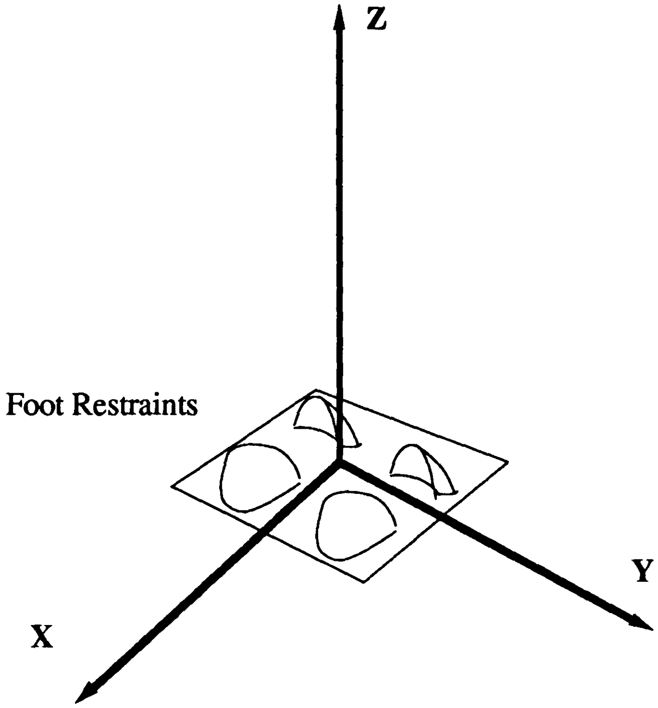

Figure 6-2: Coordinate Axes

OBJECT	LOCATION (wrt Origin) X (m)	Y (m)	Z (m)
Right Handrail:			
Sensor Measurement Point	0.7	-0.36	1.5
Task Application Point	0.61	-0.36	1.5
Left Handrail:			
Sensor Measurement Point	0.7	0.4	1.5
Restraint Point	0.61	0.4	1.5
Foot Restraint:			
Sensor Measurement Point	0	0	-0.032
Restraint Point	0	0	0

Table 6-1: Restraint Locations With Respect To Coordinate System for Neutral Buoyancy Testing

The most important coordinate transformation taking place is the transform between the sensor and the actual restraint point. Obviously, with a displacement between the restraint point and the actual measurement point, torques are developed which must be transformed back into the actual reactions. As can be seen from Table 6-1, the handrails have a 0.09 m displacement in the X-axis alone. This has no effect on tasks involving X-Force or X-Torque, but will have an effect on the other tasks. Most notably, forces in the Y and Z direction will be converted to torques.

This conversion must also occur for the foot restraints, although here there is a 0.032 m displacement in Z. All of these conversions are implemented in the program *smaug.c* available in Appendix A.

6.3 NBS Testing Procedure

Section 6.1 provided a description of the tasks to be conducted in neutral buoyancy, while this section describes the exact procedure.

A typical test session covered three hours and involved three subjects being tested. Initially, the computer was set up and the underwater electronics placed in the underwater box. The uplink/downlink cable was connected and the battery briefly attached to confirm that the electronics and software was operational. Confirming this, the sensors were attached to their specific handrails or foot restraints, and then connected to the electronics box. The box and sensors were then handed off to two divers, who attached the sensors to the test rig. At this point the battery was hooked up again to confirm that all was still operating normally (note that the battery was not hooked up when testing was not being conducted to prevent unnecessary draining). Finally, a scuba tank was placed near the test set-up. This tank included a regulator with a long hose, allowing the subject to remain essentially unencumbered. The subject then entered the water and adjusted their weight to achieve neutral buoyancy. For safety purposes all the subjects were scuba certified by a nationally recognized organization through at least the Openwater I level. This experience allowed them to trim their buoyancy well, although less emphasis was placed on achieving perfect neutrality in attitude. The subject was always watched by a safety diver on scuba, who also served as a relay between subject and the surface.

At this point testing was ready to begin. The subject first grasped both handrails and a calibration data set was taken to record the bias values of the channels, for the first data run: two-point restraint case, handrail and task board. The subject then performed the 12 tasks by the following method: the test conductor signalled the safety diver (who was near the surface) to start and began data recording, the safety diver informed the subject, who conducted the task and signalled completion by releasing the task board. This release prompted the safety diver to signal the surface to stop data recording. Calibration sets and data runs on the tasks were then taken for two remaining cases: task board and foot restraints, and handrail, task board, and foot restraints. In all cases task completion was signalled by releasing the task board handrail. This system saved a great deal of time by keeping the subject underwater, avoiding lengthy trips to the surface for explanation and consultation. This system was greatly aided by hand signals between the surface, safety diver, and subject, as well as by the presence of safety divers who were also subjects, and therefore knew the test procedure well. Many questions and difficulties were resolved by hand signals between the safety diver and subject.

The actual tasks were conducted in six sets: ±Fx, ±Fy, ±Fz, ±Tx, ±Ty, ±Tz. The subject was told to apply the force or torque in the positive direction for a count of ten, pause for a five count, and then apply in the negative direction for a ten count. This allowed for more data to be taken by avoiding too many pauses, and the opposite applications were clearly demarcated in the data even without the five count separation. The subjects were also told to apply full effort to conduct the tasks, allowing peak achievable reaction values to be recorded. The subjects paused between each two task set for 1-2 minutes, to prevent fatigue. Although not strictly regimented, this procedure worked well, allowing full data runs to be taken for each of the three restraint cases for a single subject in thirty minutes.

Two important assumptions during testing were made, and discussed in Chapter 3. First, that in all tasks the chain link modeling the subject was assumed to maintain constant joint angles. While maintenance of a single orientation was to prove difficult for the two-point handrail-task board restraint case, as the lower body had a tendency to torque, the upper body (which was the area described by the chain link) was more static. This constraint made comparison to the mathematical models far easier, and allowed measurement of a full scope of reactions. For while astronauts may not be constrained to a single orientation for all tasks, humans tend to have preferred orientations, and some tasks may require particular orientations. The second assumption was that the subject's legs were to be moved together as a single unit. This was to prevent the subject from reducing input forces and torques by swimming, as much as to simplify the modeling process. It was decided not to enforce this constraint by actually binding the subject's legs for safety reasons.

Despite the relative alacrity with which testing could be done, limitations on the use of the MIT Alumni Pool set the final number of test subjects at six. Although far below the number desired, the six did present a cross-section of gender, size, and experience (see

Section 6.5). Six subjects also allowed each subject to get very familiar with the operations, as each subject performed 168 separate tasks during the course of data taking.

6.4 1-G Test Procedure

Normal gravity testing was conducted to compare the peak forces achievable in neutral buoyancy with those achievable on the surface. To record the surface data, a single sensor was hooked up to the task board, and standing subjects performed the same task sets as in neutral buoyancy. The sensor was fixed to the test rig, this time in the laboratory, however. Data taking was simplified, of course, since the electronics were not sealed.

It is important to note, however, that the exact dimensions of the 1-G set-up differ from the neutral buoyancy case. This was due to physical constraints in the laboratory. Table 6-2 presents the pertinent coordinate locations for 1-G testing, and should be compared to Table 6-1. As mentioned above, the left handrail is not used, and there was no foot restraint sensor. Subjects simply stood at a defined location and were asked not to move their feet.

OBJECT	LOCATION (wrt Origin)	X (m)	Y (m)	Z (m)
Right Handrail:				
Sensor Measurement Point		0.57	-0.44	1.4
Task Application Point		0.48	-0.44	1.4
Foot Restraint:				
Restraint Point		0	0	0

Table 6-2: Restraint Locations With Respect To Coordinate System for 1-G Testing

As there was no left handrail for the subject's use this test is most analogous to Case 2 restraint (handrail and foot restraint). The 1-G data procured was mainly used as a benchmark to the other cases. It should also be noted that the coordinate transformation mentioned in Section 6.2 need not be changed for this case as the X-axis displacement is unchanged.

6.5 Test Subjects

As mentioned above, there were six subjects used in this experimentation. Table 6-3 shows some important information about the subjects. It should also be noted that all the subjects were right-handed and performed the tasks with their right hands. This was due mainly to the lack of available left-handed subjects, although by maintaining the same model formulations (in Chapter 3), subject-to-subject comparisons were simplified.

Subject #	Gender	Height (m)	Mass (kg)	Forearm Length (m)	Upper Arm Length (m)	Chest Width (m)	Back Length (m)	Upper Leg Length (m)	Lower Leg Length (m)
1	F	1.68	53	0.254	0.2794	0.3937	0.4699	0.3937	0.4953
2	M	1.80	112	0.267	0.3175	0.4699	0.5842	0.4318	0.4445
3	M	1.73	68	0.254	0.2794	0.4318	0.508	0.4699	0.4318
4	M	1.83	88	0.318	0.2921	0.4572	0.5334	0.4191	0.508
5	M	1.80	88	0.267	0.3175	0.4699	0.5842	0.4445	0.4445
6	M	1.73	82	0.254	0.2794	0.4826	0.5588	0.4445	0.4445

Table 6-3: Test Subject Parameters

The measurement error in height was ± 0.03 m, for the other body dimensions, ± 0.01 m. The error in mass was ± 1 kg. A major parameter not included in the table is the amount of experience performing tasks in neutral buoyancy simulation. There was no data base of actual hours available, so a qualitative approach rates test subject 2 as being by far the most experienced, while the other five have similar backgrounds. As mentioned above, all six were certified divers.

Chapter 7: Data Analysis- Modeling

As mentioned before, force-torque versus time profiles (also called reaction profiles) were recorded for a number of test subjects, while performing a variety of tasks. These profiles will be used in several ways: to attempt to confirm the static KCL models described in Chapter 3, to attempt to develop a new static model based on those models (also discussed in Chapter 3), and for use in designing a methodology for estimating physiological workload.

Figure 7-1 presents such a profile as an example of the type used throughout this chapter. Here test subject 1, while in restraint Case 1 (using the left handrail as a restraint while performing tasks using the right handrail), is applying a ±X torque. The task duration was approximately 30 seconds (indicating 15 full sets of data were taken), and the non-zero reactions are plotted below. The heavy line indicates the X-torque while the dashed line represents a Y-torque which was also being applied. This was included in the plot to emphasize the fact that defined tasks, such as ±Tx, produce a wide variety of applied reactions of all types, not just the specified reaction. The subject applied +X torque for roughly 10 seconds, rested (with torque values between 0 and 1.5 N-m) for 8 seconds, and applied -X torque for another 8 seconds of the test duration. This plot was taken directly from the *smaug.c* output of the right handrail sensor.

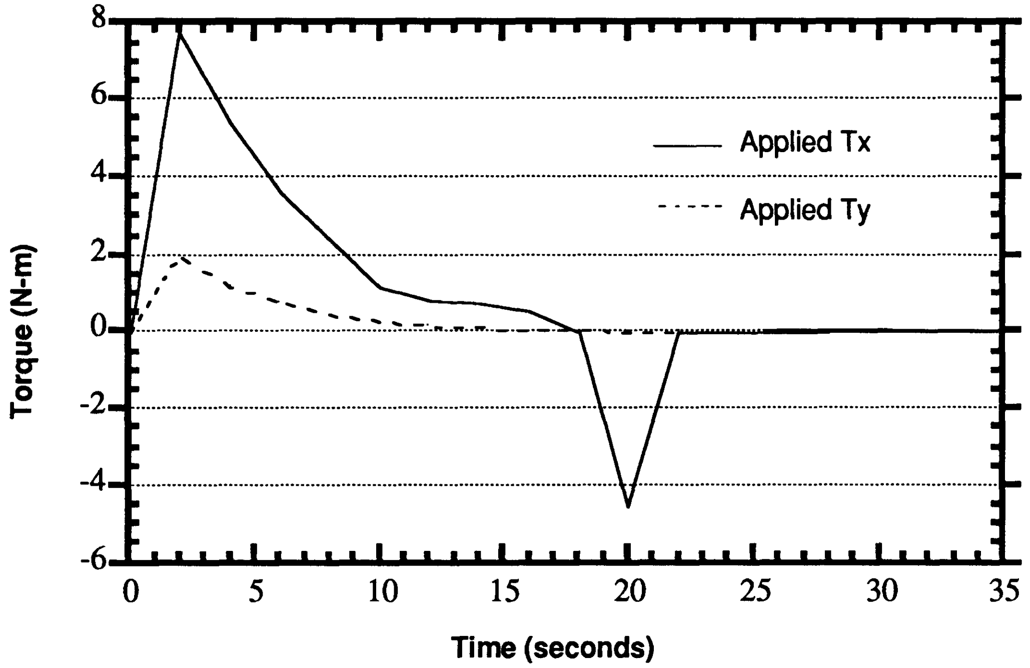

Figure 7-1: Sample Reaction Profile

Obviously, any single task generates three sets of plots, one for each sensor; and in each set the three forces and three torques are graphed. The KCL models are then used by presenting the right handrail plots as input values to *Kinematic Chain Link*, and comparing the results to the actual measured output at the left handrail and/or foot restraint sensors.

7.1 Confirming the Two Point Models

This section concentrates on confirming or denying the validity of the kinematic chain link models developed in Chapter 3. To do so, the resultants of the right handrail sensor were used as inputs to *Kinematic Chain Link* (available in Appendix A). This spreadsheet was customized for the specific subject undergoing testing, in terms of body segment lengths and joint angles. These angles were deduced through knowledge of the test rig dimensions, as well as through videotape recordings of the tasks being conducted. However, the calculations do not account for small variations in the joint angles of the chain link during testing. Error analyses have found that a 5 degree angle change in a single joint produces a mean 2% error in predicted measurements of torque. This holds true for all three torques, and is regardless of the direction of joint motion. Obviously, there is error variance between joints, as joint angle changes operating over longer lever arms produce greater errors. The largest of these is the mean 7% error caused by a five degree change in Ø8y, an angle operating over the subject's back (see Figure 3-5). While 2% is a small error, the cumulative effect of 11 joint angle errors could have had a severe impact on the validity of the predictive model, although this was not found to be the case. Due to this potential impact, a full joint measurement error analysis was conducted, and is included in Appendix E. This joint angle measurement error, along with the sensor measurement error (also discussed in Appendix E), will be cited throughout this chapter as potential error sources.

The results of the *Kinematic Chain Link* calculations were then compared to the actual output measured, and a normalized root-mean-square error calculated. The normalized RMS error is defined as:

$$\text{RMS Error}_{\text{normalized}} = \sqrt{\sum_{1}^{n} \left(\frac{M_i - P_i}{M_i}\right)^2} \qquad (7.1\text{-}1)$$

where M represents the actual value measured at the restraint sensor, P represents the value predicted by the KCL model for the same input, and n represents the total number of data points compared. This value provides a non-dimensional parameter for comparison of the various tasks and restraint cases. An example from each of restraint Cases 1 and 2 is worked through fully, and these are followed by Table 7-1, which presents the mean normalized RMS values by reaction type and restraint case.

Another assessment of error mentioned in the following section is the mean error, defined as the mean of the absolute value of the difference between the measured and predicted profiles. This is presented as Equation (7.1-2), with n, M, and P retaining their meaning from the previous equation.

$$\text{Mean Error} = \frac{\sum_{1}^{n} |M_i - P_i|}{n} \qquad (7.1\text{-}2)$$

This value is used in addition to the normalized RMS error because it provides an intuitive quantification of trends seen in the plots, as well as an easy comparison to the sensor measurement error.

7.1.1 Case 1 - Two Handrails

As mentioned in Chapters 3 and 6, the subjects performed tasks with their right hands on the right handrail/task board while their left hand provided support. The subject's lower body was unrestrained in these sets of tasks, so it is here in the Case 1 restraint tests where fluid effects (predominantly water drag) can be expected.

Figures 7-2 through 7-9 provide an example of a task conducted under this restraint condition. The graphs below represent a 40 second segment of a one minute ± Fy task conducted by subject 3 on 20 January 1990. The -Fy portion of the task has been omitted to allow closer examination of the presented profile, as the segment shown is generally representative.

Figures 7-2 and 7-3 are the measurements taken at the right handrail, the input forces and torques to both the model and subject. This specific task was selected because the subject applied a force resultant which had large components in two force axes, as well as exhibiting some + X and + Y torque. This allows the reader to see the results when a complex input is applied.

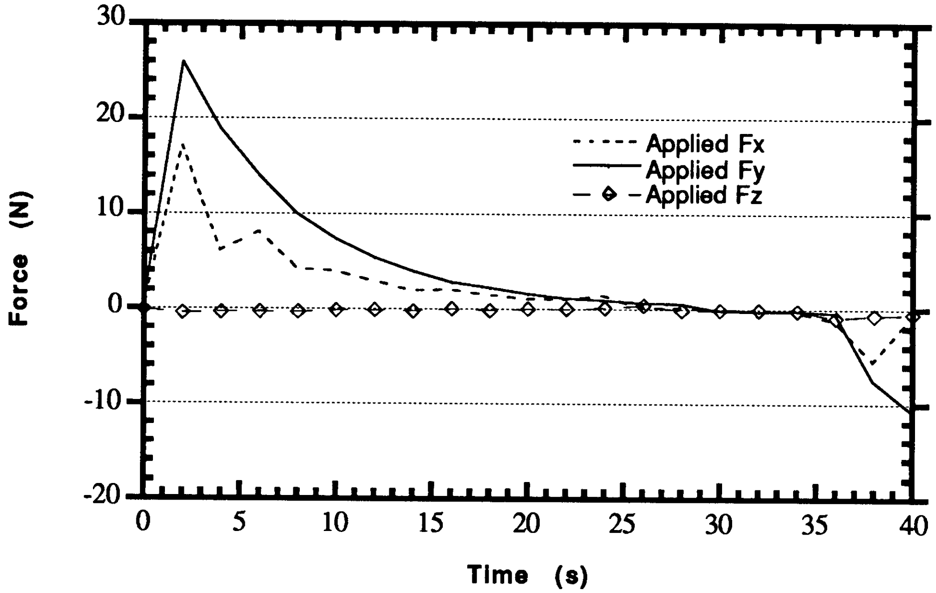

Figure 7-2: Case 1- Applied Forces

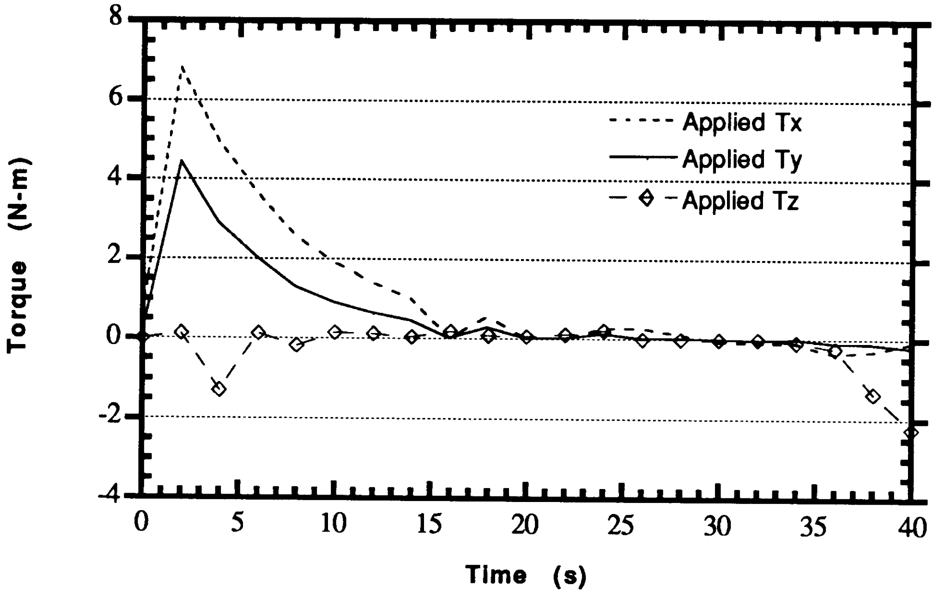

Figure 7-3: Case 1- Applied Torques

As mentioned above, these two figures represent the reactions which produced the following six figures. Each figure represents a different reaction (Fx, Fy, Fz, Tx, Ty, Tz), and presents both the values measured at the left handrail, as well as the values predicted by *Kinematic Chain Link.* For the values presented in the following six figures, the actual positive direction of the reaction is the opposite of the input reaction. This display method was adopted as it allows for easy visual comparison of the applied and measured reactions. Such a comparison allows study of the conservation of reactions far more easily then using the defined axis convention. Such a visual study tends to confirm a basic conservation of reactions, although some changes in orientation (retarded by fluid effects) were observed. At this juncture it may prove crucial to note again the sensor measurement error, namely ± 3.72 N in force, and ± 0.99 N-m in torque for Fx and Tx; ± 1.86 N, and ± 0.5 N-m for the remaining reactions. Again, details concerning sensor measurement error can be found in Appendix E: Error Analysis.

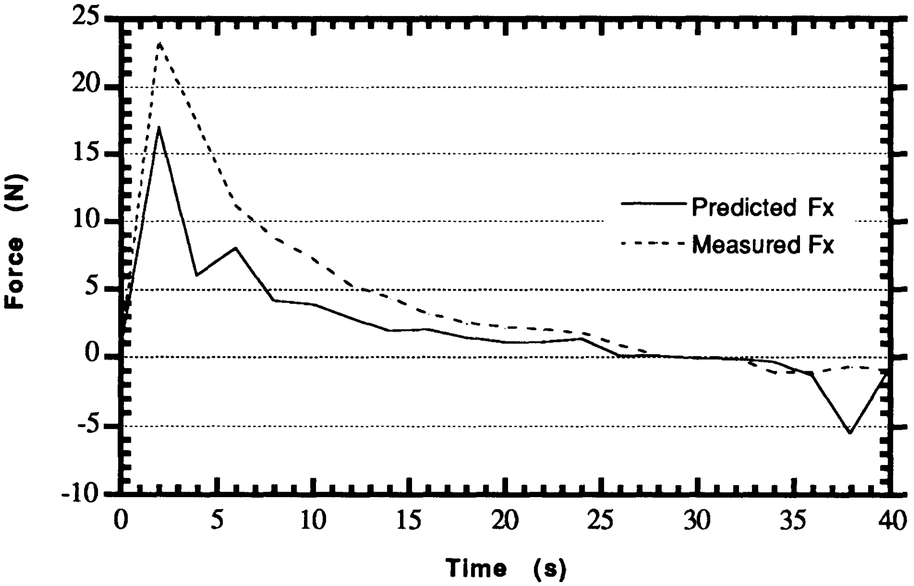

Figure 7-4: Case 1- Fx

Figure 7-4 shows a marked difference between the actual and predicted X forces at the left handrail, which is mitigated somewhat when the measurement error is considered. Of note then, is the smooth slope of the measured data at the 4 and 38 second marks, when the predicted data follows the sharp jag seen at the input (Figure 7-2). This indicates the existence of an unbalanced force which resulted in subject rotation (about the Z axis). This may have been due to the subject correcting for drift while performing the force application. The mean error observed was 2.17 N, within the measurement error range of ± 3.72 N.

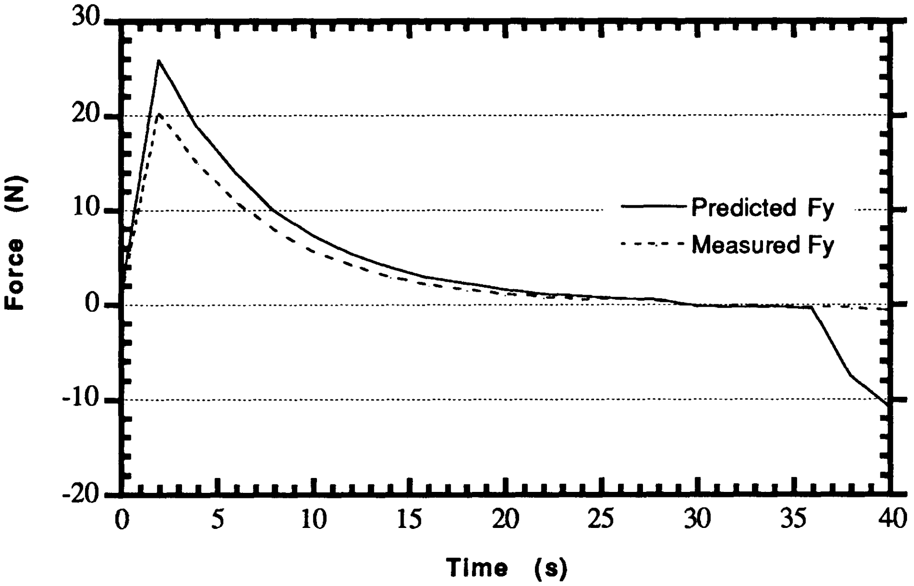

Figure 7-5: Case 1- Fy

In Figure 7-5, the measured and predicted values seem to mesh quite closely between 8 and 36 seconds. The mean error was 1.83 N, for a measurement error of ± 1.86 N. Unlike the previous figure, the predicted value was generally greater than the measured value.

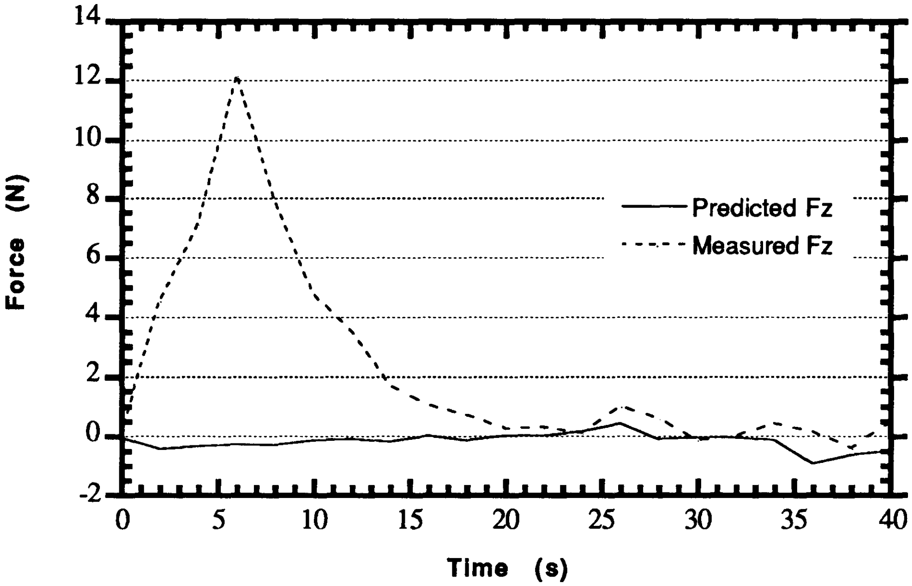

Figure 7-6: Case 1- Fz

The marked difference between the predicted Fz value, which follows the input, and the value actually measured at the left handrail, indicates that an unbalanced -Fz force was applied. Such an application would result in a -X torque probably necessitated to counter subject changes in orientation. Despite the discrepancy in the plots, the mean error was but 2.39 N.

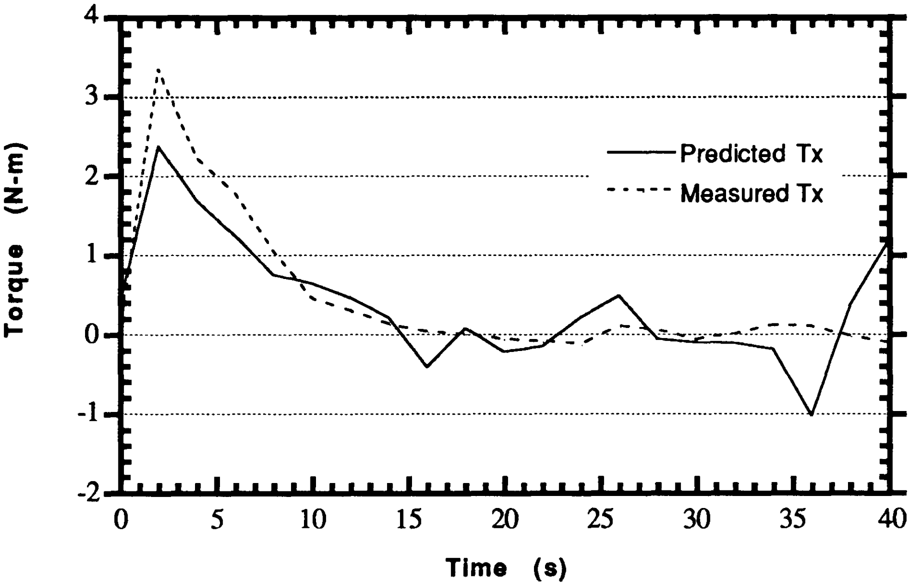

Figure 7-7: Case 1- Tx

For the peak values of Figures 7-7 and 7-8 the model values and the measured output differ greatly. The obvious deduction is that the discrepancies are the result of a subject undergoing an orientation change. In Figure 7-7, the KCL model predicts a low torque output due to the mitigating effects of X torques produced by the applied forces Fy and Fz. The actual Fy resultants seen in Figure 7-5 are lower than predicted, due to interactions producing torques, resulting in a greater required Tx and Fz to brake the rotation. After the first 8 seconds, the model and measured results seem to match more closely. This is generally true for all the plots, indicating that the subject remained in a new orientation, and ceased movement. It is also generally seen that the measured values are smoother than the accompanying predictions. This illustrates the role of water drag in absorbing much of the rotational energy. For Figure 7-7, the mean error value was 0.381 N-m.

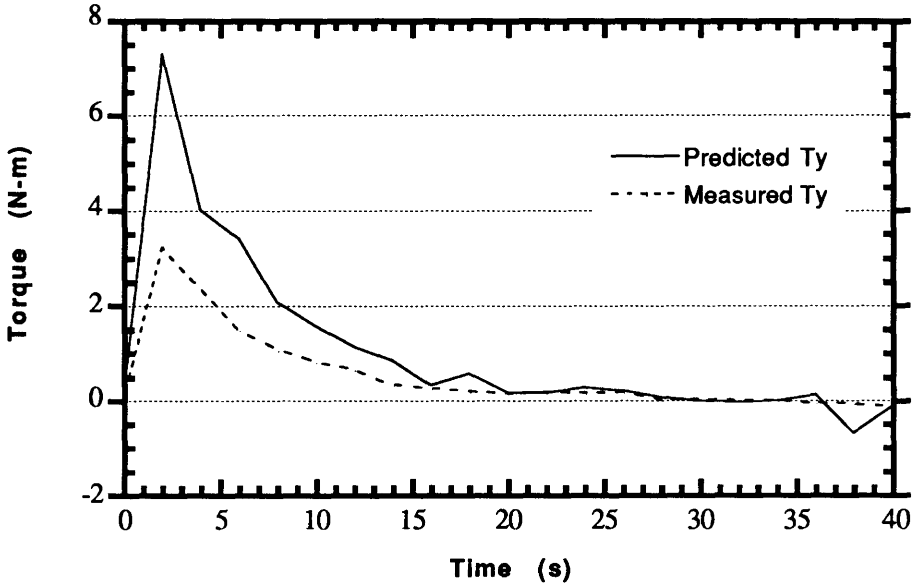

Figure 7-8: Case 1- Ty

The applied and measured results for Ty fail to match closely, indicating an unbalanced moment about the Y axis. The model is again accounting for mitigating forces which were instead involved in producing motion. This fact once again delineates the truly static nature of the Case 1 model. Although a harness system restraining the lower body orientation was considered and discarded as unsafe, such a device may have alleviated some of the problematic results for this case. The mean error for this plot was recorded as 0.571 N-m, the one of three cases in this example where the mean error exceeded the expected measurement error (± 0.5 N-m).

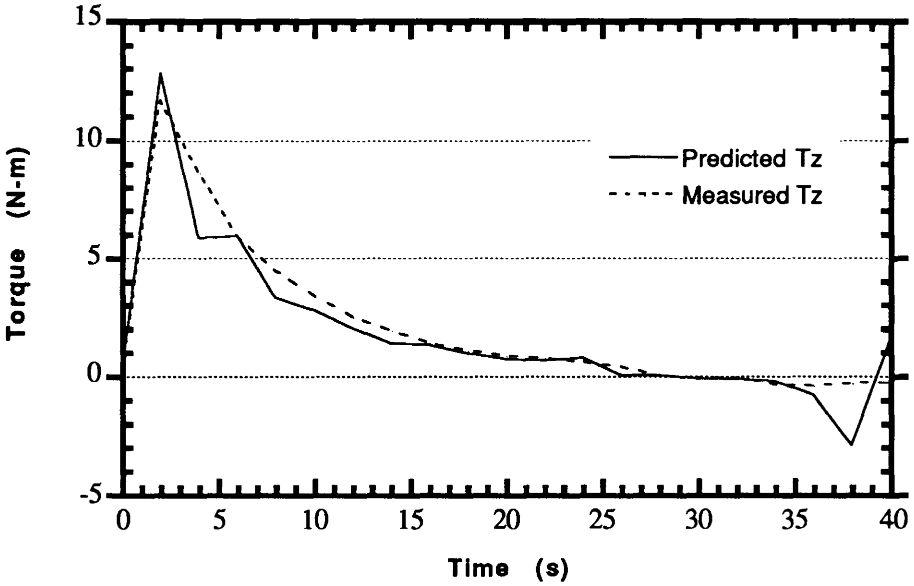

Figure 7-9: Case 1- Tz

Although Tz represents another case where the mean error (0.610 N-m) is greater than the measurement error, a visual comparison between the actual and predicted results seems to indicate a good match. It is interesting to note that the input Z torque is virtually zero for much of the task duration (Figure 7-3), while torques near 12 N-m are seen in the above plot. This is explained by the fact that both Fx and Fy force applications can produce Z torques also. It is this type of interaction which complicates analysis, but which also explains the apparent lack of reaction conservation. Except for the produced rotations, all of the net forces and torques are generally conserved. This is especially clear in the final 15 seconds, indicating a cessation of movement. However, no braking reactions are noted stopping this movement. This reveals the drag effects of movement in water; in true EVA, the subject would continue rotating until a braking reaction was applied.

As is generally seen, the static KCL model produces poor results for a restraint case where motion occurs, and conservation of reactions cannot be measured due to the braking effects of the fluid environment. Dynamic analyses discussed in Section 3.1.2 estimate this effect to be on the order of 16 N-m against the direction of rotation, for the X and Y axes. This fact accounts for the sharp discrepancies between the model and measured values when near the peak outputs (peak angular acceleration). Although the presence of braking reactions applied by a subject maintaining a specific orientation would allow for conservation of reactions to be confirmed, it would not increase the accuracy of the KCL model. To be an accurate predictor of the reactions measured for this case a valid model would have to account for the dynamic motions involved. This topic, and methods for confirming rotation and fluid effects as the cause of the inaccuracies, are discussed in detail in the conclusions Section 9.1.1.

7.1.2 Case 2 - Right Handrail and Foot Restraints

The layout of this section is virtually identical to the previous section. Again, a task is broken down into its reaction components as an example. This particular task was a ± Fx task performed by subject 1 on 28 January 1990. During the Case 2 testing, the subjects were fastened into foot restraints and performed the tasks with their right hands. The left handrail sensor was not used. One reason that this particular task was selected is that extensive videotape documentation exists. This documentation generally confirms the joint angle values used, and the fact that no significant subject motion or orientation change occurred. Thus, one can expect the results to be relatively free of fluid effects.

Unlike the example presented above, the entire task duration was roughly 35 seconds. A decision had been made between the test dates shown, to speed up each task, allowing more runs to be conducted; two separate runs being more valuable than a single longer one.

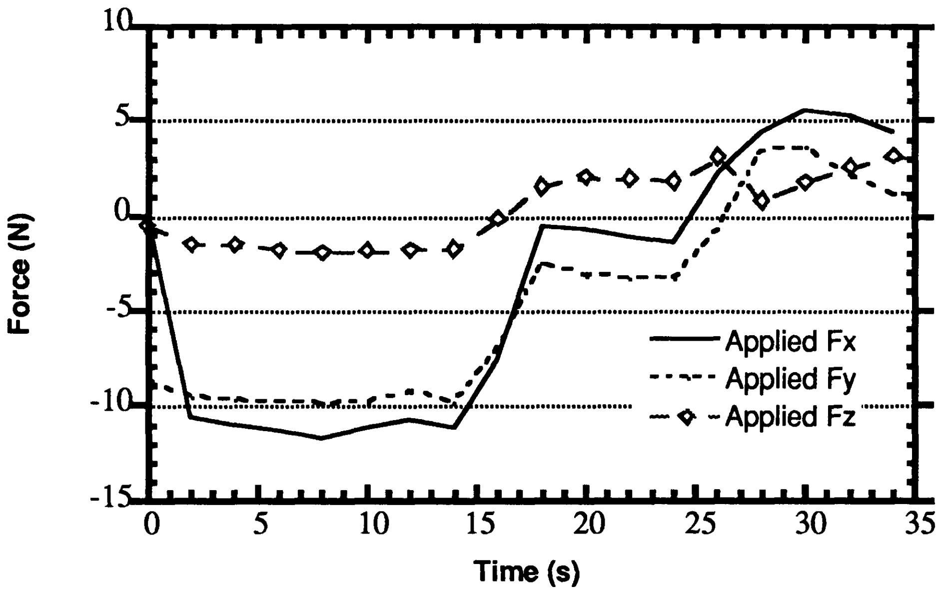

Figure 7-10: Case 2- Applied Forces

Figure 7-10 provides a display of the forces the subject applied to the right handrail during the task duration. It is immediately clear that the subject performed the task in reverse order, applying -Fx prior to +Fx. This type of event occurred several times and became obvious when the *smaug.c* output was generated. The run itself, however, remains extremely suitable as an example. The 7-second "rest" period is clearly seen between 17 and 24 seconds, even though the subject is still applying some force. The actual force resultant which the subject applied had a large Y component, and a small Z component, indicating that the subject was pulling out and to the slightly lower right for the first seventeen seconds, and pushing in and to the upper left for the final 11 seconds. This is borne out by the videotape and resulted from the fact that subject 1 had a shoulder height 0.15 m below the handrail height. This differential resulted in a tendency for the subject to pull down and to the right, and push up and to the left. The peak forces for this particular task are well below the subject's mean peak (see Chapter 8).

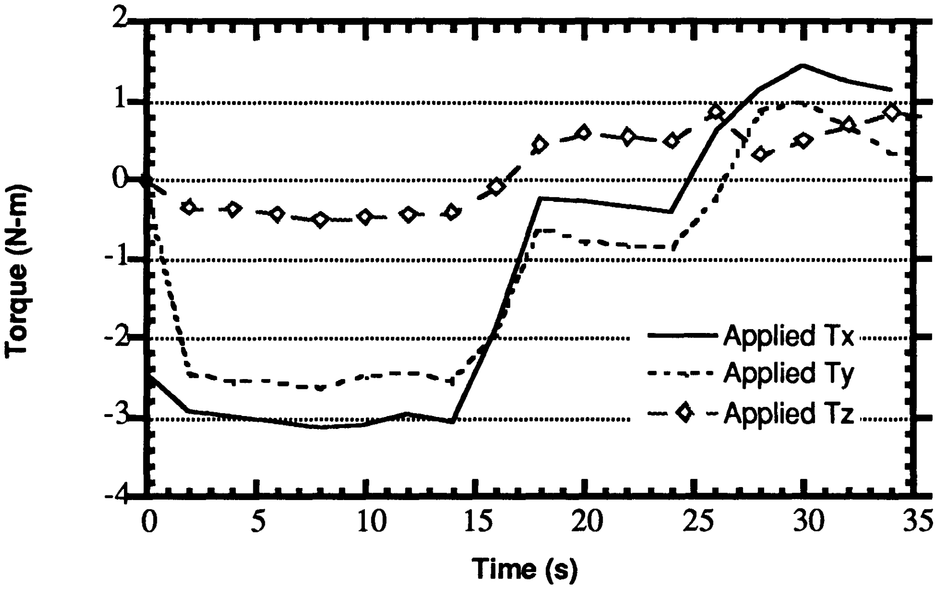

Figure 7-11: Case 2- Applied Torques

As can be seen from Figure 7-11, slight torques were also developed during the task, well below the subject's mean peak values.

Figures 7-12 through 7-17 provide the comparison between the reactions measured by the foot restraint sensor and the values predicted by *Kinematic Chain Link*. As was done in the example for Case 1, these six figures have their positive and negative coordinate directions reversed from the established standard. This once again allows easy visual comparison between the input reactions and the output measured at the subject's feet. For the foot restraints, the out-of-plane force and torque are Fz and Tz respectively, unlike the handrails. As a result, measurement error for the following graphs is ± 1.86 N for Fx and Fy, ± 3.72 N for Fz, ± 0.5 N-m for Tx and Ty, and ± 0.99 N-m for Tz.

As fluid effects error is not expected, three identified error sources exist. The first is the sensor measurement error just mentioned, and the second is any joint angle measurement error, as discussed previously. However, there is expected to be little joint angle error for this task, as the videotape was carefully studied. The final source of error is compliance in the foot restraints. The rubber water-ski bindings used allowed a large amount of flexibility, preventing the full transference of reactions through the foot restraint, to the sensor. To prevent this loss of reactions into binding flexure, more rigid bindings were considered. This idea was dropped, due to safety considerations. It is actually due to their compliance that the rubber bindings allowed swift egress for subjects.

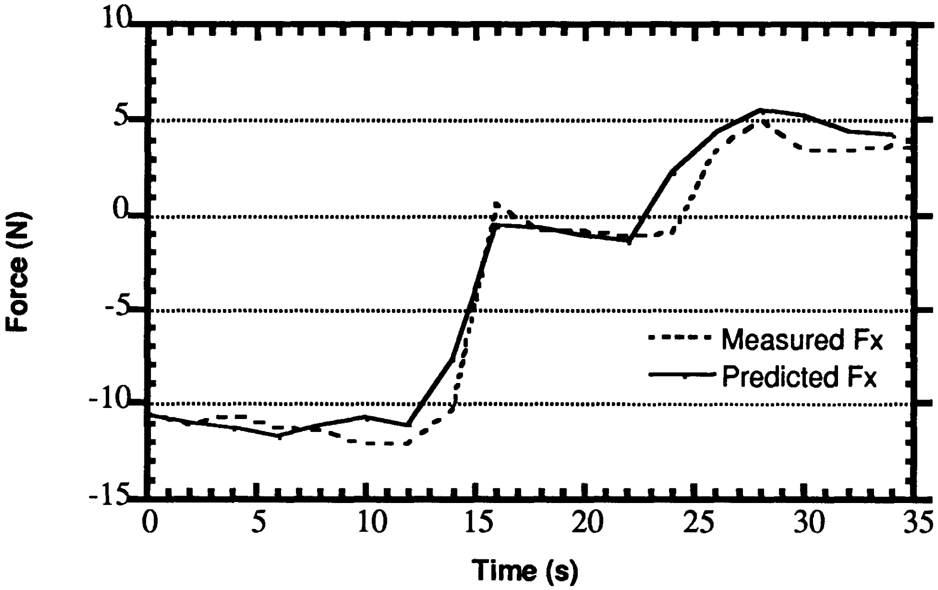

Figure 7-12: Case 2- Fx

Figure 7-12 illustrates the accuracy of the static KCL model when lower body motion is inhibited. The mean error for Fx during this task was 0.83 N, compared to 2.17 N in Figure 7-4 above. This error fits well within the potential ± 1.86 N measurement error.

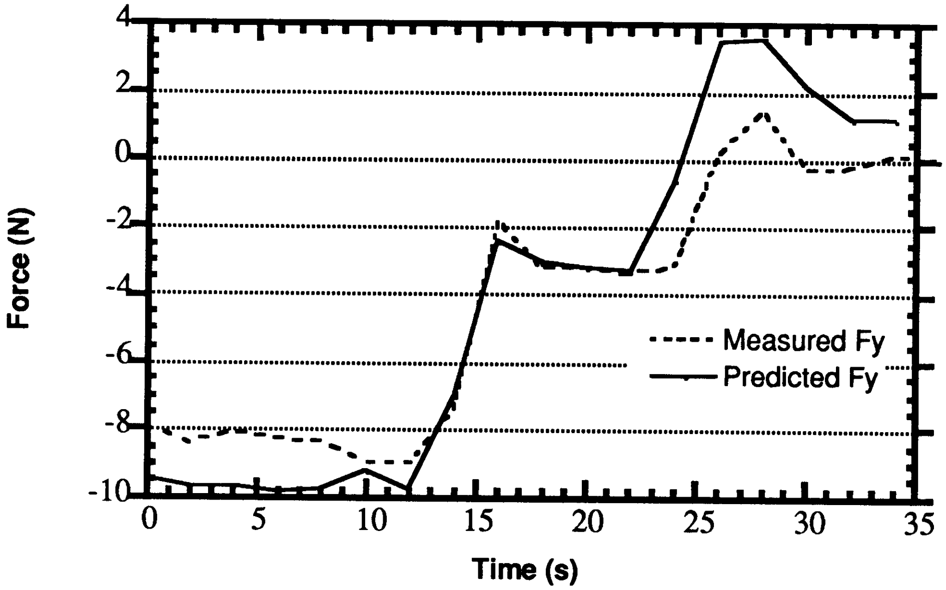

Figure 7-13: Case 2- Fy

Figure 7-13 has a mean 1.45 N error, once again within possible measurement error. The overestimated + Fy force between 22 and 35 seconds is primarily responsible for this error, and may be evidence of compliance.

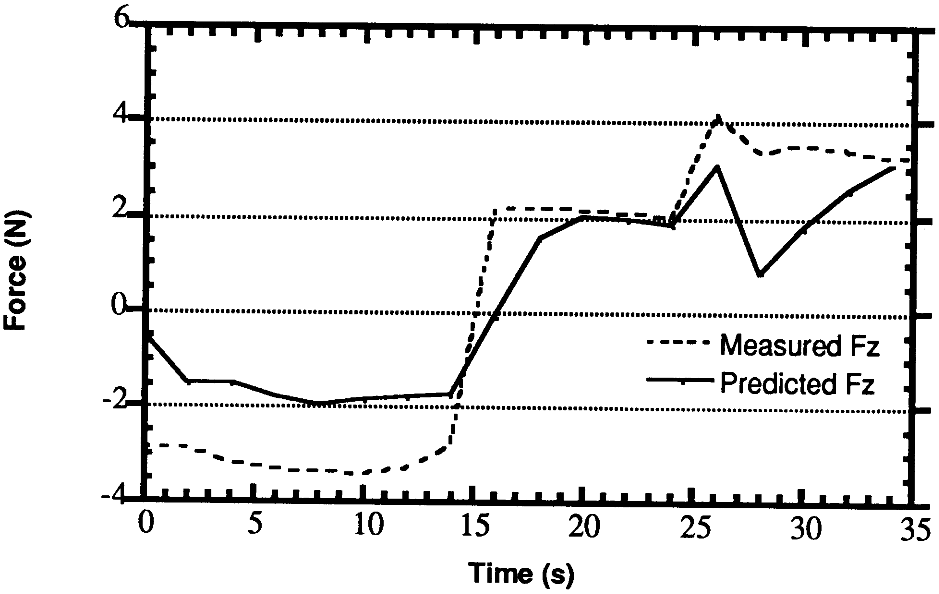

Figure 7-14: Case 2- Fz

Although exhibiting the correct general profile, the predicted and measured values in Figure 7-14 net a mean error of 1.03 N. This discrepancy is large given the low magnitude of the Z force measured when compared to the other two forces. Foot restraint compliance cannot be the cause of this error, as the measured values would have to be of lower magnitude than predicted. It is important to remember, however, that the possible ± 3.76 N measurement error almost completely encompasses this plot.

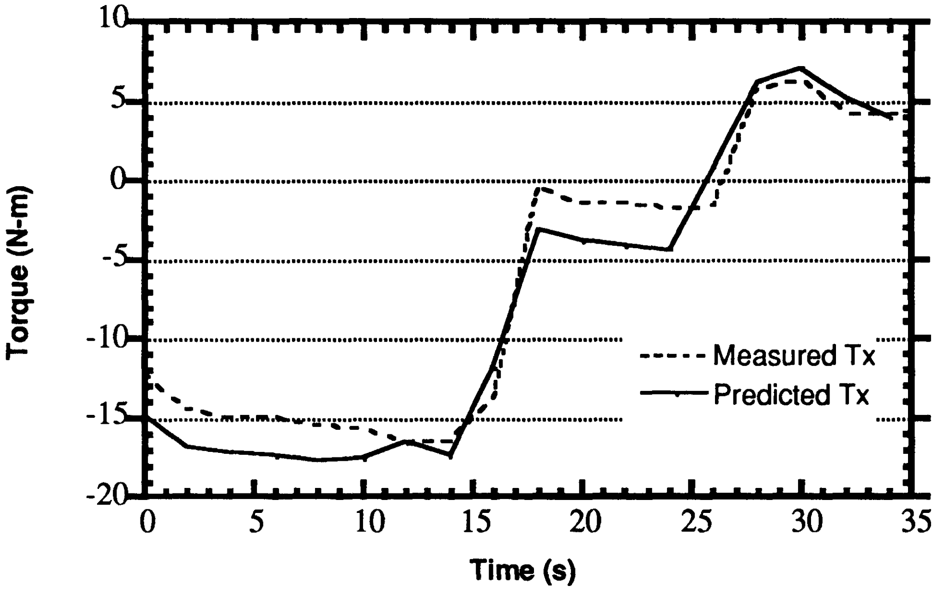

Figure 7-15: Case 2- Tx

With a mean error of 1.81 N-m, Figure 7-15 is outside the measurement error range. Compliance may be the cause, as the magnitude of the measured value is nearly always less than that of the predicted value. It is expected that if compliance is the error causing agent, that the binding would flex to a certain point and then stop, this point being when the maximum output is reached. This would indicate that the peak magnitudes of the measured and predicted profiles should be nearly exact, as it is here that compliance should no longer occur. By the same token, the greatest compliance should occur when resting, and when progressing from resting to peak output. This supposition is well borne out by Figure 7-15.

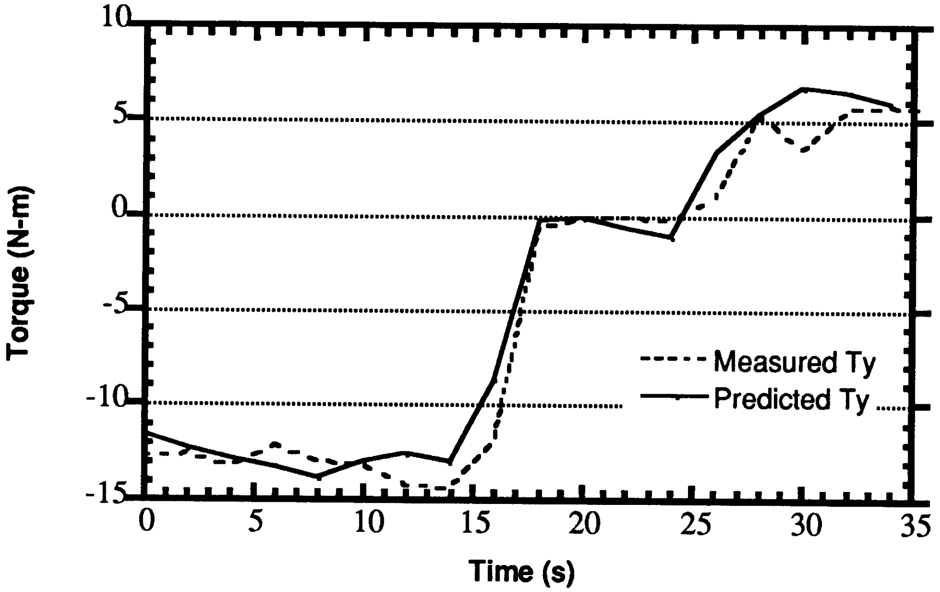

Figure 7-16: Case 2- Ty

Figure 7-16 shows a generally good match between the prediction and measured values, although the error is outside the measurement error bounds (0.924 N-m). Compliance does not seem to be the cause of the error for at least the first 18 seconds of the task.

The Ty magnitudes, ranging from +14 N-m to -7 N-m (utilizing the correct coordinate system), appear large when compared to the -2.5 to 1 N-m range of the input in Figure 7-11. This is explained by the magnitude of the X-force applied (a -11 to 6 N range), which acts across a 1.5 m lever arm (the vertical distance from the restraints to the right handrail) to produce a Y-torque in the opposite direction as the X-force. A rough analysis shows that a peak -11 N Fx creates a +16.5 N-m Ty across the lever arm, which added to the -2.5 N-m input Ty provides the +14 N-m seen at the foot restraint (-14 N-m in the coordinate system of Figure 7-16).

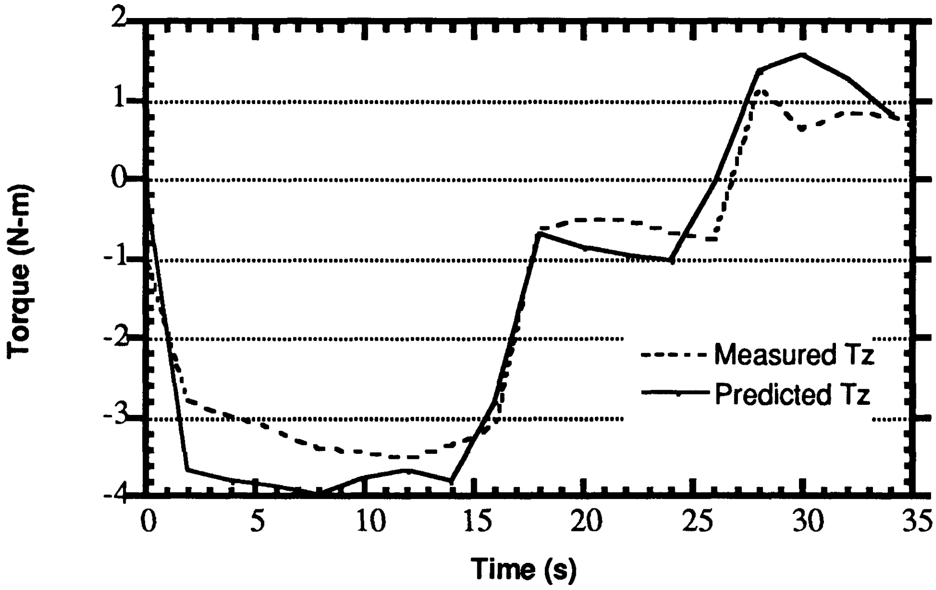

Figure 7-17: Case 2- Tz

The error in Figure 7-17 could be attributed to compliance, however, it does not exhibit the expected matching of peak magnitudes. The mean error is very low for this reaction (0.42 N-m), especially considering the measurement error range of ± 0.99 N-m.

Comparing the examples in Case 1 and Case 2 shows the relatively high quality of the model when used under Case 2 restraint conditions. This is due to the absence of motion and fluid effects as error sources. The additional error causing effect of compliance in the foot restraints may have an effect on the Case 2 results, however, this is not significantly greater than the existing sensor and joint angle errors. Over the entire range of data Case 2 produces substantially lower normalized RMS errors. This is especially true for the transverse axes torques, Tx and Ty, which are impacted the most by subject rotation. These values are collected in Table 7-1.

Reaction Type	Case 1	Case 2
Fx	18.35	11.01
Fy	22.12	8.76
Fz	24.43	2.09
Tx	46.87	3.86
Ty	50.50	5.24
Tz	25.65	3.03

Table 7-1: Mean Normalized RMS Errors

The net results of these sections is that the KCL model is a reasonably accurate predictor of the reaction profiles generated by Case 2 tasks, and is a poor predictor of Case 1 tasks, due to dynamic motion in a fluid environment.

7.2 Developing the Three Point Model

As discussed in earlier sections, it was hoped to use the confirmed KCL models for the previous cases to develop an empirical model capable of predicting reaction outputs for restraint Case 3, where the subject performs tasks with the right handrail while using both the left handrail and the foot restraints. The presence of two restraint points invalidates direct application of KCL theory, but may allow solutions derived based on the KCL models developed above. The simplest such solution would be the case where the reaction values measured at the left handrail or foot restraints in Case 3 were simple fractions of those for the previous case. To discover if the reaction distribution process occurring in Case 3 was a simple superposition of the two models requires considerable data analysis.

Given a set of reaction inputs, a test subject in restraint Case 3 creates a corresponding set of reaction outputs at both the left handrail and foot restraints. If the profiles for the left handrail are then compared to the predictions based on the Case 1 KCL model, they will differ by some factor. So for six profiles (Fx, Fy, Fz, Tx, Ty, Tz), six such factors can be found (labeled A-F in Chapter 3). The same process is completed for the same task using the measurements at the foot restraints and the Case 2 KCL model predictions, resulting in six more factors (G-L).

For any Case 3 task, these 12 factors can be found. To support the empirical model, however, these factors must provide good correspondence between the profiles, and must be constants regardless of the task. The Fx profiles of a single task is analyzed to determine A and G in the first example below. Analysis of the other tasks again looks for A and G, hoping to confirm them as constants. The error sources found in Case 3 should not be substantially different than those for Case 2, and include restraint compliance, sensor error, and joint angle measurement error; values which did not have a great adverse effect on the Case 2 model's fidelity. Prior to examining the plots, however, it must be noted, as an area of concern, that the KCL model for Case 1 could not be confirmed as valid in the preceding section.

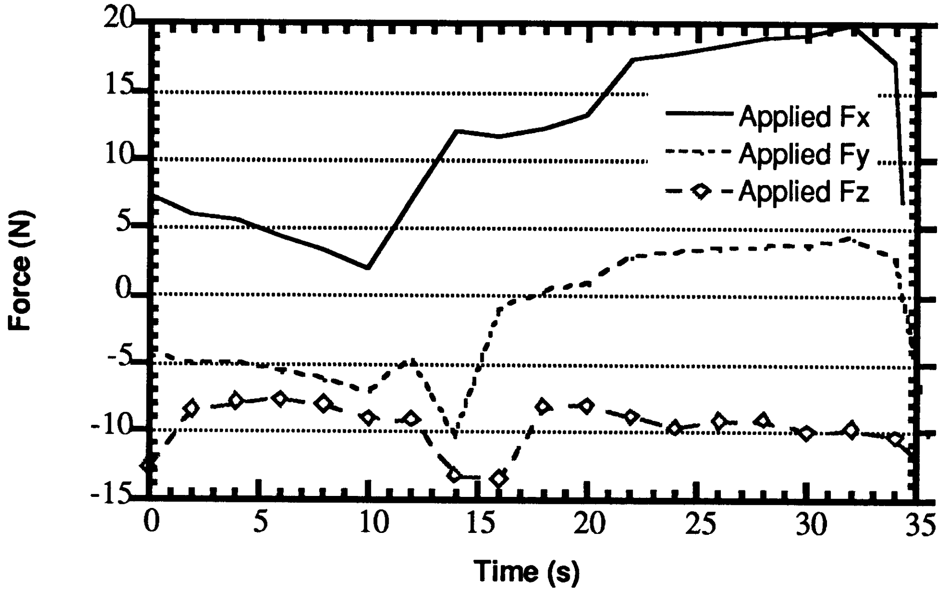

Figure 7-18: Case 3- Applied Forces

Figures 7-18 and 7-19 provide the applied force and applied torque profiles, respectively, for a segment of a Fx task conducted by test subject 5 on 10 February 1990. Through examination of the right handrail applied reactions, as well as the output for all of the Case 3 tasks analyzed, conservation of reactions was confirmed.

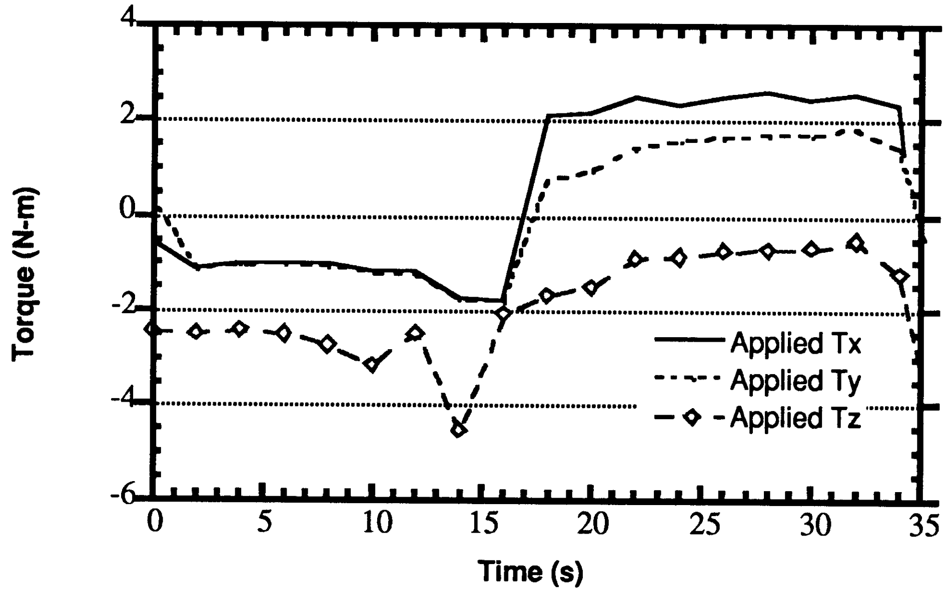

Figure 7-19: Case 3- Applied Torques

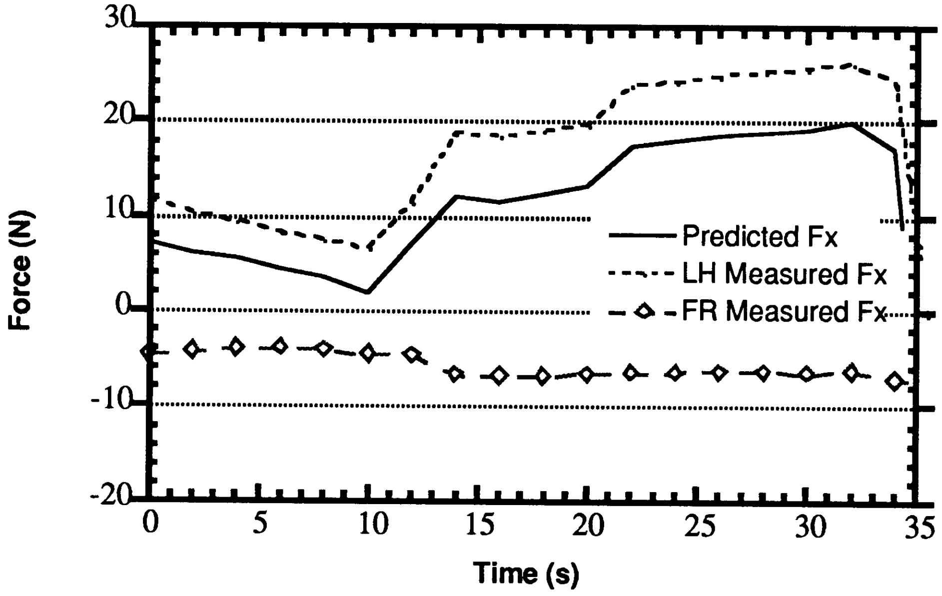

Figure 7-20: Case 3- Fx

Figure 7-20 shows the relationship between the predicted net Fx profile, and the values measured at the restraints. Once again, the coordinate directions on the measured values are reversed for easy comparison to the predicted values. As can be seen, the force at the foot restraint is a relative constant, as the subject uses the left handrail to resist the applied Fx. To achieve a "best fit" an A value of - 0.767, and a G value of 0 were estimated.

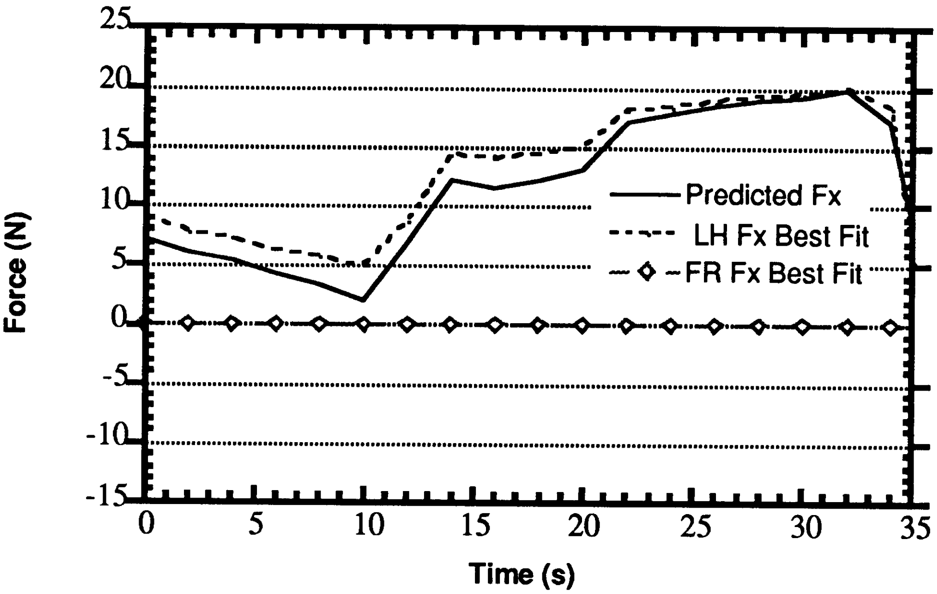

Figure 7-21: Case 3- Fx Best Fit

Employing these values produces Figure 7-21. The normalized RMS error of the fit is 2.43, which was one of the lowest errors of the sets evaluated. Further calculations for this example produced constants B, H, C and I as -0.046, 0, -6.816, and 0.069, respectively, with RMS normalized errors of 142.5 in Fy and 18.47 in Fz.

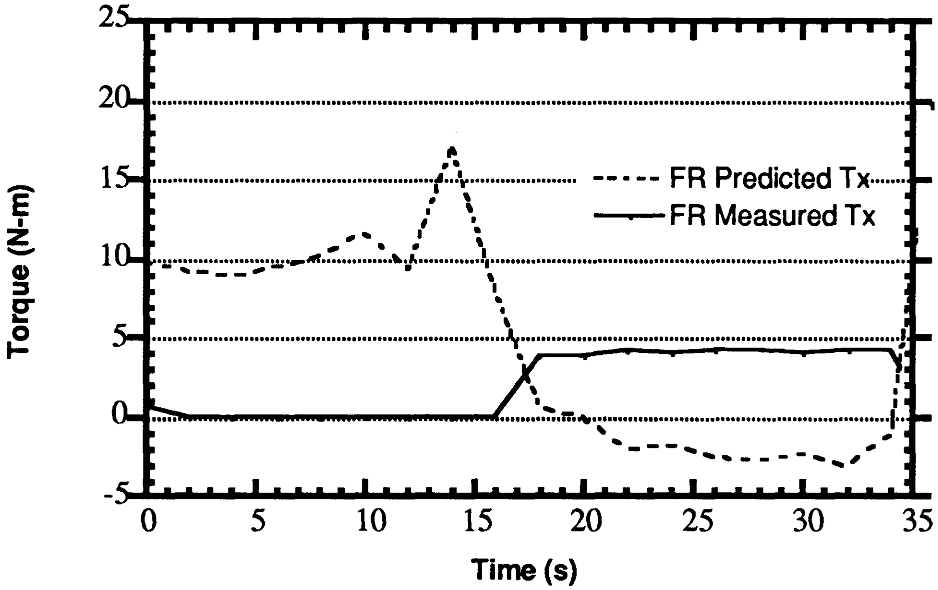

Figure 7-22: Case 3- Tx Foot Restraints

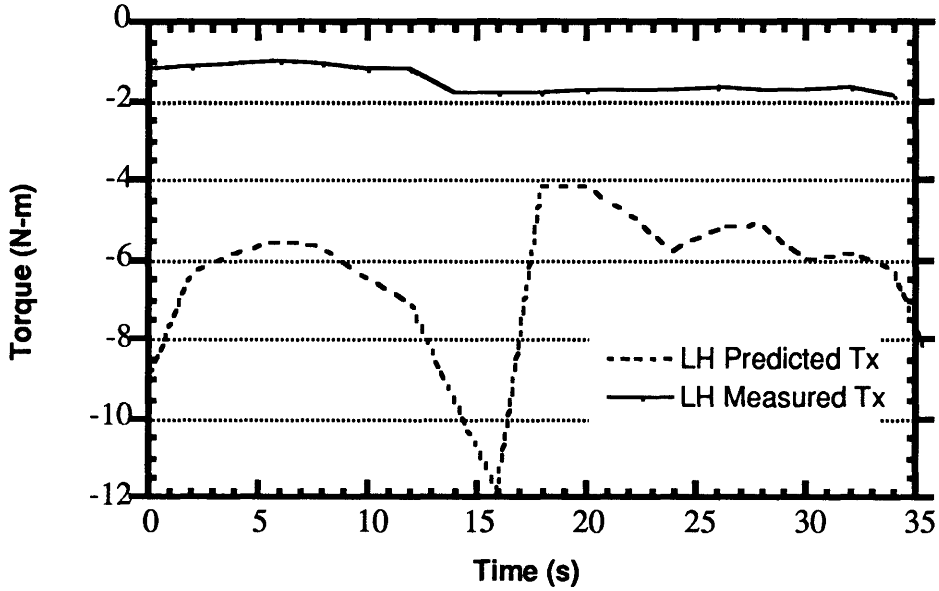

Figure 7-23: Case 3- Tx Left Handrail

A continuation of this procedure would lead to estimates at the remaining constants for the torque cases. Figure 7-22 and 7-23, however, illuminate the absence of any proportional relationship between the torque predictions and measurements. Examining Figure 7-22, the Fy force at the right handrail which would normally produce high Tx for Case 2 (foot restraints), is instead being countered by Fy at the left handrail. This Fy application is in addition to the one being applied at the left handrail to maintain conservation of forces, and is not proportional to the Case 1 left handrail prediction. This third reaction path, between the foot restraints and left handrail, is what makes Case 3 statically indeterminate. While a superposition of the measured data at the restraints provides the magnitudes and types of reactions transferred on this path, a predictive model based on proportional distribution between restraint points cannot be confirmed. There appears to be no set of constants, A through L, which describe the distribution of reactions between the two restraints. This does not imply that a consistent relationship between the input and restraint reactions does not exist, it simply does not appear that the relationship can be described by such a set of constants.

7.3 Estimating Workload

This section serves to illuminate how the data garnered for this section could be used to estimate physiological workload. The "Lauru Platform" used by L. Brouha recorded force profiles along all three axes using piezoelectric crystals, and these profiles were used to estimate the workload involved in creating those forces [Brouha, 1960]. The subjects performed tasks on the platform, and the force-time areas (the areas under, for example, the absolute value of the curve in Figure 7-1) were correlated to the subjects' oxygen consumption rate. As mentioned in Chapter 1, high correlations were discovered, ranging between 0.83 and 0.96.

The force sensing device, however, provided an innate limitation on how good an estimate could be. The force-sensing crystals measure force as a function of compression, so forces rising up out of the platform could not be detected with high precision. In addition, torques which the subject applied could not be identified, nor was there any method for confirming that the net forces and moments summed to zero.

The present hardware allows for the entire force environment on a body to be assessed, so that a true picture of the required reaction output can be gleaned. Thus the six degree-of-freedom force/torque sensors allow for reaction-time area assessment for a full range of full-body activities.

Calculating the reaction time areas for a given task requires the input profiles and output measurements. Case 1 measurements do not provide a good basis for this type of analysis since unquantifiable effort is being expended into motion. However, the Case 2 example task provides an excellent series of figures (7-10 through 7-17) to consider. In this analysis the prediction profiles are ignored, and the areas under the absolute values of all the curves are calculated. Adding together these values despite the unit difference between forces and torques gives a net expenditure value. The addition of force-areas and torque-areas can be conducted as long as a correlation to another simultaneously measured value, such as heart rate and oxygen consumption, is made. Once such a correlation is made and confirmed, the Case 2 predictive model can be used with high confidence to estimate energy expenditure without having to conduct the task.

To accurately make the the correlation between the reaction-time areas seen in the figures above and physiological workload still remains as an open area of investigation. The correlative data which Brouha developed, while providing a guideline for the methodology, does not cover the full range of subject motion and action in the neutral buoyancy environment. In addition, the physiological cost difference between the surface and neutral buoyancy vary tremendously, and depend on such things as water temperature and depth. Therefore, correlations between reaction-time areas created for a particular task and the oxygen intake for that task must be made. These oxygen consumption figures would then provide a bridge to the body of physiological data already existing, as it, along with heart rate, are the most commonly accepted measures of effort.

In one respect, the neutral buoyancy environment is ideal for oxygen consumption measurement. Compressed air must be provided for the subject in any event, and with the addition of an instrumented regulator, oxygen data becomes readily available. It is even possible that an accurate off-the-shelf scuba tank gage could provide benchmark data for tasks involving continuous, generally constant, effort. Further discussion of this issue is available in Chapter 9.

Chapter 8: Data Analysis- Peak Reactions

This chapter concentrates on examining the peak reactions achieved by the test subjects while performing the tasks discussed in Chapter 6. For this investigation, the peak values (both maximum and minimum) from the force-torque profiles used in the previous chapter were recorded. As each subject performed several repetitions of the same task for the same restraint case, an average (mean) peak reaction was calculated. It is these averages which are used below, and they are given simply as a magnitude (absolute value), with no reference to the direction of the reaction. This average data is available in Appendix D: Data.

The first section of this chapter simply presents the peak values for a given reaction by restraint case, and examines the plots for trends. The following section then looks for any correlation (using linear and higher order least square curve fits) between the peak reactions and two subject parameters: height and mass.

8.1 Peak Reactions versus Restraint Case

8.1.1 Presentation of Graphs

What follows is a series of twelve figures, one for each type of reaction (±Fx, ±Fy, ±Fz, ±Tx, ±Ty, ±Tz). For each reaction the average peak magnitude for each subject and each restraint case is displayed. Case 1 refers to a subject performing tasks on the right handrail while using the left handrail as a restraint. Case 2 refers to the use of the right handrail and the foot restraint alone, while Case 3 involved the use of both handrails and the foot restraint. This nomenclature was developed in Chapter 3, and the details of how the tasks were conducted is available in Section 6.3. "1-G" refers to benchmark data taken under normal gravity conditions, this process was detailed in Section 6.4. There exist gaps in the data indicating sections of test runs which were invalidated for various reasons. It is useful to note again here that the error on each peak reaction used to calculate these mean peaks was ± 3.72 N in force and ± 0.99 N-m in torque for the X direction, half those values for the in plane reactions.

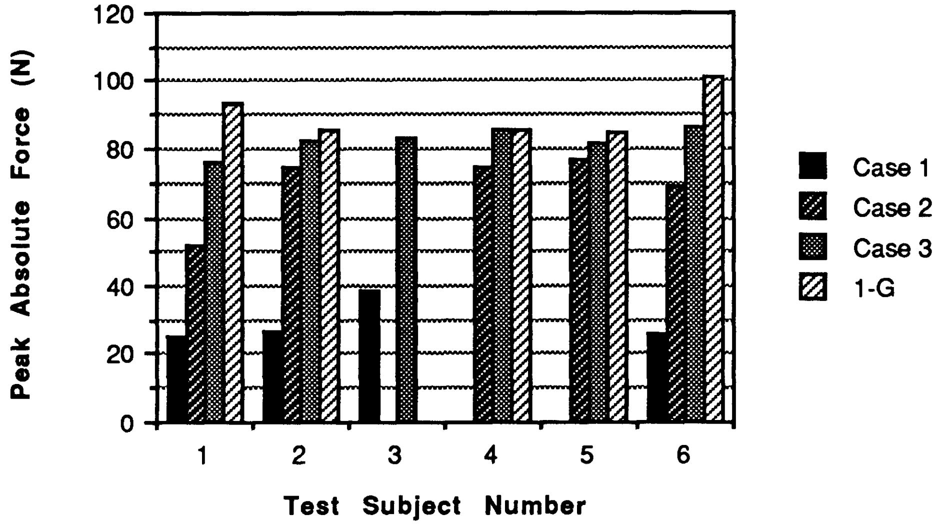

Figure 8-1: Peak +X Force v. Restraint Cases

As an example, Figure 8-1 presents the mean peak forces achieved by each of the six test subjects for the four restraint cases. As can be seen, there appears to be a trend of increasing peak output for each successive restraint case culminating in the tasks conducted in normal gravity, regardless of the subject. A Student's, or t-, test was performed on the data to confirm these trends, the results of these tests are collected in Table 8-1 in Section 8.1.2.

The only outside correlation to these peaks was found in Seireg's paper [Seireg, 1970]. He reports that a study performed in 1967 found that a diver standing on the bottom of a water tank was able to achieve a +X force peak of 27 N compared to a 1-G benchmark of 222 N. The test performed is not particularly comparable to any of these restraint cases, however. In the 1967 test, no mention is made of foot restraints, and no data on the static friction available on the pool bottom is given. In addition, the task was performed with the arm alignment through the subject's center of mass to avoid creating turning moments. If the subject in this study was applying this force one-handed without foot restraints, it is not surprising that the forces seen in Figure 8-1 are larger. What may be surprising is the smaller peaks achieved under 1-G conditions in the present study, this may have been the result of the 1-G test set-up, which exhibited compliance in the ±X direction.

The remaining eleven figures follow, often with some notation. In general however, Section 8.1.2 is used to confirm the observed trend that peak output increases for each successive restraint case.

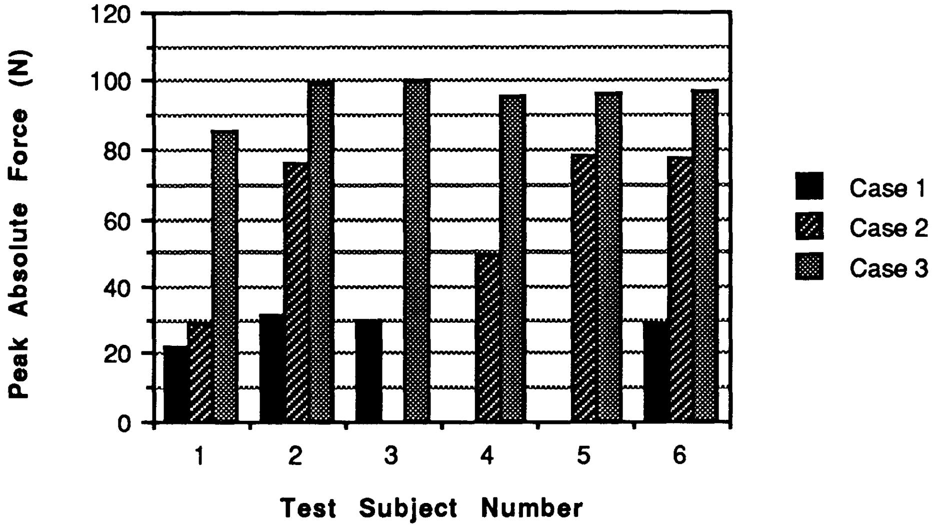

Figure 8-2: Peak -X Force v. Restraint Cases

Due to the vagaries of data acquisition, 1-G benchmarks were not obtained for the tasks in the negative coordinate directions. However, the relationship between the neutral buoyancy restraint cases is still available.

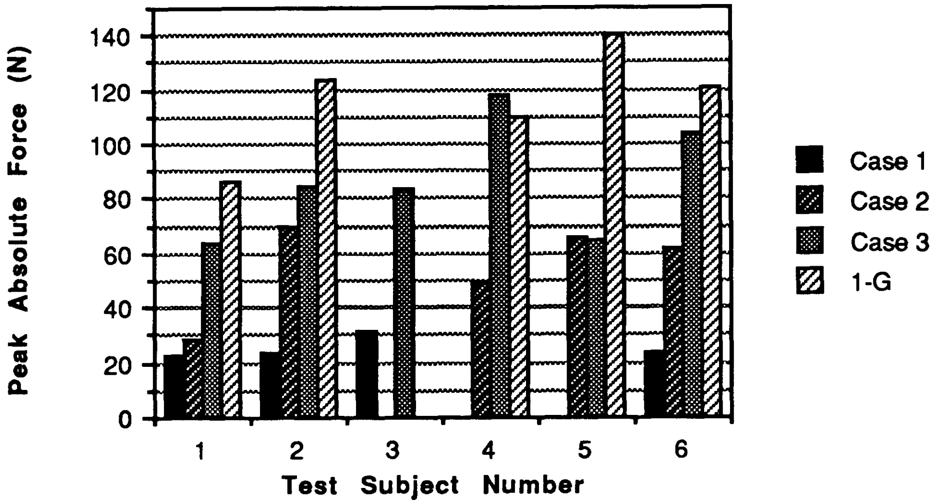

Figure 8-3: Peak +Y Force v. Restraint Cases

In this Figure (8-3) it is interesting to note that the peak 1-G force achieved by subject 4 is less than the peak force for restraint case 3. The subject mentioned during the course of 1-G testing that he was not exerting himself fully due to a slight illness. This could not only explain the incongruity in the graph, but illuminates the problems associated with human factors experimentation. With laboratory and time constraints, testing was confined to only six subjects, and 1-G testing to a single two day span. As a result, illness and other elements influence the data, whereas testing done on a far larger pool of subjects over a greater period of time could reject many of these effects.

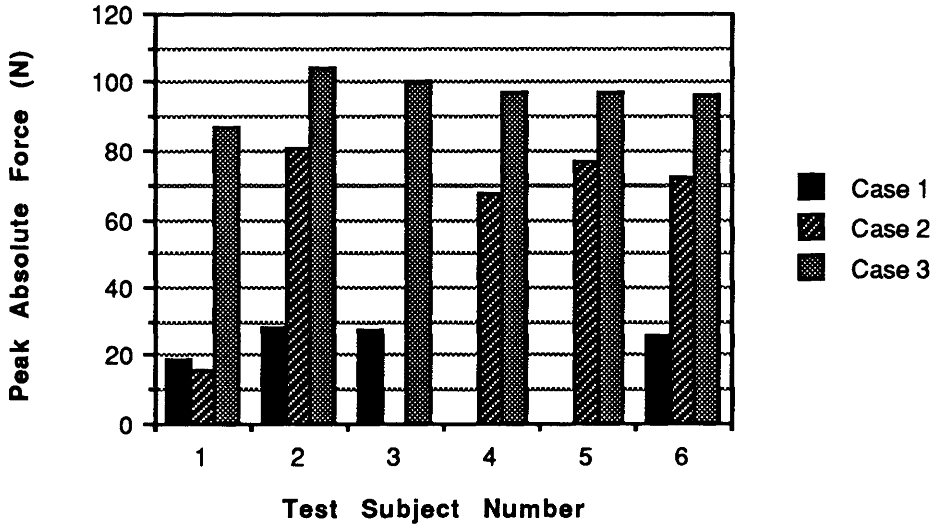

Figure 8-4: Peak -Y Force v. Restraint Cases

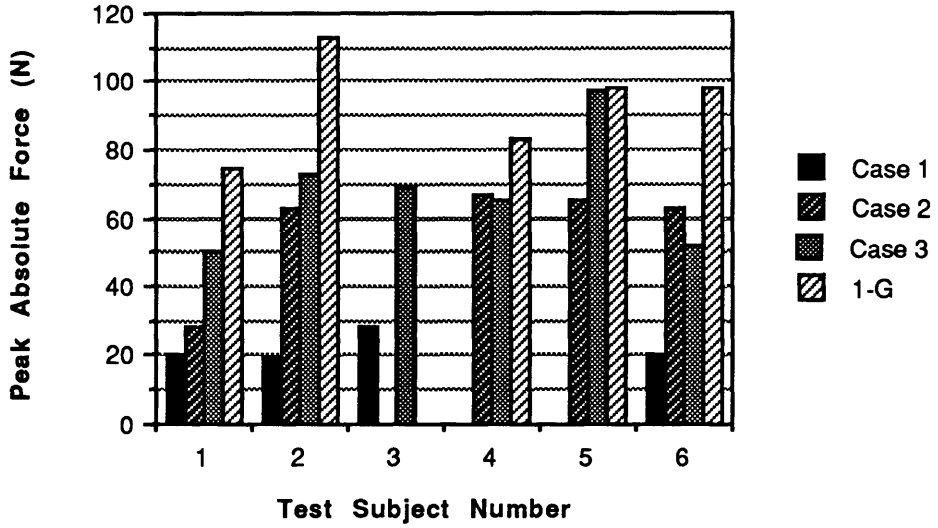

Figure 8-5: Peak +Z Force v. Restraint Cases

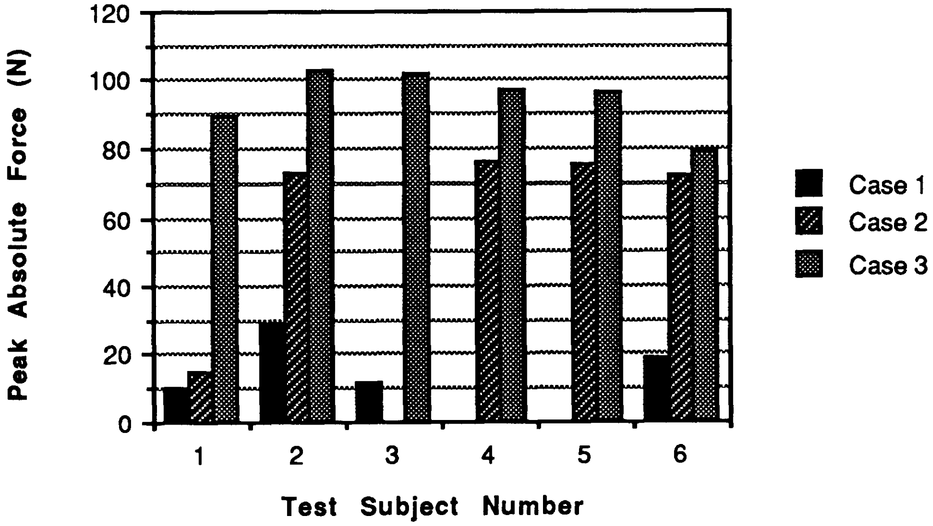

Figure 8-6: Peak -Z Force v. Restraint Cases

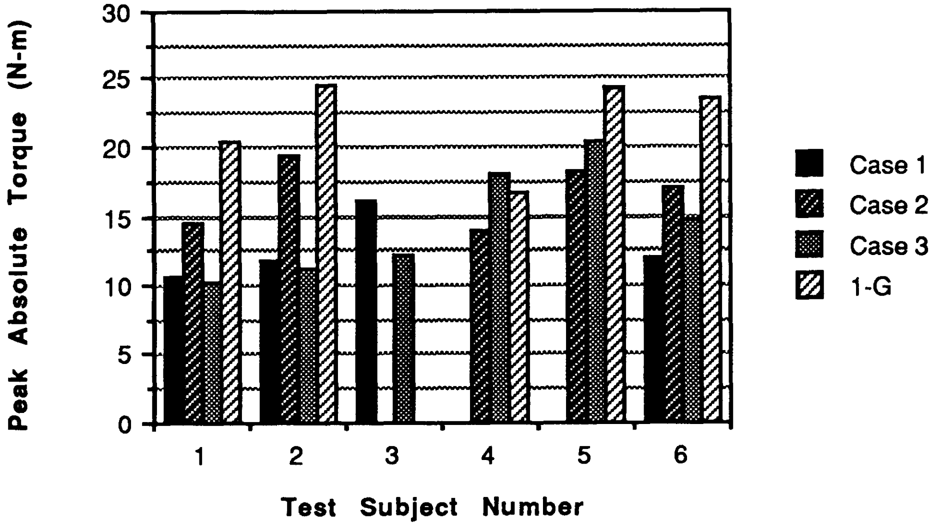

Figure 8-7: Peak +X Torque v. Restraint Cases

Two points can be made about Figure 8-7. The first is a comparison to a similar test done on a KC-135 parabolic flight by C.E.Whitsett [Whitsett, 1964]. In this test a subject torqued a handle in the same manner as was done for the +Tx task. The peak torque achieved was about 5.4 N-m. This task is most analogous to the Case 1 restraint (two handrails), but was lacking the additional handrail to provide support. This fact, in itself, may explain why the Case 1 torques recorded are between 1.85 and 2.96 times greater. In addition, given the restraints on "weightless" time available on a parabolic flight, the subject in Whitsett's study was only able to exert the torque for two seconds, which may have prevented achievement of higher peak torques.

The second item of note is that for half the subjects, peak torque achieved for Case 2 restraint was higher than for Case 3. As expected, this shows up as a low confidence on a t-test performed on the two sets of data (0.625), but there appears to be no systematic explanation, especially as this trend is not seen for -Tx (see Figure 8-8).

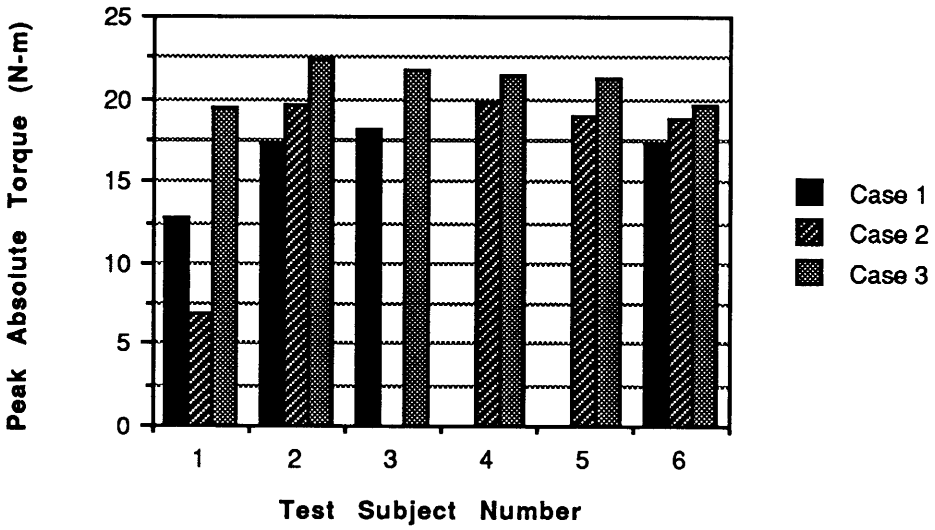

Figure 8-8: Peak -X Torque v. Restraint Cases

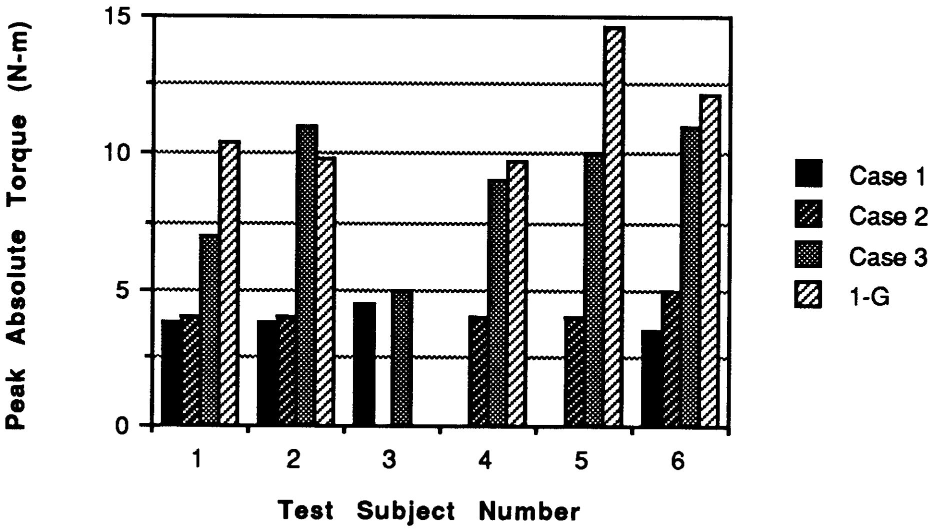

Figure 8-9: Peak +Y Torque v. Restraint Cases

It is interesting to observe that the magnitude of the torques achieved in the Y and Z directions are significantly lower than those achieved in the X direction. This is supported by various references, including [Chaffin, 1984], which indicate that humans are inherently stronger for the type of motion exhibited in performing the ±Tx task.

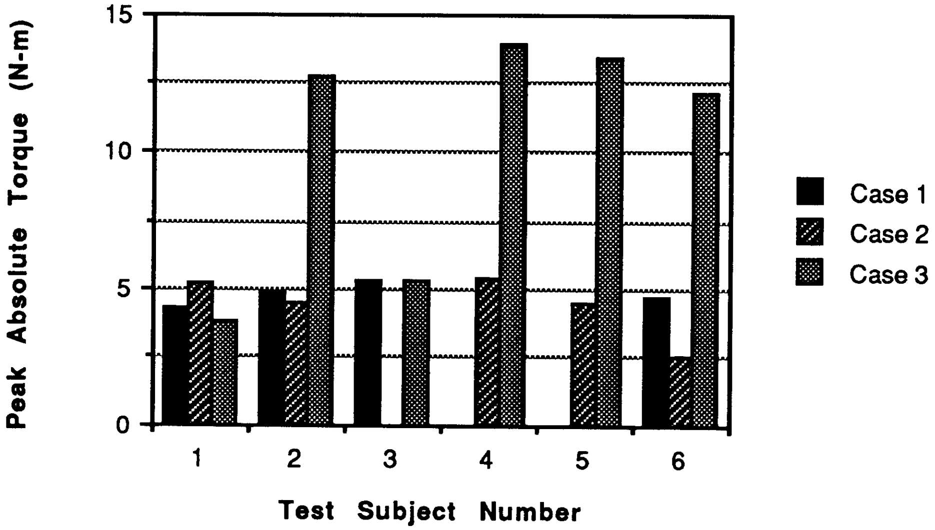

Figure 8-10: Peak -Y Torque v. Restraint Cases

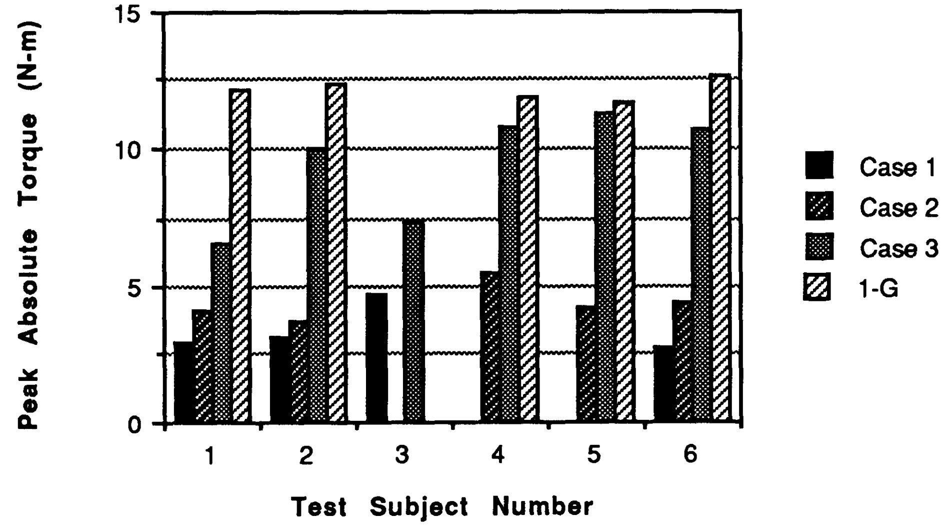

Figure 8-11: Peak +Z Torque v. Restraint Cases

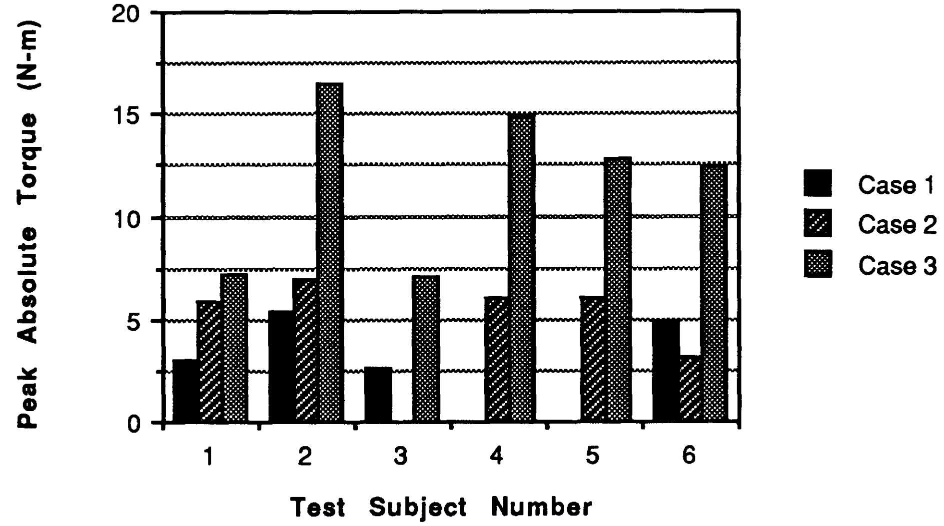

Figure 8-12: Peak -Z Torque v. Restraint Cases

8.1.2 Peak Reactions versus Restraint Cases: Correlation

In this section, the Student's test or t-test was performed on the data in an attempt to confirm or deny the trend noticed in the previous figures. Namely, that as a subject is more fully restrained, they can apply higher peak reactions. The author considers the single handrail and foot restraint (Case 2), more restraining than the two handrail restraint system (Case 1), as it more fully limits the motion of the subject's body. The t-test will also be used to confirm that the peaks achieved in neutral buoyancy, regardless of restraint type, are lower than those achieved in normal gravity.

A t-test is used to give a statistical confidence figure to a perceived trend. If two different batches of data are compared using a t-test, the test provides a confidence (between 0 and 1) that those two batches are the result of two different phenomena. It achieves this through use of the standard deviation of the difference between the means of the two batches, as well as the batch size itself. Thus, the test is purely a statistical one, unrelated to the process(es) at work. These tests were performed on a Macintosh™ SE using *StatView™ 1.0*.

Table 8-1 below displays the minimum confidence value for each reaction type, comparing each restraint case against all the others. Although the confidence value given is a minimum, StatView actually presents a confidence range. The range a particular comparison is in can be determined from the minimum values presented in Table 8-1. These ranges are shown in Table 8-2. It was decided that a 0.95 confidence or better would indicate a clear trend. This number was chosen as it encompasses three standard deviations of the data. Those cases which did not achieve this level of confidence are denoted with an asterisk in Table 8-1.

Reaction	1 v. 2	1 v. 3	1 v.1-G	2 v. 3	2 v.1-G	3 v.1-G
Fx +	0.995	0.9995	0.9995	0.975	0.975	* 0.9
Fx -	0.95	0.9995		0.99		
Fy +	0.95	0.9995	0.995	0.995	0.9995	0.95
Fy -	0.95	0.9995		0.975		
Fz +	0.975	0.9995	0.995	0.95	0.995	0.975
Fz -	0.975	0.9995		0.975		
Tx +	* 0.9	* 0.6	0.975	* 0.625	0.9995	0.99
Tx -	* 0.6	0.995		* 0.9		
Ty +	* 0.6	0.99	0.99	0.995	0.995	* 0.9
Ty -	* 0.625	0.95		0.975		
Tz +	* 0.625	0.995	0.9995	0.995	0.9995	0.975
Tz -	0.975	0.975		0.975		
All Forces	0.9995	0.9995	0.9995	0.9995	0.9995	0.9995
All Torques	0.95	0.9995	0.99	0.9995	* 0.9	* 0.6

Table 8-1: T-Test Confidence Values for Comparison of Restraint Cases

Maximum Confidence	Minimum Confidence
1	0.9995
0.9995	0.995
0.995	0.99
0.99	0.975
0.975	0.95
0.95	0.9
0.9	0.625
0.625	0.6

Table 8-2: T-Test Confidence Ranges

An examination of Table 8-1 shows very high confidence figures for the majority of comparisons. This is especially true when all the forces (regardless of direction) were compared for each restraint case, confirming the general trend. Of the twelve cases which did not meet the confidence criterion, 11 involved torques. The single case outside those 11 was a minimum confidence of 0.9 for restraint Case 3 versus normal gravity when applying positive X force. Five of the comparisons failing the confidence test are torque applications for Case 1 versus Case 2. Therefore, it would be difficult to claim on the basis of this data that the single handrail and foot restraint provide better conditions to apply torque than the two handrail case. This makes some sense when one considers the fact that both restraint systems have the same number of restraint points, the major difference being the size of the lever arm involved (0.76 m between handrails, 1.5 m (in Z) from the right handrail to the foot restraints).

The trend of higher peak force output from Case 1 to Case 2 to Case 3 to normal gravity, is clearly confirmed however, especially Case 1 versus 3. This is probably the single most obvious conclusion gleaned from this area of data analysis. The upward trend for peak torques other than ±Tx, when omitting the Case 1/Case 2 comparison, is also confirmed.

When noting the comparison for all torques, a 0.6 confidence is observed, for Case 3 restraint versus the 1-G case. A strong reason for this may be that the subject did not have a left handrail for the 1-G case, so that this test is more comparable to Case 2 (which had 0.9 confidence), rather than to Case 3 where the subject has foot restraints and two handrails.

8.2 Peak Reactions versus Subject Parameters

In this section the relationship between peak reactions and two subject parameters: height and mass, were considered. The driving reason behind this comparison was to determine what other parameters beyond restraint case might be influencing the peak force. If it were found that the reaction output varied strongly with either parameter, regardless of restraint type, then the results noted in the previous section may have been driven by the parameter and not the restraint case. Height and mass were chosen over other parameters due to the fact that they were easily quantifiable, other variables such as physical strength or experience were not.

To perform this investigation, the peak values for a given reaction were compared against the subject parameters for each separate restraint case. Both linear and higher order curve fits were applied, and examined to see if they were of the same form regardless of restraint case. "Same form" indicates the same slope for a linear curve fit, or the same shape for higher order fits. Polynomial fits up to the fifth order were attempted, however, only some samples are shown.

8.2.1 Peak Reactions: Correlation with Subject Height

Figure 8-13 provides an example of what is being attempted with this type of correlation. Each of the sets of peak +X forces (one set per restraint case) is being displayed versus subject height in meters. Linear fits were then performed on each set and the results shown. The value beside each linear fit, R^2, refers to the square of the correlation coefficient, a perfect fit having an R value of 1.000. R^2 is also referred to as the coefficient of determination.

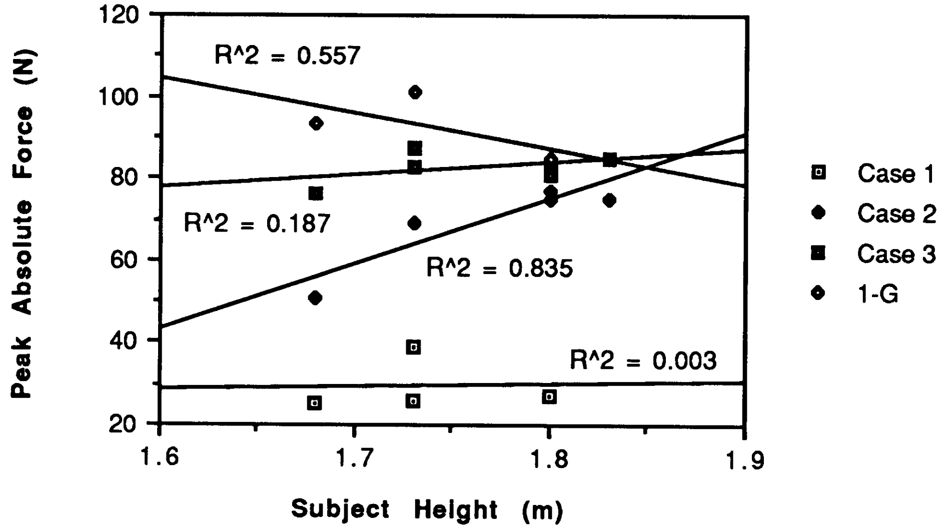

Figure 8-13: Correlation: Peak +Fx versus Subject Height- Linear Fits

As can be immediately seen, only the least squares linear fit to Case 2 has a high level of correlation (R^2 = .835). In addition, there is no similarity between the slopes of any two lines. Such a similarity might indicate a linear relationship between subject height and peak

+Fx force regardless of restraint case. Such a relationship cannot be conjectured from this data.

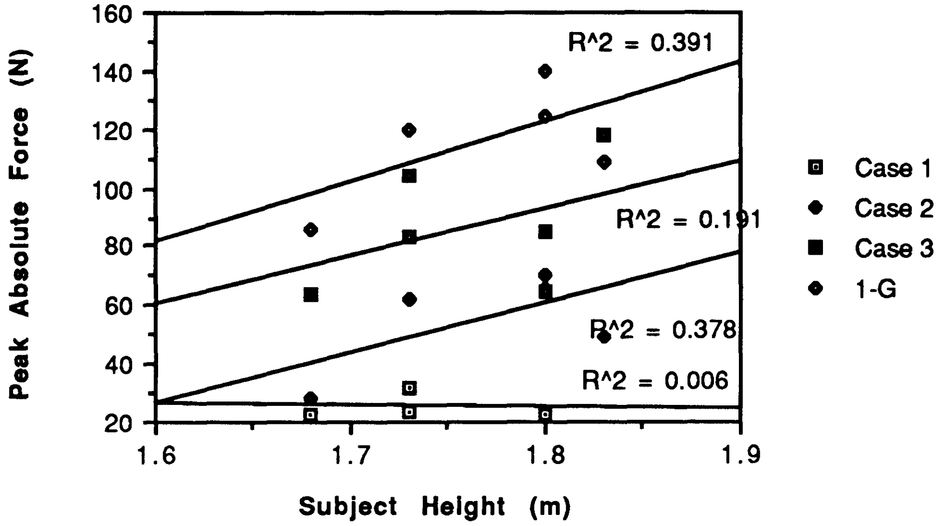

Figure 8-14: Correlation: Peak +Fy versus Subject Height- Linear Fits

Figure 8-14 is a further example of the type of results linear fit attempts produced. This comparison provides the closest slopes between any cases, with the slopes of Cases 2 and 3 within 96% of each other. However, the correlation coefficients remain woefully low. For no linear fit attempt for the parameter height, was an R-squared value better than 0.835 achieved.

Obviously, there is no clear linear relationship between peak reactions and subject height. Higher order fits were then investigated, to look for any trends therein.

Figure 8-15 shows an example second order fit.

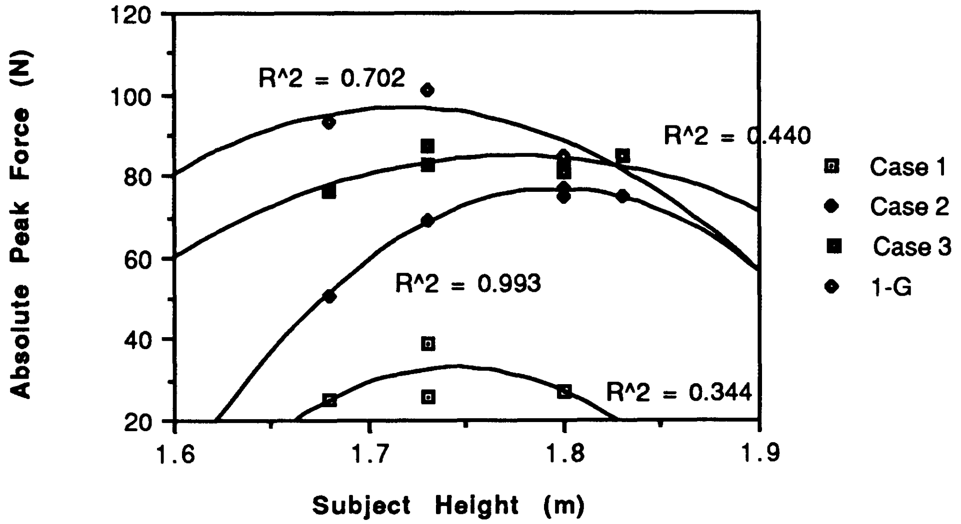

Figure 8-15: Correlation: Peak +Fx versus Subject Height- Second Order Fits

As is clearly shown, the fits become better as the order increases. This is also true for fourth and fifth order fits versus third, but the increase is slight. What can also be seen is the lack of any similarity in the fits regardless of case.

These plots are representative of all the reactions. Although the fits to the data appear to indicate higher (third and up) order correlations between subject height and peak reactions; this correlation does not seem independent of restraint case. Rather, it appears to be a simple function of the fact that correlation improves as the order of the fit approaches the number of data points. It would appear, therefore, that restraint case is a far more important influence on peak output reactions than height.

It should also be noted that there was little variety in the height of subjects tested, due to the restricted pool of test subjects, i.e. subjects available for the several hours of testing and preparation, as well as being dive qualified. The height range was between 1.68 and 1.83 meters, a 0.15 meter range, with a mean of 1.762 m and a standard deviation of only 0.057 m (3% of the mean).

The subjects' masses were also not as varied as would be liked, but here there were values from 53 to 112 kg, a 59 kg range, with a mean of 81.833 kg and a standard deviation of 20.044 kg (24% of the mean).

8.2.2 Peak Reactions: Correlation with Subject Mass

The same investigation conducted for height was conducted again for subject masses. Figure 8-16 shows a linear fit attempt for +Fx.

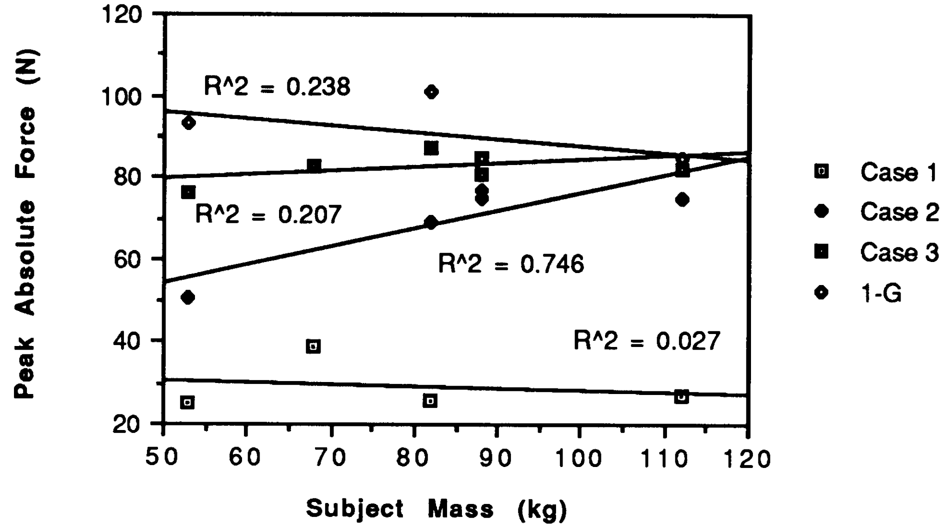

Figure 8-16: Correlation: Peak +Fx versus Subject Mass- Linear Fits

As before we see poor fits which improve with each successive higher order, although reaching a plateau of sorts from third-order on. Again, there appears to be no underpinning relationship between output reactions and subject mass.

8.2.3 Peak Reactions' Correlation- Conclusions

There appears to be little in the way of strong correlations of any order between peak output reactions and either subject mass or height. For the height case, it becomes apparent when considering the standard deviation of the subjects' height that few conclusions should be attempted, especially in the light of the least-squares fits.

While the same is not true for the masses, due to a larger variety, once again the fits provide no conclusive data. As a general rule, linear fits showed increasing output with height or mass, but are extremely inconclusive. As an attempt to provide statistical support to this vote of "no confidence", t-tests were performed on both the height and mass data, producing matrices similar to Table 8-1.

Table 8-3 presents the height-based t-tests. Once again, the values shown in this table are minimum confidences that the two sets of data were produced by different processes. In other words, it provides numerical support for or against a supposition that greater height indicates a greater ability to produce peak reactions. The range of confidence can once again be found in Table 8-2.

The four values compared in Table 8-3 are the four different heights found in the subject pool in ascending order. Height 1 represents subject 1 at 1.68 m, height 2 represents subjects 3 and 6 at 1.73 m, height 3 represents subjects 2 and 5 at 1.80 m, and height 4 represents subject 4 at 1.83 m. In the cases where two subjects had the same height value, an average of both subject's peak reactions for a particular case was used. If, due to the incompleteness of the data, two values were not available, only the single value was used.

Reaction	1 v 2	1 v 3	1 v 4	2 v 3	2 v 4	3 v 4
Fx +	0.975	0.625	0.625	0.625	0.625	0.625
Fx -	0.625	0.625	0.625	0.625	0.625	0.6
Fy +	0.975	0.9	0.95	0.6	0.6	0.6
Fy -	0.625	0.625	0.625	0.625	0.9	0.625
Fz +	0.95	0.95	0.9	0.625	0.6	0.625
Fz -	0.625	0.9	0.625	0.9	0.9	0.6
Tx +	0.9	0.975	0.625	0.625	0.95	0.625
Tx -	0.9	0.9	0.625	0.625	0.625	0.625
Ty +	0.99	0.9	0.625	0.625	0.625	0.9
Ty -	0.625	0.625	0.625	0.625	0.625	0.625
Tz +	0.95	0.625	0.625	0.6	0.6	0.625
Tz -	0.6	0.625	0.625	0.9	0.9	0.9
All Forces	0.9995	0.9995	0.9995	0.625	0.625	0.625
All Torques	0.995	0.9995	0.975	0.975	0.625	0.9

Table 8-3: T-Test Confidence Values for Comparison of Subject Heights

As may be inferred from the curve fit attempts, little confidence is found in any height based assertion. If a minimum level of confidence is once again set at 0.95, only 16 comparisons meet that criteria. Fourteen of those are in comparisons involving height 1. Height 1 represents the height of subject 1, who is physically weaker than the other subjects. Since the t-tests do not tend to confirm any height based trends between any other two height levels, it is doubtful that the process at work between height 1 and the others is solely the result of the height difference.

Table 8-4 fills a similar matrix for masses and was developed in the same manner as the matrix for heights. Five cases were compared: mass 1 being 53 kg and representing subject 1; mass 2, 68 kg, subject 3; mass 3, 82 kg, subject 6; mass 4, 88 kg, subjects 4 and 5; and finally, mass 5, 112 kg, subject 2.

Reaction	1 v 2	1 v 3	1 v 4	1 v 5	2 v 3	2 v 4	2 v 5	3 v 4	3 v 5	4 v 5
Fx +	0.625	0.95	0.625	0.625	0.625	0.625	0.6	0.625	0.6	0.625
Fx -	0.975	0.625	0.625	0.625	0.625	0.625	0.625	0.625	0.625	0.625
Fy +	0.625	0.95	0.995	0.95	0.625	0.625	0.625	0.625	0.6	0.6
Fy -	0.9	0.625	0.625	0.625	0.625	0.625	0.625	0.625	0.95	0.975
Fz +	0.625	0.9	0.975	0.95	0.625	0.625	0.6	0.625	0.9	0.625
Fz -	0.9	0.625	0.625	0.9	0.625	0.625	0.625	0.625	0.625	0.6
Tx +	0.625	0.975	0.625	0.95	0.6	0.625	0.625	0.6	0.6	0.6
Tx -	0.9	0.625	0.625	0.9	0.9	0.625	0.625	0.625	0.625	0.625
Ty +	0.6	0.9	0.9	0.625	0.625	0.625	0.625	0.625	0.625	0.625
Ty -	0.625	0.625	0.625	0.625	0.625	0.625	0.625	0.625	0.625	0.625
Tz +	0.625	0.625	0.625	0.625	0.6	0.625	0.6	0.6	0.9	0.9
Tz -	0.625	0.625	0.625	0.625	0.625	0.625	0.625	0.9	0.9	0.9
Forces	0.9995	0.9995	0.9995	0.9995	0.625	0.625	0.6	0.6	0.9	0.625
Torques	0.975	0.995	0.995	0.995	0.9	0.99	0.625	0.625	0.625	0.6

Table 8-4: T-Test Confidence Values for Comparison of Subject Masses

Looking once again at a 0.95 confidence cutoff, Table 8-4 has 20 out of 140 elements meeting that criteria (compared to 16 of 84 in the height table). Seventeen of those are in comparisons involving subject 1 alone. As it has already been indicated that subject 1 may be a pre-biased case, other comparison sets must be examined before confirming any mass based trend. Cursory observation of Table 8-4 reveals that the trend seemingly confirmed by pairings involving subject 1 (indicating increasing peak reactions with increasing mass) is not borne out by any other pairing. Thus, this data indicates no strong correlation between subject mass and peak reactions.

It seems likely therefore, that a driving factor in the magnitude of peak reactions output by the subject pool is highly dependent on restraint case, especially for forces, and is not heavily influenced by subject mass. It is also probable that subject height does not provide a strong influence, although the lack of variety in the subject height pool makes any conclusion strained.

Chapter 9: Conclusions and Suggestions for Further Research

To a large extent, the conclusions derived from the investigations in this work are presented completely in the two preceding chapters. This chapter, while it does recap many of the findings, serves mainly as a watershed from which the ideas for future research on these, and similar, topics may grow. Obviously, the experimental apparatus in Chapter 5 provides a powerful tool for investigating neutral buoyancy biomechanics. In addition, it could also be used to provide benchmarks for comparisons between astronauts and telerobotic or robotic servicers. The suggestions for further research, while using the conclusions in this document, tend to concentrate on how to use this research tool to the widest extent. It should be noted that the two topics mentioned in the chapter title are interwoven throughout the following text.

9.1 Static Modeling

9.1.1 Restraint Case 1- Two Handrails

Of the two static models which were to be confirmed with actual sensor data, Case 1 contained the greatest amount of error between predicted and measured results. This was due to the fact that, unlike Case 2 where the subjects' feet were restrained, subjects in Case 1 had their lower bodies free. This allowed for rotations to occur, leading to a breakdown in reaction conservation. Under actual zero gravity conditions, these rotation producing moments would be accounted for when the subject applied equal-and-opposite braking forces to stop rotation. In neutral buoyancy the subject does not need to apply this braking force, as fluid drag retards the rotation of its own accord. The KCL models cannot account for the kinetic energy lost into the fluid, producing poor predictions. These problems are exacerbated because applied forces as well as torques interact to produce these rotations, leading to a general, rather than a specific, failure of the KCL model. As a result, the KCL model cannot be recommended for use as a predictor of the reactions seen in this restraint case.

Although it is clear that the KCL model should not be used as a reaction predictor for this type of restraint if rotations occur, it would be beneficial to confirm that the rotation and fluid effects are the variables responsible for the breakdown. To accomplish this, the author presents two methodologies.

The first is to prevent the rotations from occurring. A simple and safe method is to request that the subjects maintain a desired orientation, despite the fact that in actual operations such a constraint might not exist. Rotations will still occur; however, braking reactions would become necessary and appear on the sensors. As long as subject reaction time was short, general reaction conservation should be confirmed. Less safe is some restraint system which immobilizes the lower body. However, such a restraint system could not work without producing a reaction profile of its own, which must, in turn, be measured. Thus, such a test rig would look like restraint Case 3. If Case 3, which prevents rotation, does not exhibit conservation of reactions, then rotation/fluid effects may not be the primary factor. As might be expected, however, restraint Case 3 did generally exhibit conservation of reactions. Reasons for lack of complete conservation in all cases are discussed in Chapter 7, and center around compliance in the foot restraint binding system. This allowed forces to be expended into the bindings rather then being transmitted to the sensor. Such a situation was allowed to continue because compliant bindings allowed the subjects easy egress in the event of an emergency. Barring this fact, however, the Case 3 data supports the idea that rotation and fluid effects are the factors responsible for the breakdown of the Case 1 model.

The second idea would be to develop a graphic program which uses the applied and measured reaction values at both handrails, as well as the model of fluid drag effects mentioned in Chapter 3, to display the rotation of the subject. This mathematical model would use dynamic motion equations of the type developed in [Cousins, 1987] (see

Chapter 2). Both handrails would provide data to the model, the results being an animated three-dimensional display. This dynamic graphic display could then be compared against videotape of the task being performed to see if the rotations match. This would require synchronization of the display and tape, animation software, and a reasonably powerful and fast graphic station. The display and videotape could be compared quickly as a general confirmation, or frame-by-frame for a complete conservation of reactions analysis. If the rotations match, this would indicate that the cause of KCL model error is probably subject rotation and fluid effects.

9.1.2 Restraint Case 2 - Right Handrail and Foot Restraints

The addition of foot restraints prevented the error causing motions found for tasks conducted with restraint Case 1, greatly increasing fidelity between the KCL model and the measured reactions. The addition of foot restraints also added a new source of error, however, to the pre-existing sensor measurement and joint angle measurement errors. The foot restraints used in testing exhibited compliance, allowing some of the magnitude of the reactions to be lost into flexure of the binding rather than being transmitted to the sensor. This new error source was not of the magnitude of the errors in Case 1, therefore the author is hesitant to advocate more rigid foot restraints unless greater safety precautions are taken.

The quality of the predictive model is quite good, despite existing errors. The addition of some form of accurate real-time joint angle measurement system, as well as system upgrades to reduce sensor noise towards their theoretical minimums could virtually remove much of the existing inaccuracy. Even without these upgrades, the KCL model appears to be valid for the range of tasks and variables tested in the neutral buoyancy environment.

9.1.3 Restraint Case 3 - Both Handrails and Foot Restraints

As seen in Chapter 7, the proposed empirical model for describing the distribution of reactions in this indeterminant restraint case could not be supported through testing. No set of constants was found which described how reactions were divided between the right handrail-left handrail and right handrail- foot restraint reaction paths, regardless of task or subject. The interactions along one reaction path caused changes in the reactions on the other path which were not proportional to the values seen in the previous restraint cases. The combination of interactions between the paths exhibits itself as reactions along a path between the foot restraints and left handrail, and these values could be determined from the measured data by applying conservation of reactions. Examination of this data found the interactions on this path to be time and task varying which disallows the empirical model proposed as an accurate predictor of the results.

The three-point data did prove somewhat useful however, as confirmation of dynamic motion as the error-causing agent in Case 1, as mentioned above.

An obvious area for future research would be an investigation of the actual type of systematic reaction distribution occurring for the three-point case, if one exists.

9.2 Energy Expenditure

As discussed in Section 7.3, the reaction-time areas gleaned from the recorded reaction profiles provides a method for non-invasively estimating physiological workload. To get useful data on this subject, however, a correlation to some other commonly used yardstick for energy consumption must be found. Among the choices are heart rate measurement and calculation of the rate of oxygen consumption. Oxygen (in the form of compressed air in tanks) is an essential consumable in neutral buoyancy testing. A simple glance at the air pressure gage prior to, and immediately following a test run provides a first cut at the amount and rate of oxygen consumption. It seems an obvious choice, therefore, to correlate the reaction-time areas to oxygen consumption as a first step in energy expenditure research.

This type of research would require some changes in the testing process. Among them would be the inclusion of a more precise regulator gage, perhaps one linked to a data collection system. In addition, tasks of longer duration should be performed, to allow for aerobic activity to dominate, permitting an accurate correlation to be made.

An important area of further research for both energy expenditure estimation and static modeling is in the regime of more complex tasks. Testing should be conducted with longer tasks composed of several of the simple tasks performed in this research. The KCL model for Case 2 should be able to provide a good prediction of the task outputs as long as the subtasks (± Fx, ± Fy, ± Fz, ± Tx, ± Ty, ± Tz) can be identified. This is also true for energy expenditure.

9.3 Peak Reactions

Chapter 8 presents interesting data on the peak forces and torques applied by the subject pool. The most important conclusion derived from the data is that the method of restraint of a subject has a strong influence on his or her peak reaction magnitude. A subject supported by a left handrail while performing tasks on a right handrail produced lower peaks than any other restraint cases. This was certainly true for forces, although the gap between this restraint case and Case 2 for torque application is small. Restraint Case 2 represents a subject in foot restraints, performing tasks on the right handrail, unsupported by the left hand. As mentioned this system did not provide a clear advantage in torque output over Case 1, but did provide an advantage in forces. It was also less advantageous in all respects to restraint Case 3, as was Case 1. Case 3 has a subject using both the left handrail and the foot restraints for support while performing tasks on the right handrail. In this restraint system higher peak reactions were seen regardless of type. Benchmarks in normal gravity were taken and compared to all three cases, and as expected, peak reactions were higher in 1-G than for any neutral buoyancy restraint case.

In order to illuminate what factors, other than restraint case, might be influencing peak reaction output, the subjects' height and mass were examined as parameters. These were selected as two values which were quantifiable, and seemed likely to have an influence. No mass or height-dependant influence was discovered, although the lack of variability in the subject pool (especially for height) weakens any conclusions. Further testing should be performed with a greater range of subject heights to confirm the lack of any height-based influence on peak reactions.

9.4 Suggestions for Further Hardware Development and Research

9.4.1 Distributed Data Acquisition

Section 5.6 presents a distributed data acquisition scheme which, if implemented, would allow for greater noise rejection and a much higher data rate. Achieving data rates around 20 Hz (a 40-fold higher data rate than at present), would allow for accurate dynamic force modeling of human activity. The tasks and models in this study are essentially static, greater data rates would allow the same test architecture to be used to examine this type of dynamic tasks and modeling.

In addition to the data acquisition hardware upgrades, advances in software upgrades would be useful also. The present system records data in the rawest form, as bridge voltages, which are later processed. Now that the system's viability has been confirmed, the further processing could be incorporated in real-time. This combination of the functions of *puff.c* and *smaug.c* would allow immediate assessment of test activities. Obviously, the original software would be retained to allow for debugging of future problems. What may also be useful is the conversion of *Kinematic Chain Link* into a module of *smaug.c*. Such a module would take the right handrail inputs and calculate the model predictions in real time, along with the present output. These software upgrades would require a faster topside computer with greater memory capacity. It should not be difficult however, to find a better computer than the present 6 MHz, 10 Mb PC-XT machine, *Mycroft*.

9.4.2 Underwater Signaling Upgrade

This device was to have been implemented for this research. An underwater signal, such as a light, would be used as the start/stop cue to the test subject, rather than the present series of hand signals. The signal would be tripped by the data acquisition program, allowing for more accurate measurements of task duration. The disadvantage to such a system is that it removes a degree of feedback between the test conductor and the subject. During this research, such feedback proved necessary time and again, as the hardware, software, and tasks were all being broken in.

9.4.3 Instrumented Regulator

As mentioned in Section 9.2, the subject's air supply regulator gage would provide a good method of estimating oxygen consumption. Such data could then be used to correlate the reaction-time areas discussed in Chapter 7. Such instrumented breathing apparatuses exist, and the presence of a safety diver rules out much of the danger associated with problems with such a device. In fact, during this testing, no problems were ever encountered which placed a subject in danger, as the restraints could be removed and the subject was always near the surface.

9.4.4 Reconfigurable Test Set-Up

Developing a test rig in which the relative locations of the handrails and foot restraints could be changed easily underwater, would allow for examination of reach envelopes. In particular, a subject's ability to apply various reactions at various points in his or her reach envelope could be determined.

9.5 Final Note

A major suggestion of the author applies to all human factors testing. Test more. More subjects, with more variety, for longer durations. Limitations on access to testing facilities, limited numbers of scuba subjects, and hardware problems combine to restrict or invalidate amounts of data. However, to draw conclusions across a population requires a semi-representative sample. The author notes with pleasure that the FAFNIR (Force Assessment For Neutral-buoyancy Investigation and Research) data acquisition system is moving to an environment where long duration testing will be possible, and will be able to investigate the many questions which this work raises, but leaves unanswered.

References

Bowden, Mary L. *Dynamics of Manual Assembly of Large Space Structures in Weightlessness*. S.M. Thesis, Massachusetts Institute of Technology, January 1981.

Brouha, Lucien. Physiology in Industry: Evaluation of Industrial Stresses By the Physiological Reactions of the Worker. Pergamon Press, New York, 1960, 99-108.

Chaffin, D., and Andersson, G. Occupational Biomechanics. Wiley, New York, 1984.

Coermann, R. R. *Mechanical Vibrations*. Ergonomics and Physical Environmental Factors. Occupational Safety and Health Series Number 21, International Labor Office, Geneva, 1970.

Cousins, Daniel . *Biomechanics of Extravehicular Activity and its Neutral Buoyancy Simulation*. Ph.D. Thesis, Massachusetts Institute of Technology, June 1987.

Epsilonics- Anonymous, *Modern Strain Gage Transducers... Their Design and Construction*. Articles from Epsilonics, October 1981 - August 1983.

Hanson, Dotson, Jau, South. *A Force-Torque Sensor Subsystem for the Space Shuttle Remote Manipulator System*. Jet Propulsion Laboratory, Pasadena, 1988.

Huston, R. L., and Passerello, C. E. *On the Dynamics of a Human Body Model*. Journal of Biomechanics, 1971, 4, 369-378.

ICS- Anonymous. Model 6A21 Analog Input Card Reference Manual. Industrial Computer Source, San Diego, 1988.

Nubar, Y., and Contini, R. *A Minimum Principle in Biomechanics*. Bulletin of Mathematical Biophysics, 1961, 23, 377-391.

Omega Engineering. Omega Complete Pressure, Strain, and Force Measurement Handbook and Encyclopedia. Volume 26. Omega Engineering, Stamford, 1988, E41-E44.

Paines, J.D.B. *A Review of Hydrodynamic Forces in Neutral Buoyancy Simulation of Microgravity EVA or IVA*. MIT Space Systems Laboratory Report # 17-86, Cambridge, 1986.

Roozbazar, Aziz. *Biomechanical Modeling of the Human Body*. Proceedings of the Human Factors Society 17th Annual Meeting, October 16-18, 1973, 181-191.

Seireg, A., Baz, A., and Patel, D. *Supportive Forces on the Human Body During Underwater Activities*. Presentation at the 4th Annual ASME Biomechanics Conference June 1-2, 1970, Washington D.C.

Suggs, C. W., and Abrams, C. F. *Simulation of Whole Body Dynamics*, 1973, Personal Communication to Roozbazar, A.

Tomusiak, Marian. *Simulation of Zero-G Dynamics of Assembly of Large Space Structure Components*. S.M. Thesis, Massachusetts Institute of Technology, May 1978.

Whitsett, C. E. *A Mathematical Model to Represent Weightless Man*. Aerospace Medicine, January 1964, 11-16.

Young, Warren C. Roark's Formulas for Stress and Strain, Sixth Edition. McGraw-Hill, New York, 1989.

Appendix A: Software

Written in Microsoft C™ for use on a 6 MHz IBM PC-XT™:

1) puff.c	data acquisition software

Written in Think C™ for use on a Macintosh SE™:

2) smaug.c	data reduction/conversion software

Written in Microsoft Excel™ for use on a Macintosh SE™:

3) Kinematic Chain Link	static human modeling software
4) Moments of Inertia	dynamic human modeling software
5) Sensor Design	force/torque sensor modeling software

Puff.c Fafnir Data Acquisition Software

Written in Microsoft C™ for the IBM PC-XT

```
/*_ puff.c  Thu Feb 8 1990  Written by: S.Chakraborty & S.Druker */
/*
 *    Program for data acquisition on the 6A21 Analog Input Card
 *    from Industrial Computer Source.
 *    Includes some data breakdown, formatting, and masking
 *    Card is hooked up in Mycroft, in the funky Fafnir setup.
 *    First Written:  Mon Jan 15  1990  by: S.Druker and S.Chakraborty
 *    Works best under Zortech C compiler with : ztc puff.c
 *    For Microsoft C : cl puff.c
 *    Thanks to Rob Sanner, Terry Fong, Ender St. John, Sandy Alexander
 */

#include      <stdio.h>
#include      <conio.h>
#include      <string.h>
#include      <stdlib.h>
#include      <time.h>
#include      <io.h>

/* Set Default Filename */
char    filename[80]   = "fafnirss.dat";

/* Set Port Parameters for IBM I/O */
#define PORT_0        0x0300
#define PORT_1        PORT_0 + 1
#define PORT_2        PORT_0 + 2
#define PORT_3        PORT_0 + 3

/*
 *    gain on bits 5,6 and bit 7 is RUN/HOLD
 *    Gain Mask is defined below for default gain of 1
 *    gain of 10 is 0x20, gain of 100 is 0x40 or 0x60
 */

#define GAIN          0x00
#define RUN_HOLD_ZERO   0x00
#define RUN_HOLD_ONE    0x80

/*
 *    port0 controls channel select through bits 0-4,
 *    through the actual value of the 5 bit number.
 *    Status (for polled mode) is bit 1 on port1, we'll look for that
 */
```

```
#define STATUS        0x02

/* Define Variables */
int main(int argc, char* argv[])
{
    long          time = 0;
    FILE          *fp;
    unsigned char   channel= 0x00;
    unsigned int   number1;
    unsigned int   number2;
    unsigned int   number3;
    unsigned int   number4;
    unsigned int   number5;
    unsigned int   number;
    unsigned int   h;
    unsigned int   g = 0;
    unsigned char   i;
    unsigned char   j;
    unsigned char   k;

  /* Check for filename validity */

    if (argc > 1)
        strcpy(filename,argv[1]);

    if ((fp = fopen(filename, "r")) != (FILE*) NULL)
    {
        fprintf(stderr,"fafnir: file \"%s\" exists.\n", filename);
        exit(-2);
    }

    fclose(fp);
    if ((fp = fopen(filename, "w")) == (FILE*) NULL)
    {
        fprintf(stderr, "fafnir: could not open file \"%s\".\n",
            filename);
        exit(-2);
    }


    /* Start actual data acquisition, continue until ESC hit */

    printf("Fafnir data acquisition program commencing, data being\n");
    printf("written to file \"%s\".\n", filename);
    printf("Hit ESC to stop taking dat, Ctrl-Break will abort with\n");
    printf("possible loss of data.\n");

    /* Channel select and record time */
    for(channel = 0x00; ;channel = (channel + 1) % 0x06, time++ )
    {
        /* write out time if desired, 4 make a complete data set */

        /* fprintf(fp,"\n%ld\t",time); */
```

```
    /* ESC section */
    if (kbhit())
          if (getch() == 27) break;


/* module channel select */
    for (i = 0x00; i < 4; i++)
    {

          /* Write out i/o channel if necessary */
          /* fprintf(fp,"\ti %d\t",i); */

          /* invert i/o select, and bit shift*/
          /* since lower two bits are read only*/
          j = ~i;
          j = j << 2;

          outp(PORT_3, j);

          /* Channel select write */
          outp(PORT_0, GAIN | channel | RUN_HOLD_ZERO);

          /* Wait ten milliseconds for settle */
          k += 5;

          /* Configure Port to Read Values */
          outp(PORT_0, GAIN | channel | RUN_HOLD_ONE);
          while (!(inp(PORT_2) & 0x02)) ; /* wait for high */
          while (  inp(PORT_2) & 0x02 ) ; /* wait for low */
          outp ( PORT_0, GAIN | channel | RUN_HOLD_ZERO);

          /* Read in both ports and store as two-byte value*/
          number1 = inpw(PORT_0);
          number2 = inpw(PORT_1);
          number2 = number2 << 8;
          number = number2 | number1;

          /* mask out overrun error */
          number3 = number & 32768;

          /* mask out polarity*/
          number4 = number & 16384;
          number4 = number4 >> 12;

          /*output overrun indicator or polarity*/
          if(number3 != 0)
          {
                fprintf(fp, "o");
          }
          else if(number4 != 0)
          {
                fprintf(fp, "+");
          }
          else
```

```
            {
                fprintf(fp, "-");
            }

            /* mask for data */
            number5 = number & 4095;

            /* Put number in output */
            fprintf(fp, "%d \t", number5);

            if(g++ == 23)
            {
                fprintf(fp, "\n" );
                g = 0;
            }
        }
    }
    fclose(fp);
}
```

Smaug.c Fafnir Data Reduction Software

Written in Think C™ for the Macintosh SE

```
/* Smaug.c */
/* Written by Sayan Chakraborty */
/* With much assistance from Sam Druker */
/* In Think C v4.0 on Macintosh SE */

/* Program converts data in text files */
/* From gage voltages to reactions */

/* For sequential fixed model */

/* DEFINE to 1 for debugging output,
                        0 otherwise           */

#define DEBUG 0

#define FOREVER for(;;)

# include <math.h>
# include <stdio.h>
# include <string.h>
# include <stdlib.h>

static char     dummy_buf[2048];
static  char    end_filename[] = "end";

int main(int ac, char** av)
{
        int             index;
        FILE    *infile, *outfile;
        char    NAME1[15], NAME2[15];
        float   v[25], r[19];                           /* v and r are offset one from
                                                        bottom of array (v[1]) to
                                                        corresponds to old v1, v3, r3.
*/

        /* Read files until "end" is typed */
        FOREVER
        {
                int     lineno = 0;

                printf("\nEnter Name of Source File:  ");
                scanf("%s", NAME1);
                getc(stdin);

                if (!(strcmp(NAME1, end_filename)))
                        exit(1);
```

```
                strcpy(NAME2, NAME1);

                /* delineate converted data with .n */
                strcat(NAME2, ".n");

                /* File error handling */

                if (!(infile = fopen(NAME1, "r")))
                {
                        printf("Could not open %s\n", NAME1); goto next_file;
                }

                if (!(outfile = fopen(NAME2, "w")))
                {
                        printf("Could not open %s\n", NAME2); goto next_file;
                }
                printf("Opened %s and %s for data conversion\n", NAME1, NAME2);


                FOREVER                 /* While lines o' data */
                {
                        /* Read in 24 data elements */
                        lineno++;
                        for (index = 1; index < 25;index++)
                        {

                                if (fscanf(infile, " %f", v + index) == EOF)
                                        goto next_file;

                        }
                        getc(infile);
                        printf("Read line o'data #%d\n", lineno);

                        /* Debugging Output */
#if DEBUG
                        for (index = 1; index < 6; index++)
                                        printf("%10.5f\t", v[index]);
                        if (!(lineno % 10))
                        {
                                printf("Does this look OK?\n");
                                if (getchar() != 'y')
                                {
                                        fgets(dummy_buf, 2048, stdin);
                                        break;
                                }
                                else
                                {
                                        fgets(dummy_buf, 2048, stdin);
                                }
                        }
#endif
                        /* Calibration specific to subject & day */
                        v[1] = v[1] + 3790;
```

```
v[2] = v[2] + 3433;
v[3] = v[3] + 3778;
v[4] = v[4] + 3269;
v[5] = v[5] + 3782;
v[6] = v[6] + 3446;
v[7] = v[7] + 3762;
v[8] = v[8] + 3247;
v[9] = v[9] + 0;
v[10] = v[10] + 0;
v[11] = v[11] - 0;
v[12] = v[12] - 0;
v[13] = v[13] - 0;
v[14] = v[14] - 0;
v[15] = v[15] + 0;
v[16] = v[16] - 0;
v[17] = v[17] - 0;
v[18] = v[18] - 0;
v[19] = v[19] - 0;
v[20] = v[20] - 0;
v[21] = v[21] + 0;
v[22] = v[22] - 0;
v[23] = v[23] - 0;
v[24] = v[24] - 0;


/* Calculate Resultant Reactions from Calibrated Voltages */


/* Right Handrail */
if(!(v[1] && v[3] && v[5] && v[7]))
        r[1] = 0;
else
        r[1] = -0.04119 * (v[1] + v[3] + v[5] + v[7]);
if(!(v[2] && v[6]))
        r[2] = 0;
else
        r[2] = -0.04119 * (v[2] + v[6]);
if(!(v[4] && v[8]))
        r[3] = 0;
else
        r[3] =  -0.04119 * (v[4] + v[8]);
if(!(v[2] && v[4] && v[6] && v[8]))
        r[4] = 0;
else
        r[4] = 0.01099 * (v[2] + v[4] + v[6] + v[8]);
if(!(v[1] && v[5] && v[3] && v[4] && v[7] && v[8]))
        r[5] = 0;
else
        r[5] = 0.01099 * (v[1] + v[5]);
if(!(v[1] && v[2] && v[3] && v[6] && v[5] && v[7]))
        r[6] = 0;
else
        r[6] = 0.01099 * (v[3] + v[7]);
```

```
/* Compute conversions to account for displacement between sensor and task board */
/* Note that even in cases where the torque values recorded are caused by forces */
/* Those values are printed, to make the software non-case-specific */

                    r[2] = r[2] - r[6]/(.09);
                    r[3] = r[3] + r[5]/(.09);

                    /* Left Handrail */
                    if(!(v[9] && v[11] && v[13] && v[15]))
                            r[7] = 0;
                    else
                            r[7] = -0.04119 * (v[9] + v[11] + v[13] + v[15]);
                    if(!(v[10] && v[14]))
                            r[8] = 0;
                    else
                            r[8] = -0.04119 * (v[10] + v[14]);
                    if(!(v[12] && v[16]))
                            r[9] = 0;
                    else
                            r[9] = -0.04119 * (v[12] + v[16]);
                    if(!(v[10] && v[12] && v[14] && v[16]))
                            r[10] = 0;
                    else
                            r[10] = 0.01099 * (v[10] + v[12] + v[14] + v[16]);
                    if(!(v[9] && v[13] && v[11] && v[12] && v[15] && v[16]))
                            r[11] = 0;
                    else
                            r[11] = 0.01099 * (v[9] + v[13]);
                    if(!(v[9] && v[10] && v[11] && v[14] && v[13] && v[15]))
                            r[12] = 0;
                    else
                            r[12] = 0.01099 * (v[11] + v[15]);

/* Compute conversions to account for displacement between sensor and task board */
/* Note that even in cases where the torque values recorded are caused by forces */
/* Those values are printed, to make the software non-case-specific */

                    r[8] = r[8] - r[12]/(.09);
                    r[9] = r[9] + r[11]/(.09);

                    /* Foot Restraints */
                    if(!(v[17] && v[19] && v[21] && v[23]))
                            r[15] = 0;
                    else
                            r[15] = -0.04119 * (v[17] + v[19] + v[21] + v[23]);
                    if(!(v[18] && v[22]))
                            r[13] = 0;
                    else
                            r[13] = -0.04119 * (v[18] + v[22]);
                    if(!(v[20] && v[24]))
                            r[14] = 0;
                    else
                            r[14] = -0.04119 * (v[20] + v[24]);
                    if(!(v[18] && v[20] && v[22] && v[24]))
```

```
                                r[18] = 0;
                        else
                                r[18] = 0.01099 * (v[18] + v[20] + v[22] + v[24]);
                        if(!(v[17] && v[21] && v[19] && v[20] && v[23] && v[24]))
                                r[16] = 0;
                        else
                                r[16] = 0.01099 * (v[17] + v[21]);
                        if(!(v[17] && v[18] && v[19] && v[22] && v[21] && v[23]))
                                r[17] = 0;
                        else
                                r[17] = 0.01099 * (v[19] + v[23]);

/* Compute conversions to account for displacement between sensor and task board */
/* Note that even in cases where the torque values recorded are caused by forces */
/* Those values are printed, to make the software non-case-specific */

                        r[13] = r[13] + r[17]/(.032);
                        r[14] = r[14] - r[16]/(.032);


                        /* Print out Calculated Reactions */
                        for (index = 1; index < 19; index++)
                                {
                                fprintf(outfile, "%10.2f\t", r[index]);
                                }
                        fprintf(outfile, "\n");

                        }               /* While lines o' data */
next_file:
                        printf("\nEnd of file for %s\n", NAME1);
                        fclose(infile);
                        fclose(outfile);

        }
}
```

Kinematic Chain Link Static Human Modeling Software

Microsoft Excel™ v2.2 Worksheet for the Macintosh SE

A	B	C	D
Length of Right Forearm, L1	1	Degrees	Chest Width, L3
Angle of Right Forearm, Ø1y	=(PI()*C2)/180	45	Left Shoulder Angle,Ø4x
Length of Right Upper Arm L2	1		Left Shoulder Angle,Ø5y
Right Shoulder Angle,Ø2y	=(PI()*C4)/180	45	Left Upper Arm Length,L4
Right Shoulder Angle,Ø3x	=(PI()*C5)/180	0	Left Forearm Angle,Ø6y
			Left Forearm Length, L5
	Fx	**Fy**	**Fz**
Applied Force	1	0	0
Reactions @ Right Elbow Ø1y	=-B9	=-C9	=-D9
Right Shoulder wrt Ø2y	=B11	=C11	=D11
Right Shoulder wrt Ø3x-Total	=B12	=C12	=D12
Left Shoulder wrt Ø9z	=B13	=C13	=D13
Left Elbow wrt Ø4x	=B14	=C14	=D14
Left Elbow wrt Ø5y-- Total	=B14	=C14	=D14
Left Hand wrt Ø6y	=B16	=C16	=D16
Mid-Chest wrt Ø9z	=B14	=C14	=D14
Waist wrt Ø7x	=B20	=C20	=D20
Waist wrt Ø8y -- Total Waist	=B20	=C21	=D20
Knees	=B22	=C22	=D22
Ankles	=B23	=C23	=D23

E	F
1.5	Degrees
=(PI()*F2)/180	0
=(PI()*F3)/180	45
1	
=(PI()*F5)/180	45
1	
Tx	**Ty**
0	0
=-E9+C9*SIN(B2)*B1	=-F9-B9*SIN(B2)*B1+D9*COS(B2)*B1

=E11-C11*B3*COS(B4)	=F11+B11*B3*COS(B4)+D11*B3*SIN(B4)
=E12-C12*B3*COS(B5)+D12*B3*SIN(B5)	=F12+B12*B3*COS(B5)
=E13+D13*E1*COS(H4)	=F13+E1*D13*SIN(H4)
=E14+C14*E4*COS(E2)+D14*E4*SIN(E2)	=F14-B14*E4*COS(E2)
=E15+C14*COS(E3)*E4	=F15-B14*E4*COS(E3)-D14*E4*SIN(E3)
=E16-C16*E6*SIN(E5)	=F16+B16*E6*SIN(E5)-D16*E6*COS(E5)
=E13+D13*(E1/2)*COS(H4)	=F13+D13*(E1/2)*SIN(H4)
=E20+C20*COS(H2)*H1+SIN(H2)*H1*D20	=F20-COS(H2)*H1*B20
=E21+C21*H1*COS(H3)	=F21-H1*B21*COS(H3)+D21*H1*SIN(H3)
=E22+C22*H5*COS(H6)	=F22-B22*H5*COS(H6)-D22*H5*SIN(H6)
=E23+C23*COS(K2)*K1	=F23-B23*COS(K2)*K1+D23*SIN(K2)*K1

G	**H**	**I**
Back Length, L6	2	Degrees
Waist Angle,Ø7x	=(PI()*I2)/180	0
Waist Angle,Ø8y	=(PI()*I3)/180	25
Waist Angle,Ø9z	=(PI()*I4)/180	0
Upper Leg Length,L7	1.2	
Knee/Waist, Ø10y	=(PI()*I6)/180	20

Tz

0

=-G9-C9*COS(B2)*B1
=G11-C11*B3*SIN(B4)
=G12-B12*B3*SIN(B5)
=G13-B13*COS(H4)*E1-C13*SIN(H4)*E1
=G14-B14*E4*SIN(E2)
=G15-C14*E4*SIN(E3)

=G16+C16*E6*COS(E5)

=G13-B13*(E1*0.5)*COS(H4)-C13*(E1*0.5)*SIN(H4)
=G20-SIN(H2)*H1*B20
=G21-C21*H1*SIN(H3)
=G22+C22*SIN(H6)*H5

=G23-C23*SIN(K2)*K1

J	**K**	**L**
Lower Leg Length, L8	1.2	Degrees
Knee Angle, Ø11y	=(PI()*L2)/180	45

Moments of Inertia

Dynamic Human Modeling Software

Microsoft Excel™ v2.2 Worksheet for the Macintosh SE

A Subj. Mass/Ht	B Segment	C Model	D Mass	E Density kg/m3
70	Head	Ellipsoid	=0.0306*A3+2.46	1110
1.725	Neck	Cylinder	=0.0146*A3+0.6	1110
	Torso	Ellip. Cylinder	=0.5436*A3-2.8	1030
	Upper Arm	Conic Fustrum	=0.0274*A3-0.01	1070
	Lower Arm	Conic Fustrum	=0.0189*A3-0.16	1130
	Upper Leg	Conic Fustrum	=0.1159*A3-1.02	1050
	Lower Leg	Conic Fustrum	=0.0375*A3+0.38	1090
	Hand	Sphere	=0.0055*A3+0.07	1160
	Foot	Rec. Parallel.	=0.0069*A3+0.47	1100

F Length L	G COM Nu	H Width W	I Depth D
=0.13*A4	0.5	=SQRT((6*D3)/(E3*F3))	=H3
=0.052*A4	0.5		
=0.338*A4	0.5	=0.191*A4	=(4*D5)/(F5*E5*3.1415*H5)
=0.186*A4	0.436		
=0.146*A4	0.43		
=0.245*A4	0.433		
=0.246*A4	0.433		
	0.5		
=0.152*A4	0.5	=0.055*A4	=0.039*A4

J Radius R	K Sigma	L Parameter A
=SQRT(D4/(E4*F4*3.1415))		
	=1+G6+G6^2	=(9*(K6+G6^3+G6^4))/(20*PI()*K6^2)
	=1+G7+G7^2	=(9*(K7+G7^3+G7^4))/(20*PI()*K7^2)
	=1+G8+G8^2	=(9*(K8+G8^3+G8^4))/(20*PI()*K8^2)
	=1+G9+G9^2	=(9*(K9+G9^3+G9^4))/(20*PI()*K9^2)
=((3*D10)/(E10*PI()*4))^(1/3)		

M	**N**
Parameter B	Ixx
	=(D3*(F3^2+H3^2))/20
	=(D4*(3*J4^2+F4^2))/12
	=(D5*(0.75*H5^2+F5^2))/12
=(3*(1+4*G6+10*G6^2+4*G6^3+G6^4))/(80*K6^2)	=D6*(L6*(D6/(E6*F6))+M6*F6^2)
=(3*(1+4*G7+10*G7^2+4*G7^3+G7^4))/(80*K7^2)	=D7*(L7*(D7/(E7*F7))+M7*F7^2)
=(3*(1+4*G8+10*G8^2+4*G8^3+G8^4))/(80*K8^2)	=D8*(L8*(D8/(E8*F8))+M8*F8^2)
=(3*(1+4*G9+10*G9^2+4*G9^3+G9^4))/(80*K9^2)	=D9*(L9*(D9/(E9*F9))+M9*F9^2)
	=(2*D10*J10^2)/5
	=(D11*(H11^2+F11^2))/12

O	**P**
Iyy	Izz
=N3	=(D3*(H3^2))/10
=N4	=(D4*J4^2)/4
=(D5*(0.75*I5^2+F5^2))/12	=(D5*(H5^2+I5^2))/16
=N6	=(2*D6^2*L6)/(E6*F6)
=N7	=(2*D7^2*L7)/(E7*F7)
=N8	=(2*D8^2*L8)/(E8*F8)
=N9	=(2*D9^2*L9)/(E9*F9)
=N10	=N10
=(D11*(I11^2+F11^2))/12	=(D11*(H11^2+I11^2))/12

Sensor Design Force/Torque Sensor Modeling Software

Microsoft Excel™ v2.2 Worksheet for the Macintosh

Note: Assumes Fixed Model and Al 7075-T6

A	B	C	D	E
H1	**H2**	**L**	**L2**	**Torque Res Flb**
0.375	0.28125	2	6	=(65*(A2^3))/27

F
Force Res Lbs
=(((27*E2)/(6*C2))*(1+(64*((B2/A2)^4)*((C2/D2)^3))))

G
Pyield @1
=(((35000*(A2^3))/(3*C2))*(1+(64*((B2/A2)^4)*((C2/D2)^3))))

H	I	J
Myield @1	**Pyield @2**	**Myield @2**
=((17500*(A2^3))/9)	=(((280000*(B2^3))/(3*D2))*(1+(((A2/B2)^4)*((D2/C2)^3))/64))	=((35000*(B2^3))/9)

Appendix B: Electronics Specifications

1) Analog Devices Model 2B34J Four Channel RTD/Strain Gage Conditioner
2) LM317 Adjustable Voltage Regulator
3) Power General 489 +12 to ±15 DC/DC Voltage Converter
4) For Details on the Industrial Computer Source 6A21 Analog Input Card see Reference [ICS, 1988]

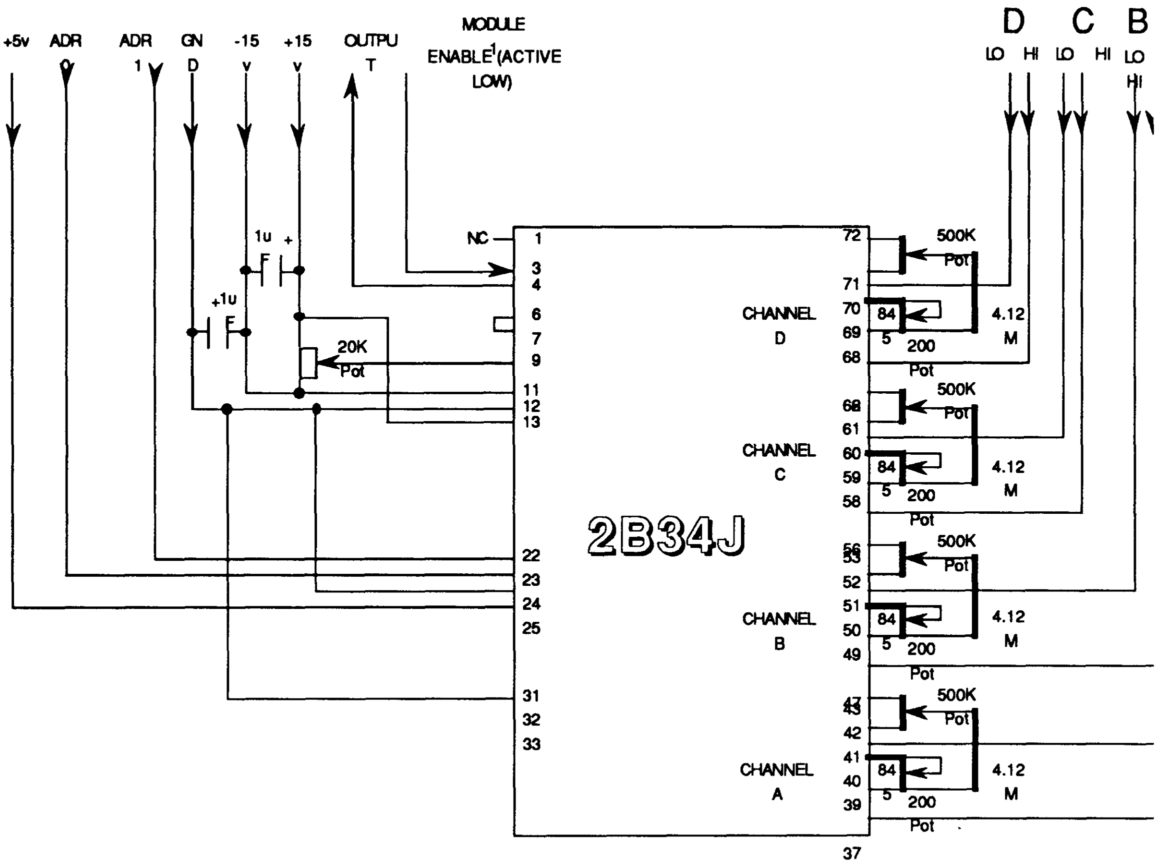

Analog Devices Model 2B34J Four Channel RTD/Strain Gage Conditioner

Specifications:

(Reproduced From Analog Devices 1984 Databook, Modules and Subsystems)

Analog Input Range	± 100	mV	
Gain	166.6	V/V	
Analog Output Range	± 5	V	@ 1 mA
Analog Output Resistance	35	Ohms	
Channel Selection Time	300	µS	
Channel Scanning Speed	> 3000	Channel/Sec.	
Input Settling Time	0.4	S	
Supply Voltage	± 15	VDC	±5%
Current	+ 35 to -15	mA	
Rated Temperature Range	0 to 70	C	
Case Size	2 x 4 x 0.4	Inches	

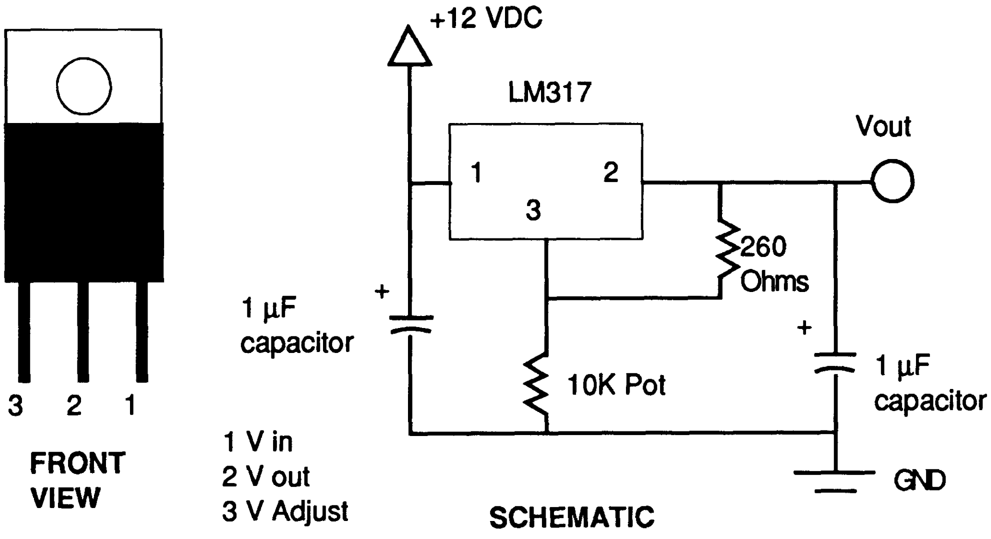

LM317 Adjustable Voltage Regulator

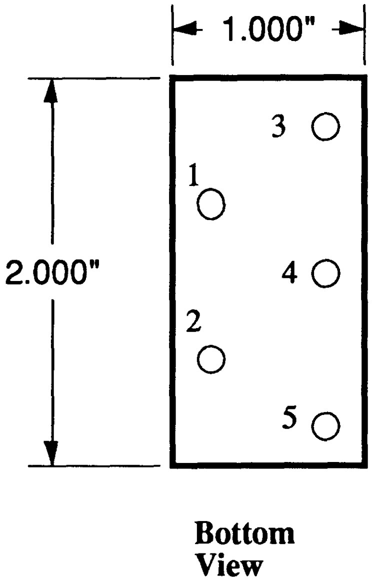

1 +12 VDC in
2 GND in
3 +15 VDC out
4 GND out
5 - 15 VDC out

Power General 489 +12 to ±15 DC/DC Voltage Converter

Appendix C: Sensor Design

Note: In this appendix, English units are often used as this is a design machined to U.S. specifications.

The basic principle behind most load cells and force-torque sensors is the measurement of strain at a point to determine the force or moment producing that strain. To that end, strain gages are attached to a flexure of known properties, which is then subjected to the reaction to be measured. These reactions can be loaded on the flexure in a variety of ways; in the case of forces they can be along the axis of the flexure or perpendicular to it, or in between. Strain gages themselves are essentially resistors whose resistance changes linearly as the gages change length. This elongation is the strain itself. It should prove interesting to look at how forces produce strain, then, to get an idea of how the device should be designed to be loaded.

C.1 Flexure Design

Assuming a square cross-section, single end cantilevered flexure of isotropic material, the bending strain produced at the measurement point by a tip force perpendicular to the long axis of the flexure is described by:

$$\text{Strain}_{\text{bending}} = \frac{FLz}{EI} \quad \text{(C-1)}$$

where F is the tip force, L the distance from the tip to measurement point, z the distance from the force measurement to the flexure centerline (one-half the thickness), E the Young's Modulus, and I the Moment of Inertia for the cross-section. If we assume a flexure thickness of b, Equation (C-1) becomes:

$$\text{Strain}_{\text{bending}} = \frac{6FL}{Eb^3} \quad \text{(C-2)}$$

If the tip force is aligned with the axis of the flexure, we have axial, rather than bending, strain. Axial strain is a function of the force, the Young's Modulus, and the cross sectional area of the flexure (the square of the flexure thickness for our case) as is seen below.

$$\text{Strain}_{\text{axial}} = \frac{F}{Eb^2} \quad \text{(C-3)}$$

Shear strain, the strain produced on the sides of a flexure when it is subjected to a perpendicular tip force, can also be measured. Assuming strain measured at a 45 degree angle, this shear strain equals:

$$\text{Strain}_{\text{shear}} = \frac{FQ}{E(1+\mu)Ib} \quad \text{(C-4)}$$

where Q is the moment of area, and μ is Poisson's ratio. Poisson's ratio is 0.3 for aluminum, and can be modeled as between 0 and 0.5 for most metals. Substituting a square cross-section with flexure thickness b, we have:

$$\text{Strain}_{\text{shear}} = \frac{3F}{2E(1+\mu)b^2} \quad \text{(C-5)}$$

If we now set the other two strain equations as a function of axial strain, we see that for large values of L/b, flexures in bending produce much more strain.

$$\text{Strain}_{\text{shear}} = \frac{3\text{Strain}_{\text{axial}}}{2(1+\mu)} \quad \text{(C-6)}$$

$$\text{Strain}_{\text{bending}} = \frac{6L\text{Strain}_{\text{axial}}}{b} \quad \text{(C-7)}$$

It was thus determined that the sensor should be able to measure all forces and torques using flexures in bending. For the final sensor design, Equations (C-6) and (C-7) became:

$\text{Strain}_{\text{bending}} = 40\ \text{Strain}_{\text{axial}}$ (C-8)

$\text{Strain}_{\text{shear}} = 1.15\ \text{Strain}_{\text{axial}}$ (C-9)

which delineates the distinct advantage bending flexures have over the other types.

C.2 General Sensor Design

A survey of material (especially [Epsilonics, 1981]), led to the concept of a "Maltese-Cross" style sensor, which would be able to measure all forces and torques in bending. This design was then modified as follows:

- The addition of side flexures to prevent the main flexures parallel to the force application direction from being loaded axially.

- Enlargement of the point at which the main flexures cross to allow attachment of task boards.

- The use of square cross-section flexures to simplify the design process.

- Side flexure length must be less than the length of the load application area (3" diameter) plus the length of two main flexures to allow the inclusion of attachment points to the backing board.

- Main flexures were not to be tapered, despite the fact that strain would vary over the length of the gage, due to the additional complexity involved.

- Strain gages to be placed at the midpoint of the main flexure.

- Strain gage bridges composed of gages on opposing faces of a given flexure.

- Wheatstone bridge configuration to be used, but two gages on opposing faces were to be perpendicular to the direction of bending, and used to compensate for temperature differences across the flexures. This indicates that the measured strain would be twice the actual strain, allowing for greater sensitivity.

These modifications led to the general sensor layout seen in Figure 5-3.

C.3 Governing Equations

It was initially determined that all beams could be modeled as fixed at both ends. This was confirmed when calibrating the sensors by applying forces of known magnitudes. The measured strain correlated to the fully fixed model rather than to a model in which the joints between the main and side flexures were modeled as simple (this is discussed further at the end of this section).

The equations which were used to design the sensor are as follows:

1) For an in-plane force, deflection of the center of a side flexure and deflection of the load application point must be equal. This prevents axial loading.

2) Tradeoff between sensitivity and strength of sensor:

- Yield force of 400 lbs, yield torque of 75 foot-lbs (values determined from references, especially [Hanson, 1988]).

- Ideal device sensitivity of better than ± 0.5 lbs, ± 0.5 ft-lbs for a minimum measurable strain of 10 μstrain. Assumes other factors would degrade performance.

The equations for the sensor are found from [Young, 1989]. Assumes force acts through center of flexures.

Deflection (y):

$$y = \frac{FL_1^3}{192\,EI_1} = \frac{FL_2^3}{192\,EI_2} \qquad \text{(C-10)}$$

where F is the applied force, E the Young's Modulus, L1 the length of two main flexures and the load application area, I1 the Moment of Inertia of the main flexure, L2 the length of the side flexure, and I2 the MoI of the side flexure. Substituting b1 for the main flexure thickness, and b2 for the side flexure thickness the following relation is found:

$$\frac{L_1^3}{b_1^4} = \frac{L_2^3}{b_2^4} \qquad \text{(C-11)}$$

L1 is equal to 2L + 3", where L is a main flexure length. From the previous section it is known that L2 < L1. Equation (C-11) provides a relationship between the four parameters which are the essence of the sensor design.

The yield equations are determined by the maximum moment equations for an applied moment or force, at both the side and main flexures. Only the in-plane forces and torques are considered as the device is plainly twice as resilient to out of plane forces and torques (all four main flexures are in bending, not just two). It may be useful to see Figure 5-7 to clarify this.

The following moment equations again assume a force or torque applied to the center of the flexure.

1) Main Flexure, applied force F:

$$M_{max} = \frac{FL_1}{8} \qquad \text{(C-12)}$$

2) Side Flexure, applied force F:

$$M_{max} = \frac{FL_2}{8} \qquad \text{(C-13)}$$

3) Main Flexure, applied torque M:

$$M_{max} = \frac{M}{8} \qquad \text{(C-14)}$$

4) Side Flexure, applied torque M:

$$M_{max} = \frac{M}{8} \qquad \text{(C-15)}$$

These moment values can then be substituted into the following equation:

$$\text{Sigma}_{\text{yield}} = \frac{6M_{\max}}{b_n^3} \qquad \text{(C-16)}$$

The yield stress, is a constant material property, and will be discussed in the next section. Beyond that, Equation (C-16) is, in reality, four equations which can be developed as yield force or torque on either main or side flexures, as a function of the thickness and length of those flexures.

The sensitivity equations are similar to those above, but instead of using the maximum moment point, the strain gage attachment point (L/2) is used. In addition, the yield stress is replaced by Young's Modulus times the measurable strain, 10 µstrain (actual strain 5 µstrain due to bridge configuration). This sensor is half as sensitive to out of plane reactions, for the same reason it is so resilient in those directions. In the following equations x is the strain gage attachment point (L/2), and L is the length of a main flexure (L = .5(L1- 3")).

1) Measurable Moment, applied force, F:

$$M = F\left(\frac{x}{2} - \frac{L_1}{8}\right) \qquad \text{(C-17)}$$

2) Measurable Moment, applied torque, T:

$$M = -\frac{3Tx}{2L_1} + \frac{T}{4} \qquad \text{(C-18)}$$

These equations can be substituted into Equation (C-19) and solved for the applied torque or force in terms of the main flexure length and thickness.

$$E(\text{strain}_{\text{measurable}}) = \frac{6M}{b_n} \qquad \text{(C-19)}$$

The four equations represented by (C-16), the two equations represented by (C-19), and the relationship (C-11) are the equations governing the sensor design. Other important points are that L2 < L1, L = .5(L1 - 3"), and x = .5L. The unknowns are L, L2, b1, and b2 if we ignore the material properties of Young's Modulus and Yield Stress. The

Microsoft Excel™ v2.2 Spreadsheet *Sensor Design* was developed using these equations to allow the four values to be iterated to a usable design. This spreadsheet is available in Appendix A.

If the joints between the main and side flexures are modeled as simple, several changes in the governing equations are found. The signs in equations relating applied reactions to produced moments are opposite from those in a fully fixed model. This pattern of signs (positive moment as a result of a positive axial force) was not seen in actual calibration, rather negative moments resulted from the (defined) positive force. As a result the fixed model was assumed as mentioned above.

C.4 Material Selection

Obviously, the spreadsheet could not be used until a material and its properties could be specified. As seen by Equation (C-16) a high yield stress allows for greater sensor strength. (C-19) reveals that a low Young's Modulus allows greater flexibility, and thus more sensor sensitivity. Thus materials were compared by the nondimensional ratio sigma/E. Better transducer materials have higher ratios.

While this was a major consideration, the materials' linearity of response, hysteresis, cost, and machinability were also considered. Usable temperature range was not considered important, as use in the pool kept operating temperatures between 70 and 85 degrees F. Eight common transducer materials were considered, and they are shown in Table C-1. All characteristics save for the sigma/E ratio are rankings from 1-10 given by [Epsilonics, 1983], with a higher number indicating a better suitability for user as a transducer (i.e. high linearity, low hysteresis, low cost, easy machinability).

#	Material	Ksigma/E	Linearity	Hysteresis	Cost	Machinability
1	410 Steel	4.83	7	7	7	4
2	630 Steel	6.49	8	7	6	6
3	631 Steel	7.59	8	8	6	6
4	Al2024-T6	4.34	6	7	5	8
5	Al6061-T6	4	5	4	6	7
6	Al7075-T6	6.73	7	6	5	8
7	Be-Cu Alloy	10	8	8	2	5
8	6Al 4V Ti	10	7	7	2	3

Table C-1: Material Comparisons

Given this set of comparisons, the material field was narrowed as follows:

1) Excluded on basis of low sigma/E ratio: 1, 4, and 5.

2) Excluded due to high cost: 7 and 8.

3) Material 2 was dropped as it had no particular advantage over material 3.

The remaining materials, 631 stainless steel and 7075 aluminum were both used in different versions of the *Sensor Design* spreadsheet. It was found that an aluminum sensor meeting the yield strength and sensitivity requirements was about 9 inches on a side. The corresponding steel sensor was 2 inches, with all other dimensions correspondingly small. The cost of machining and instrumenting such an intricate sensor would be very high in comparison to the other sensor. The cost of the extra material required for the aluminum sensor would be far outweighed by the cost involved in attaining the high precision necessary in the small work area of the steel sensor. Thus the material choice was Al 7075-T6.

Appendix D: Data

Includes the mean peak reactions data used in Chapter 8.

Note: All forces in Newtons, all torques in Newton-meters.

1) Data Taken for Restraint Case 1, Taken 1/20/90, 1/21, 2/24, 2/25.
For information on the test subjects see Section 6.5.

CASE 1

Reaction	Subject # 1	2	3	6
Fx +	24.87	26.84	38.66	26.02
Fx -	21.97	31.43	29.76	29.13
Fy +	23	23.3	31.67	23.95
Fy -	19.03	28.08	27.45	25.78
Fz +	20.43	19.9	28.07	20.23
Fz -	10.11	29.43	11.85	18.87
Tx +	10.58	11.85	16.07	12.05
Tx -	12.68	17.39	18.2	17.26
Ty +	3.85	3.8	4.53	3.55
Ty -	4.31	4.88	5.31	4.7
Tz +	2.97	3.17	4.74	2.79
Tz -	3.05	5.38	2.59	4.86

2) Data Taken for Restraint Case 2, Taken 1/27/90, 1/28, 2/24, 2/25.
For information on the test subjects see Section 6.5.

CASE 2

Reaction	Subject # 1	2	4	5	6
Fx +	51.45	74.62	74.74	76.82	69.03
Fx -	29.03	76.13	49.78	78.74	77.98
Fy +	28.38	70	49.35	65.99	62.18
Fy -	15.98	80.69	67.69	76.71	71.78
Fz +	28.01	62.95	67.02	65.24	62.46
Fz -	15.21	72.86	76.28	75.49	72.27
Tx +	14.57	19.48	13.91	18.19	17.15
Tx -	6.91	19.67	19.85	18.96	18.74
Ty +	3.73	4.11	4.43	4.23	5.4
Ty -	5.18	4.54	5.37	4.55	2.58
Tz +	4.1	3.75	5.49	4.22	4.43
Tz -	5.82	6.87	5.97	6.07	3.19

3) Data Taken for Restraint Case 3, Taken 2/10/90, 2/11, 2/24, 2/25.
For information on the test subjects see Section 6.5.

CASE 3

Reaction	Subject # 1	2	3	4	5	6
Fx +	76.32	82.48	82.98	85.13	81.26	86.62
Fx -	85.77	99.62	100.5	95.98	96.29	97.21
Fy +	63.71	84.55	83.35	118.07	65.09	103.61
Fy -	86.86	104.03	100.54	97.13	97.23	96.39
Fz +	50.56	72.89	69.32	65.49	97.36	52.14
Fz -	89.79	102.71	101.58	97.25	96.51	79.21
Tx +	10.25	11.19	12.24	18.12	20.49	14.66
Tx -	19.43	22.33	21.78	21.45	21.25	19.57
Ty +	6.61	10.69	5.1	9.1	9.59	11.08
Ty -	3.85	12.77	5.33	13.97	13.42	12.19
Tz +	6.54	9.99	7.34	10.77	11.26	10.66
Tz -	7.19	16.43	7.01	14.84	12.76	12.41

4) Data Taken for Restraint Case 4 - Normal Gravity, Taken 6/8, 6/9, 6/14/90.
For information on the test subjects see Section 6.5.

CASE 4

Reaction	Subject # 1	2	4	5	6
Fx +	93.45	85.29	85.14	84.59	101.05
Fy +	86.06	123.81	109.37	140.19	120.29
Fz +	74.59	113.14	83.16	97.99	97.87
Tx +	20.43	24.43	16.58	24.32	23.44
Ty +	10.42	9.84	9.66	14.65	12.18
Tz +	12.16	12.34	11.82	11.69	12.67

Appendix E: Error Analysis

This appendix covers two of the major causes of error discussed in Chapters 7 and 8. The measurement error associated with the conversion of subject-produced strain into reaction values affects all the data in this document. Joint angle measurement error affects the *Kinematic Chain Link* models used in Section 7.1 only. This error is produced by the inaccuracy inherent in the subject joint angle estimates.

Two other major sources of error are cited in this work: foot restraint compliance and fluid, or hydrodynamic, effects. The latter is discussed in detail in Chapter 3, while the former could not be assessed quantitatively.

E.1 Sensor Measurement Error

Sensor measurement error is mentioned extensively in Chapters 5 and 7, and therefore deserves treatment in detail. Specifically, this error refers to the accuracy of any force or torque measurement made by the FAFNIR Data Acquisition System itself. Before proceeding forward it is necessary to define several terms. *Accuracy* refers to the error limits around any given reaction measurement, and is expressed as ± A N, or N-m; where A is the accuracy value. *Range* refers to the force and torque range over which the accuracy remains constant. In general this indicates the range of linear sensor behavior. *Resolution, precision,* and *sensitivity* are used interchangeably, and refer to the smallest increment which will produce a recognizable change in the values being read. Sensitivity more specifically refers to the smallest detectable change *from zero,* however, this distinction was not found to be important during this analysis.

Strain-gaged sensors based on flexures in bending depend on the linear relationship between moment and strain to produce results. At yield stress, the sensor material loses this linear behavior, therefore the sensor range is limited by this value. Equation (C-16) provides the limiting range for this sensor at ± 2393 N and ± 117 N-m, compared to a design goal of ± 1179 N and ± 102 N-m (for the out of plane direction). However, these ranges were not the final values. The analog-to-digital conversion board used had a limited range of ± 4.095 V divided into millivolt increments. It was found via calibration, that a 1 millivolt change corresponded to a 0.165 N change in force, and a 0.044 N-m change in torque. Thus, the A-to-D board limited the overall range to ± 676 N, and ± 181 N-m. Choosing the lowest range for both force and torque results in an operational range for the sensors at ± 676 N and ± 117 N-m, in the out-of-plane direction (half that for the in-plane coordinates). Note that values are for the out-of-plane direction unless otherwise specified.

As just mentioned, the smallest increment available was 1 millivolt, limiting the precision to worse than ± 0.165 N, and ± 0.044 N-m, for the out-of-plane direction (in-plane errors are half of the out-of-plane values). It was found in testing that changes in force or torque at a ± 10 millivolt level produced recognizable changes in the sensor under constant bias conditions (bias is discussed in the next paragraph); resulting in accuracies of ± 1.65 N and ± 0.44 N-m. Much of this degradation could be due to line noise, and would be virtually eliminated by upgrades described in Section 5.6. This is the minimum limit on sensor accuracy; however, it did not prove to be the overriding error factor. As an aside, it is interesting to note that the design reaction accuracies in Table 5-1 were determined using 10 μstrain as the minimum resolvable strain. Analyzing the output of this sensor, puts the actual value close to 9.2 μstrain, indicating a good design approximation.

When using the sensors, voltages are converted to digital values with a 1 millivolt precision, and are then converted to force and torque values. To accomplish this, the values are first adjusted to account for any bias in the sensors. If this bias was constant throughout testing, this calibration could be accomplished without inducing more error. Unfortunately, fluctuation in the bias occurred during testing, at levels greater than the accuracy determined above. Examination of the data revealed a mean ± 12.56 mV variation in the bias. However, if only values within two standard deviations of the bias mean are considered, this value is reduced to ± 6.90 mV. The bias fluctuations were relatively constant for the three sensors, at ± 11.36, ± 10.67, and ± 15.12. This range represents a maximum 0.73 N difference from sensor to sensor, so even without eliminating "outliers", the sensors were assumed to be interchangeable.

The bias fluctuation was found to be slightly dependent on the day of testing. Four sessions were conducted and the mean fluctuations were recorded at ± 34.04 mV, ± 15.24 mV, ± 4.56 mV, and ± 10.96 mV respectively. However, when values outside two standard deviations were again removed, these values became ± 6.90 mV, ± 6.40 mV, ± 4.56 mV, and ± 8.98 mV. This is only a 0.73 N difference between the extremes, so the data from separate testing sessions were also analyzed interchangeably.

Combining the sources of error results in ± 22.56 mV including outliers, and ± 16.90 mV removing them. Since the data reduction software does not incorporate any removal of points outside two standard deviations, the more conservative value of ± 22.56 mV is selected. This error results in reaction errors of ± 3.72 N, and ± 0.99 N-m for out-of-plane forces and torques. These values can be compared with the initial design goal of ± 2.224 N and ± 0.678 N-m.

E.2 Joint Angle Measurement Error

An examination of the kinematic modeling equations in Chapter 3, or their software implementation in Appendix A will reveal that the various joint angles play a large part in the final models. The predicted torque values depend on the length of various lever arms, and are thus sensitive to joint angle. To use the models properly, accurate joint angle information on the subjects being tested must be provided as inputs to *Kinematic Chain Link*.

There are two difficulties associated with acquiring accurate joint angle information. First, joint angle values change during the duration of testing, and since no real-time joint angle measurement system is available, small changes must be ignored. The second problem is related in that study of videotape and the test rig can only provide angle estimates of limited accuracy. This accuracy is estimated by the author to be in the ± 5 degree range for any of the eleven joints in the model. Therefore, a sensitivity analysis was performed on the static models for restraint cases 1 and 2 to discover the impact of joint angle measurement errors on the model output.

The error analysis covered a ± 10 degree range, and was performed by varying the joint angles for a constant reaction input to the software, and observing changes in the output. Reactions of unitary value were selected for all six directions as the input, and the angles remain as defined in Chapter 3. Note that all angle deflections measured are absolute values, no difference dependant on direction was noted over the ± 10 degree range.

Figure E-1 shows the percentage torque prediction error (force prediction is not influenced by joint angle) as a function of joint angle measurement error for joint Ø1y in Case 1 for Subject 2, as well as a best linear fit. Percentage error is defined as the absolute value of the altered output minus the base output, over the base output.

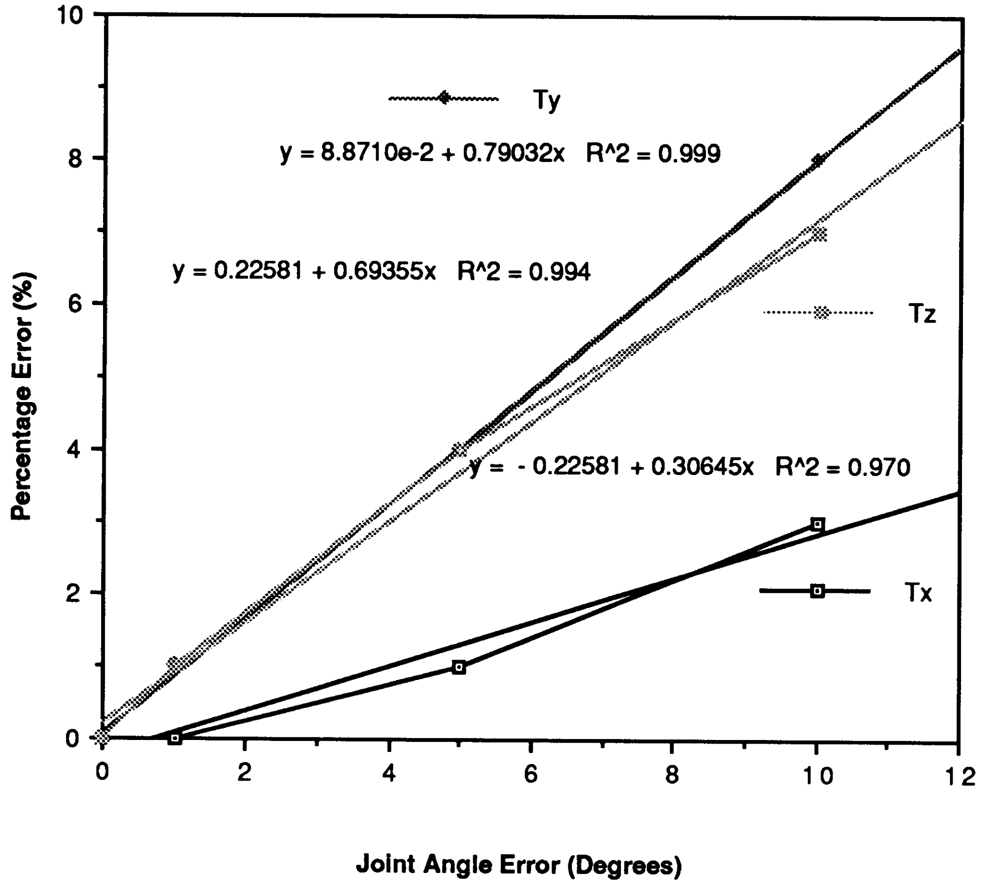

Figure E-1: Angle Deflection versus Percentage Error

Table E-1 collects the percentage errors for all angles and six reactions for restraint Case 1, while Table E-2 provides the same data for Case 2. Little variation between the six test subjects was seen, therefore the values presented in the following three tables are means across all subjects.

	1 Degree			5 Degrees			10 Degrees		
Joint Angle	% Error: Tx	Ty	Tz	Tx	Ty	Tz	Tx	Ty	Tz
Ø1y	0	1	1	1	4	3	3	8	6
Ø2y	0	0	1	1	1	7	3	1	14
Ø3x	0	0	2	2	2	9	5	4	19
Ø4x	0	0	2	1	2	9	2	4	19
Ø5y	0	0	1	1	1	7	3	1	14
Ø6y	0	1	1	1	4	3	3	8	5
Ø7x	*	*	*	*	*	*	*	*	*
Ø8y	*	*	*	*	*	*	*	*	*
Ø9z	0	1	3	0	6	15	0	11	28
Ø10y	*	*	*	*	*	*	*	*	*
Ø11y	*	*	*	*	*	*	*	*	*

Table E-1: Case 1- Percentage Errors

% Error:	1 Degree			5 Degrees			10 Degrees		
Joint Angle	Tx	Ty	Tz	Tx	Ty	Tz	Tx	Ty	Tz
Ø1y	0	1	0	1	7	1	2	13	3
Ø2y	0	0	0	1	1	3	1	2	6
Ø3x	0	1	1	1	4	4	3	6	7
Ø4x	*	*	*	*	*	*	*	*	*
Ø5y	*	*	*	*	*	*	*	*	*
Ø6y	*	*	*	*	*	*	*	*	*
Ø7x	0	0	2	2	1	7	3	2	15
Ø8y	0	2	2	0	12	8	0	24	15
Ø9z	0	1	1	0	5	3	0	9	6
Ø10y	0	2	1	0	8	6	0	16	12
Ø11y	0	2	1	0	10	7	0	21	13

Table E-2: Case 2- Percentage Errors

* indicates angles not included in the model

It can be seen from the tables that joints acting over longer links (such as Ø7-9) usually result in greater percentage errors, as would be expected.

Since total joint angle measurement error would result from all the joints in the model, mean percentage error values for a 5 degree variation in each angle were calculated and presented in Table E-3. Note that assuming a 5 degree error for every joint is a gross overestimate of the error, but does provide a feel for the magnitude of the discrepancy.

	Case 1			Case 2		
	Tx	Ty	Tz	Tx	Ty	Tz
Change +5	0	14	44	2	19	23
Change -5	0	13	47	3	16	24
Alternating	1	3	13	1	20	17

Table E-3: Cumulative Errors